Data-driven modeling and control of dynamical systems using Koopman and Perron-Frobenius operators

by

Bowen Huang

A dissertation submitted to the graduate faculty

in partial fulfillment of the requirements for the degree of

DOCTOR OF PHILOSOPHY

Major: Electrical Engineering (Systems and Controls)

Program of Study Committee:
Umesh Vaidya, Co-major Professor
Venkataramana Ajjarapu, Co-major Professor
Baskar Ganapathysubramanian
Ananda Weerasinghe
Zhengdao Wang

The student author, whose presentation of the scholarship herein was approved by the program of study committee, is solely responsible for the content of this dissertation. The Graduate College will ensure this dissertation is globally accessible and will not permit alterations after a degree is conferred.

Iowa State University

Ames, Iowa

2020

DEDICATION

I would like to dedicate this thesis to my beloved parents, Xiu Lixin and Huang Tiemin, without whose support I would not have been able to complete my Ph.D. degree.

TABLE OF CONTENTS

Page

LIST OF TABLES

Page

LIST OF FIGURES

Page

ACKNOWLEDGMENTS

I would like to take this opportunity to express my thanks to those who helped me with various aspects of conducting research and the writing of this thesis. First and foremost, Prof. Umesh Vaidya for his guidance, patience and support throughout this research and the writing of this thesis. His insights and words of encouragement have often inspired me and introduced me to the charming side of operator theory, dynamical systems and control, and renewed my hopes for completing my graduate education. I would also like to thank my head teacher in high school, Yang Baochen for his guidance throughout the initial stages of my career and developing important habits of self-study with his inspirational teaching style. I would additionally like to thank my colleagues, particularly Subhrajit Sinha, Sai Pushpak, and Ma Xu for collaborating with me and for being there whenever I wanted to exchange opinions on our research.

ABSTRACT

This dissertation studies the data-driven modeling and control problem of nonlinear systems by exploiting the linear operator theoretic framework involving Koopman and Perro-Frobenius operator. A systematic linear-operator based controller design procedure has been established, which can be used to solve a variety of nonlinear control problems, including feedback stabilization using control Lyapunov functions, optimal quadratic regulation using Koopman eigenfunctions and convex optimization formulation of optimal control problem using P-F and Koopman operator approximation.

As the core of data-driven modeling, we first propose a new algorithm for the finite-dimensional approximation of the linear transfer Koopman and Perron-Frobenius operator from time-series data. We argue that the existing approach for the finite-dimensional approximation of these transfer operators such as Dynamic Mode Decomposition (DMD) and Extended Dynamic Mode Decomposition (EDMD) does not capture two important properties of these operators, namely positivity and Markov property. The algorithm we propose preserves these two properties. We call the proposed algorithm as naturally structured DMD (NSDMD) since it retains the inherent properties of these operators. Naturally structured DMD algorithm leads to a better approximation of the steady-state dynamics of the system regarding computing Koopman and Perron- Frobenius operator eigenfunctions and eigenvalues. However, preserving positivity property is critical for capturing the real transient dynamics of the system. This positivity property of the transfer operators and it's finite-dimensional approximation play an important role for controller and estimator design of nonlinear systems.

To solve the feedback stabilization problem for nonlinear control systems, we tried to take advantage of the Koopman operator framework. The Koopman operator approach provides a linear representation for a nonlinear dynamical system and a bilinear representation for a nonlinear control system. The problem of feedback stabilization of a nonlinear control system is then transformed to the stabilization of a bilinear control system. We propose a control Lyapunov function (CLF)-based approach for the design of stabilizing feedback controllers for the bilinear system. The search for

finding a CLF for the bilinear control system is formulated as a convex optimization problem. This leads to a schematic procedure for designing CLF-based stabilizing feedback controllers for the bilinear system and hence the original nonlinear system. Another advantage of the proposed controller design approach outlined in this dissertation is that it does not require explicit knowledge of system dynamics. In particular, the bilinear representation of a nonlinear control system in the Koopman eigenfunction space can be obtained from time-series data.

Next, we study the optimal quadratic regulation problem for nonlinear systems. The linear operator theoretic framework involving the Koopman operator is used to lift the dynamics of nonlinear control system to an infinite-dimensional bilinear system. The optimal quadratic regulation problem for nonlinear system is formulated in terms of the finite-dimensional approximation of the bilinear system. A convex optimization-based approach is proposed for solving the quadratic regulator problem for bilinear system. We applied a variety of examples and compared the simulation results between our framework and conventional LQR control using linearized model.

For more general optimal control problems, finally we provide a density-function based convex formulation for the optimal control problem of the nonlinear system. The convex formulation relies on the duality result in the stability theory of a dynamical system involving density function and Perron-Frobenius operator. The optimal control problem is formulated as an infinite-dimensional convex optimization program. The finite-dimensional approximation of the optimization problem relies on the recent advances made in the data-driven computation of the Koopman operator, which is dual to the Perron-Frobenius operator. Simulation results are presented to demonstrate the application of the developed framework.

CHAPTER 1. INTRODUCTION

With the increasing complexity of modern industrial processes, aerospace systems, transportation systems, power grid systems, modeling the accurate physical system model could be a difficult or even impossible task for researchers and engineers. Even in the case an accurate physical system model can be established, the mathematical formulation still could be too complex to apply the classical controller design procedure, and impossible for the system monitoring and performance evaluation. For this reason, traditional nonlinear control system design methodologies, including the Lyapunov based method, backstepping method and feedback linearization, which depend on an accurate model of the plant, has become impractical for control issues in these kinds of enterprises.

In the meantime, based on the establishment and development of the IoT(Internet of Things) technology, a large amount of diversified time-series data(Big Data) can be generated at high speed by industrial equipment and collected both in the form of stored historical data from prior measurements and online data in real-time during process runs. Using these data, both on-line and off-line, to directly design controllers, predict and assess system states, evaluate performance, make decisions, or even diagnose faults, would be very significant, especially under the lack of accurate process models. Hence, the data-driven control(DDC) or model-free control method is introduced for the identification of the process model and the design of the controller based entirely on experimental data collected from the plant.

1.1 Literature Survey

In this section, we will first go through the history of the data-driven control theory (DDC) and the Linear operator theory, including Koopman and Perron-Frobenius operator, and their application to data analysis. Then a detailed literature review on the Koopman operator identification and Perron-Frobenius operator identification will be given.

The term "data-driven" was first proposed in computer science and has only entered the vocabulary of the control community in recent years. The concept of Big Data Yin and Kaynak (2015) has been well-developed in meteorology, genomics, complex physics simulations, biological and environmental research, finance, and business to healthcare. In the era of Big Data, the data acquiring, storing, computing, and communicating have become much easier, and a large amount of data could be analyzed and explored online by merits of the advanced hardware and software technologies. All of these enable DDC to be necessary and possible technologically.

In general, the definition of Data-driven control Hou and Wang (2013); Van Helvoort (2007); Heusden (2010) is given by all control theories and methods in which the controller is designed by directly using on-line or off-line I/O data of the controlled system or knowledge from the data processing but not any explicit information from mathematical model of the controlled process, and whose stability, convergence, and robustness can be guaranteed by rigorous mathematical analysis under certain reasonable assumptions.

The standard approach to control systems design can be divided into two steps, system identification and controller design for the required performance. According to the controller design procedure, the data-driven control method can be classified as indirect and direct methods.

The direct method, e.g., Formentin et al. (2013), is to map the experimental data directly onto the controller without any model to be identified in between. The SPSA-based DDC method (SPSA) is a direct controller approximation method based on SPSA (simultaneous perturbation stochastic approximation) proposed by Spall in Spall et al. (1992). This method uses only closed-loop measured data rather than a mathematical model of the controlled plant to tune the parameters of the controller Spall and Cristion (1993); Spall and Chin (1997); Spall and Cristion (1998); Spall (2009). Iterative feedback tuning (IFT) was proposed by Hjalmarsson in 1994 Hjalmarsson et al. (1994). It is a typical data-driven control scheme involving iterative optimization of the parameter of the fixed controller according to an estimated gradient of a control performance criterion. At each iteration, the estimate is constructed from a finite set of data obtained partly from the normal operating condition of the closed-loop system and partly from a special experiment in which the output of the plant is fed back in the reference signal of the closed loop.

The indirect method, however, is still retaining the standard two-step approach, first identify a model, then find a controller based on such a model. Hence the typical objective of the system identification step is to have the approximated model as close as possible to the physical model. In the history of data-driven and nonlinear control area, there already exists a wide range of approaches in the literature, including model-free adaptive control Krstic et al. (1995), extremum-seeking Ariyur and Krstić (2003), gain scheduling Rugh and Shamma (2000), feedback linearization Charlet et al. (1989), describing functions Vander Velde (1968), sliding mode control Edwards and Spurgeon (1998), singular perturbation Kokotovic et al. (1976), geometric control Brockett (1976), back-stepping Kokotovic (1992), model predictive control Camacho et al. (2003); Mayne et al. (2000), reinforcement learning Sutton and Barto (2018), and machine learning control Hansen et al. (2008); Brunton and Noack (2015). The subspace approach is an important branch of the indirect methods in DDC methodologies, including the subspace approach Huang and Kadali (2008); Katayama (2006); Van Overschee and De Moor (2012), the data space approach Fujisaki et al. (2004); Ikeda et al. (2001); Park and Ikeda (2009), and the data-driven simulation approach Markovsky et al. (2005, 2006); Markovsky and Rapisarda (2008). The subspace approaches exploit the idea that system dynamics are represented as a subspace of a finite-dimensional vector space, which consists of the time series data of input/state/output or input/output. The Approximate dynamic programming(ADP) has been proposed in Werbos et al. (1990); Werbos (1992) as a solution to optimal control problems forward-in-time. ADP combines reinforcement learning using adaptive critic structures with dynamic programming. ADP includes four main schemes: heuristic dynamic programming, dual heuristic dynamic programming, action-dependent heuristic dynamic programming, i.e., Q-learning WATKINS (1989); Watkins and Dayan (1992); Weissensteiner (2009), and action-dependent dual heuristic dynamic programming. Iterative learning control (ILC) was first proposed by Uchiyama in Japanese in 1978 Uchiyama (1978), which did not get much attention. After one critical report Arimoto et al. (1984) was published in 1984, ILC was extensively studied and significant progress was made in both theory and application in many fields. For a system that repeats the same task in a finite interval, ILC is an ideal technique to learn from the repetitive dynamics to achieve better control performance. ILC has a very simple controller structure and requires little prior knowledge of the system. It can guarantee learning error

convergence as the number of iterations approaches infinity. A more comprehensive and systematic summary of the ILC research can be found in Chen and Wen (1999); Moore (2012).

However, most of the above existing methods are generally tailored to a specific class of problems, require considerable mathematical and computational resources, or don't readily generalize to new applications. The Koopman operator and Perron-Frobenius operator approximations are playing a more and more important role in the generalized data-driven system identification and control methodology.

The Koopman operator formalism was first proposed in the early work of Koopman (1931), where he introduced the linear transformation called Koopman operator, $\mathbf{U}$, and realized that this transformation is unitary for the Hamiltonian dynamical system (the $\mathbf{U}$ notation comes from the unitary property). This observation by Koopman inspired John von Neumann to give the first proof for a precise formulation of ergodic hypotheses, known as *mean ergodic theorem* Halmos (1973). In 1932, Koopman and von Neumann wrote a paper together, where they introduced the notion of the *spectrum of a dynamical system*, i.e. the spectrum of the associated Koopman operator, and noted the connection between chaotic behavior and the continuous part of the Koopman spectrum Koopman and Neumann (1932). For several decades after the work of Koopman and Von Neumann, the notion of Koopman operator was mostly limited to the study of measure-preserving systems as the unitary operator in the proof the mean ergodic theorem or discussions on the spectrum of measure-preserving dynamical systems Petersen (1989); Mane and Levy (1987). It seldom appeared in other applied fields until it was brought back to the general scene of dynamical system by two articles in Mezić and Banaszuk (2004); Mezić (2005). Both papers discussed the idea of applying Koopman methodology to capture the regular components of data in systems with a combination of chaotic and regular behavior.

In 2009, the concept of Koopman modes was applied to a complex fluid flow in Rowley et al. (2009), where the Koopman Mode Decomposition(KMD) is shown promising in capturing the dynamically relevant structures in the flow and associated time scales. This work also showed that KMD could be computed by a numerical decomposition technique known as Dynamic Mode Decomposition (DMD) in Schmid (2010). Since then, KMD and DMD have been massively used in analyzing the nonlinear flows Schmid et al. (2011); Pan et al. (2011); Seena and Sung (2011); Muld et al. (2012);

Hua et al. (2016); Bagheri (2013); Sayadi et al. (2014). A review of the Koopman theory in the context of fluid flows can be found in Mezić (2013). The other applications of KMD include model reduction and fault detection in energy systems for buildings Georgescu and Mezić (2015); Georgescu et al. (2017), coherency identification and stability assessment in power networks Susuki and Mezic (2011); Susuki and Mezić (2013), extracting spatio-temporal patterns of brain activity Brunton et al. (2016a), background detection and object tracking in videos Kutz et al. (2015); Erichson et al. (2016) and design of algorithmic trade strategies in finance Mann and Kutz (2016).

Parallel to the applications, the identification of the Koopman spectrum from data has also seen a lot of progress in recent years. For post-transient systems, the Koopman eigenvalues lie on the unit circle and Fourier analysis techniques can be used to find the Koopman spectrum and modes Mezić and Banaszuk (2004). For dissipative systems, the Koopman spectral properties can be computed using a theoretical algorithm known as *Generalized Laplace Analysis* Mohr (2014); Mohr and Mezić (2014). For the system application with transient behavior, DMD is the popular technique for Koopman identification. The idea of Extending DMD was introduced for numerical computation of the Koopman spectrum by sampling the state space and using a dictionary of observables. The linear algebraic properties of the algorithm are discussed, and new variations are suggested in Chen et al. (2012); Tu et al. (2013). Other new variants of DMD, e.g., Multi-resolution DMD Kutz et al. (2015) and DMDc Proctor et al. (2016), are also introduced in to unravel multi-time-scale phenomena and account for linear input to the system. Considering the scalability of the available data, improvements of DMD are also devised to handle larger data sets Hemati et al. (2014); Guéniat et al. (2015), different sampling techniques Brunton et al. (2013); Tu et al. (2013) and noise Dawson et al. (2016); Hemati et al. (2017). The convergence of DMD-type algorithms for Koopman identification was discussed in Arbabi and Mezic (2017); Korda and Mezić (2018b); Mezic and Arbabi (2017). Once the system information is obtained by Koopman operator identification, these techniques can be widely applied to the data-driven prediction and control. An example of optimal controller is designed based on finite-dimensional Koopman linear expansion of nonlinear dynamics in Brunton et al. (2016b). In Surana (2016); Surana and Banaszuk (2016), a system identification framework is developed to build state estimators for nonlinear systems. More recent works have shown successful application of

Koopman linear predictors for nonlinear systems Korda and Mezić (2018a), and optimal controllers of Hamiltonian systems designed based on Koopman eigenfunctions Kaiser et al. (2017). The feedback control of fluid flows using Koopman linear approximation is demonstrated in a model-predictive control framework Peitz and Klus (2019); Peitz (2018); Arbabi et al. (2018).

Another important component in the operator-theoretic methods, the Transfer operator $\mathbf{P}$ or known as Perron-Frobenius(P-F) operator, which is the left ad-joint to the Koopman operator, also attracted a lot of attention lately for problems involving dynamical system analysis and design. In particular, transfer operator-based methods are used for identifying steady-state dynamics of the system from the invariant measure of transfer operator, identifying almost invariant sets, and coherent structures Dellnitz and Junge (2006); Froyland and Dellnitz (2003); Froyland and Padberg (2009). The spectral analysis of transfer operators is also applied for reduced-order modeling of dynamical systems with applications to building systems, power grid, and fluid mechanics Budisic et al. (2012); Surana and Banaszuk (2016); Arbabi (2017). Similar to the Koopman operator, the P-F operator is also a linear operator defined on the functional space. Hence the operator-theoretic methods can always provide a linear representation of a nonlinear system by shifting the focus from the state space to the space of measures and functions. In particular, the transfer operator methods are used for almost everywhere stability verification Vaidya and Mehta (2008a); Rajaram et al. (2010a), controller design Vaidya et al. (2010b), nonlinear estimation Vaidya (2007); Mehta and Vaidya (2005) and for solving optimal sensor placement problem Sinha et al. (2016); Sharma et al. (2019a). By exploiting the linearity and positivity properties of the P-F operator, a systematic linear programming based approach involving transfer P-F operator has been developed by the long series of work. Besides the novel work in this dissertation, a transfer operators-based method is proposed to obtain global optimal stabilizing control for the stochastic system in Das et al. (2017), and four different optimal control examples are demonstrated further in Das et al. (2018).

The main motivation for our work is to come up with a complete systematic data-driven system identification and control framework, based on the operator-theoretic methods involving Koopman and P-F operators. Moreover, it would also be expected if the machine learning techniques can be used for the Koopman operator identification to handle large datasets and improve the scalability of the

algorithm. In that case, the sample complexity of the algorithm can also be computed and compared with the existing deep learning algorithms in the data-driven control area, e.g., reinforcement learning.

1.2 Our Contribution

As stated in the previous section, the ultimate goal of our work is to establish a complete data-driven system identification and control framework, which could handle the large scale data set from a general nonlinear real-world system. However, most of the existing data-driven modeling and control methods are generally tailored to a specific class of problems, require considerable mathematical and computational resources, or don't readily generalize to new applications. Especially for the Reinforcement Learning model-free control, we can only provide guarantees in special cases that the state/action space is finite, while in a general nonlinear real-world case, the neural network is used to approximate the value function, and there are no guarantees on how the learned model relates to the physical model. Currently, there is no overarching framework for nonlinear control as exists for linear systems. Our proposed framework Huang et al. (2019), based on the Operator-theoretic methods hence delivers unique advantages in both the system identification and controller design procedure, as shown in Fig. 1.1.

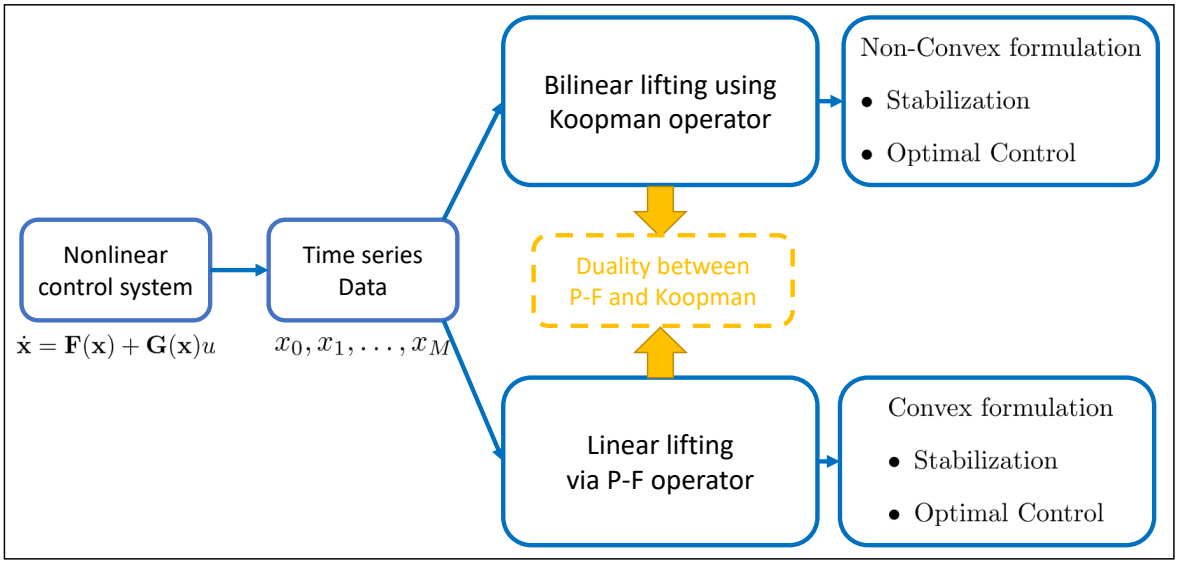

Figure 1.1: Data-Driven Identification and Control framework of Nonlinear Systems

The first step of the Operator-theoretic data-driven control framework is implemented by the Naturally Structured DMD (NSDMD) algorithm Huang and Vaidya (2018) or the Extending DMD algorithm Williams et al. (2015). Compared with the existing data-driven nonlinear control methods, especially the reinforcement learning control, our Koopman operator-based approximations formulate a linear operator formulation on the space of functions given the data generated from the nonlinear system, which carry over our intuition from linear systems to nonlinear systems. Besides that, our NSDMD algorithm for the finite-dimensional approximation of linear operator constructs a connection between the Koopman operator approximation and the P-F operator approximation, the additional constraints in the NSDMD algorithm also explicitly accounts for the positivity and Markov property in the finite-dimensional approximation. In Chapter 3, we show that preserving these properties allows one to better approximate the steady-state dynamics as captured by the spectrum (eigenvalue and eigenfunctions) of these operators but is essential to obtain the actual transient behavior of the system. We show that the problem of finding the finite-dimensional approximation of the Koopman operator using NSDMD is a least-square optimization problem with constraints and is convex. Using the adjoint property between the two transfer operators, we also construct the finite-dimensional approximation of the P-F transfer operator. The P-F transfer operator is used to compute the finite-dimensional approximation of the eigenfunction with eigenvalue one of the P-F operator capturing the steady-state invariant dynamics of the system. Structure preserving the property of our proposed NSDMD algorithm makes this possible. Furthermore, DMD and EDMD algorithm does not lead to stable finite-dimensional Koopman matrix since the largest eigenvalue of the Koopman matrix is not guaranteed to be one. Since the Koopman operator obtained using NSDMD preserves the Markov property, the largest eigenvalue is always one leading to a stable finite-dimensional approximation.

The second step consists of the controller design algorithms based on the bilinear control system model obtained from Koopman operator approximation. In Huang et al. (2019), we present a data-driven approach for feedback stabilization of a nonlinear system. Refer to Fig. 1.1 for the schematic of data-driven nonlinear stabilization. We first show that the nonlinear control system can be identified from the time-series data generated by the system for two different input signals, namely zero input and a constant input. For this identification, we make use of a linear operator theoretic framework

involving the Fokker Planck equation. Furthermore, sample complexity results developed in Chen and Vaidya (2019) are used to determine the data required to achieve the desired level for the approximation. This process of identification leads to a finite-dimensional bilinear representation of the nonlinear control system in Koopman eigenfunction coordinates. This finite-dimensional approximation of the bilinear system is used for the design of a stabilizing feedback controller. While the control design for a bilinear system is, in general, a challenging problem, we propose a systematic approach based on the theory of control Lyapunov function (CLF) and inverse optimality for feedback control design Khalil (1996). The search for CLFs for a general nonlinear system is a difficult problem. We exploit the bilinear representation of the nonlinear control system in the Koopman eigenfunction space to search for a CLF for the bilinear system. By restricting the search of CLFs to a class of quadratic Lyapunov functions, we can provide a convex programming-based systematic approach for determining the CLF Boyd et al. (1994). It is important to emphasize that while the CLF is quadratic in the lifted eigenfunction space, it is, in fact, non-quadratic and contains higher-order nonlinear terms in the original state space coordinates. The principle of inverse optimality allows us to connect the CLF to an optimal cost function. The controller designed using CLF also optimizes an appropriate cost. Using this principle, we comment on the optimality of the controller designed using CLF.

1.3 Organization of This Dissertation

This dissertation is organized as follows. In Chapter 2, we develop the basic concepts and definitions of Transfer operator and Koopman operator theory, some existing Koopman and P-F operator identification methods are also discussed in details. In Chapter 3, we proposed a new data-driven operator identification method, namely, Naturally Structured Dynamic Mode Decomposition(NSDMD), and discussed the advantage of the proposed algorithm compared to the existing Koopman identification algorithms. Chapter 4 is dedicated to finding the nonlinear stabilization control in nonlinear dynamical control systems using the Koopman operator, and we demonstrate three examples where we use the Operator-based method to design the nonlinear stabilization control and quadratic regulator based on the time-series data generated from the nonlinear system. In Chapter 5 is dedicated to further exploit an iterative method to find an optimal quadratic regulator for a nonlinear system using

Koopman operator. In Chapter 6, we provide a convex formulation for the optimal control problem of the nonlinear system. The convex formulation relies on the duality result in the stability theory of a dynamical system involving density function and Perron-Frobenius operator. Finally, we conclude this dissertation in Chapter 7 by summarizing the results.

CHAPTER 2. PRELIMINARIES

In this chapter, we review the basics of transfer operator theory. We introduce the formal definition of the Koopman operator and Perron-Frobenius operators for discrete-time and continuous-time deterministic and stochastic system.

2.1 Linear Perron-Frobenius and Koopman Operators: Discrete-time Dynamics

Consider a discrete time dynamical system

$$\mathbf{x}_{t+1} = \mathbf{T}(\mathbf{x}_t) \tag{2.1}$$

where $\mathbf{T} : \mathbf{X} \subset \mathbb{R}^n \to \mathbf{X}$ is assumed to be invertible and smooth diffeomorphism. Furthermore, we denote by $\mathcal{B}(\mathbf{X})$ the Borel-σ algebra on $\mathbf{X}$, $\mathcal{M}(\mathbf{X})$ vector space of bounded complex valued measure on $\mathbf{X}$, and $\mathcal{F}$ the space of complex valued functions from $\mathbf{X} \to \mathbb{C}$. Associated with this discrete time dynamical systems are two linear operators namely Koopman and Perron-Frobenius (P-F) operator. These two operators are defined as follows.

Definition 1 (Perron-Frobenius Operator)**.** *$\mathbb{P} : \mathcal{F} \to \mathcal{F}$ is defined as*

$$[\mathbb{P}\psi](\mathbf{x}) = \psi(\mathbf{T}^{-1}(\mathbf{x})) \left| \frac{\partial \mathbf{T}^{-1}(\mathbf{x})}{\partial \mathbf{x}} \right|$$

where $|\cdot|$ stands for the determinant. More generally, the P-F operator can also be defined on the measure space $\mathcal{M}(\mathbf{X})$ as follows[1]*:*

$$[\mathbb{P}\mu](A) = \int_{\mathbf{X}} \delta_{T(\mathbf{x})}(A) d\mu(\mathbf{x}) = \mu(\mathbf{T}^{-1}(A))$$

for all sets $A \in \mathcal{B}(\mathbf{X})$ and where $\delta_{T(\mathbf{x})}(A)$ is stochastic transition function which measures the probability that point x will reach the set A in one time step under the system mapping $\mathbf{T}$. Note that the more general definition of P-F operator on the space of measure does not require invertibility

[1] *With some abuse of notation we will use the same notation to denote the P-F operator on the space of measures and functions*

or differentiable property of the mapping $\mathbf{T}$*, we only require the mapping* $\mathbf{T}$ *to be continuous. The noninvetible case the* $\mathbf{T}^{-1}(A)$ *is defined as* $\mathbf{T}^{-1}(A) := \{\mathbf{x} \in \mathbf{X} : \mathbf{T}(\mathbf{x}) \in A\}$.

Definition 2. *[Invariant measures] are the fixed points of the P-F operator* $\mathbb{P}$ *and hence satisfies*

$$\mathbb{P}\bar{\mu} = \bar{\mu}$$

Under the assumption that the state space $\mathbf{X}$ is compact, it is known that the P-F operator admits at least one invariant measure.

Definition 3 (Koopman Operator)**.** $\mathbb{U} : \mathcal{F} \to \mathcal{F}$ *is defined as follows:*

$$[\mathbb{U}\varphi](\mathbf{x}) = \varphi(\mathbf{T}(\mathbf{x}))$$

Properties 4. *The following properties for the Koopman and Perron-Frobenius operators can be stated.*

a). For invariant measure μ *(Definition 2), it easily follows that*

$$\begin{aligned} \| \mathbb{U}\varphi \|^2 &= \int_{\mathbf{X}} |\varphi(\mathbf{T}(\mathbf{x}))|^2 d\bar{\mu}(\mathbf{x}) \\ = \quad & \int_{\mathbf{X}} |\varphi(\mathbf{x})|^2 d\bar{\mu}(\mathbf{x}) = \| \varphi \|^2 \end{aligned}$$

This implies that Koopman operator is unitary.

b). For any $\varphi \geq 0$*, we have* $[\mathbb{U}\varphi](\mathbf{x}) \geq 0$ *and hence Koopman is a positive operator.*

c). For invertible system $\mathbf{T}$*, the P-F operator for the inverse system* $\mathbf{T}^{-1} : \mathbf{X} \to \mathbf{X}$ *is given by* $\mathbb{P}^*$ *and* $\mathbb{P}^*\mathbb{P} = \mathbb{P}\mathbb{P}^* = I$*. Hence, the P-F operator is unitary.*

d). For $\psi(\mathbf{x}) \geq 0$*,* $[\mathbb{P}\psi](\mathbf{x}) \geq 0$*.*

e). The P-F and Koopman operators are dual to each other as follows

$$\langle \mathbb{U}\varphi, \psi \rangle = \int_{\mathbf{X}} [\mathbb{U}\varphi](\mathbf{x})\psi(\mathbf{x})d\mathbf{x} = \int_{\mathbf{X}} \varphi(\mathbf{y})\psi(\mathbf{T}^{-1}(\mathbf{y})) \left| \frac{\partial \mathbf{T}^{-1}}{\partial \mathbf{y}} \right| d\mathbf{y} = \langle \varphi, \mathbb{P}\psi \rangle$$

f). Let $\mu \in \mathcal{M}(\mathbf{X})$ be a positive measure but not necessarily the invariant measure of $\mathbf{T} : \mathbf{X} \to \mathbf{X}$, then the P-F operator satisfies following Markov property.

$$\int_{\mathbf{X}} [\mathbb{P}\psi](\mathbf{x}) d\mu(\mathbf{x}) = \int_{\mathbf{X}} \psi(\mathbf{x}) d\mu(\mathbf{x})$$

The linearity of the P-F operator combined with the properties 4 (e) and 4 (f), makes the P-F operator a particular case of Markov operator Lasota and Mackey (2013). This Markov property of the P-F operator has significant consequences on its finite-dimensional approximation. We will discuss this in the next chapter on set-oriented numerical methods for finite-dimensional approximation of P-F operator. To study the connection between the spectrum of these two operators, we refer the interested readers to Mezić and Banaszuk (2004) and Mehta and Vaidya (2005) (Theorem 5 and Corollary 6) for results connecting the spectrum of transfer Koopman and P-F operator both in the infinite-dimensional and finite-dimensional setting.

2.2 Linear Perron-Frobenius and Koopman Operators: Continuous-time Dynamics

Consider a continuous-time dynamical system of the form

$$\dot{\mathbf{x}} = \boldsymbol{F}(\mathbf{x}), \tag{2.2}$$

where $\mathbf{x} \in \mathbf{X} \subset \mathbb{R}^n$ and the vector field $\boldsymbol{F}$ is assumed to be continuously differentiable. Let $\boldsymbol{S}(t, \mathbf{x}_0)$ be the solution of the system (2.2) starting from initial condition $\mathbf{x}_0$ and at time t.

Definition 5 (Koopman semigroup)**.** *The Koopman semigroup of operators $\mathbb{U}_t : \mathcal{F} \to \mathcal{F}$ associated with system (2.2) is defined by*

$$[\mathbb{U}_t \varphi](\mathbf{x}) = \varphi(\boldsymbol{S}(t, \mathbf{x})). \tag{2.3}$$

It is easy to observe that the Koopman operator is linear on the space of observables although the underlying dynamical system is nonlinear. In particular, we have

$$[\mathbb{U}_t(\alpha\varphi_1 + \varphi_2)](\mathbf{x}) = \alpha[\mathbb{U}_t\varphi_1](\mathbf{x}) + [\mathbb{U}_t\varphi_2](\mathbf{x}).$$

Under the assumption that the function φ is continuously differentiable, the semigroup $[\mathbb{U}_t\varphi](\mathbf{x}) = p(\mathbf{x}, t)$ can be obtained as the solution of the following partial differential equation

$$\frac{\partial p}{\partial t} = \boldsymbol{F} \cdot \nabla p =: Lp.$$

with initial condition $p(\mathbf{x}, 0) = \varphi(\mathbf{x})$. From the semigroup theory it is known Lasota and Mackey (2013) that the operator L is the infinitesimal generator for the Koopman operator, i.e.,

$$Lp = \lim_{t \to 0} \frac{\mathbb{U}_t p - p}{t}.$$

The definition of the semigroup of Perron-Frobenius operator is given by,

Definition 6 (Perron-Frobenius semigroup)**.** *The Perron-Frobenius semigroup of operators $\mathbb{P}_t : \mathcal{F} \to \mathcal{F}$ associated with system (2.2), for each $A \in \mathcal{B}(\mathbf{X})$*

$$\int_A \mathbb{P}_t \psi(\mathbf{x}) \mu(d\mathbf{x}) = \int_{\boldsymbol{S}_{-t}(A)} \psi(\mathbf{x}) \mu(d\mathbf{x}) \tag{2.4}$$

where $S_{-t}(A) : \{\mathbf{x} \in X : S(t, \mathbf{x}) \in A\}$. Making use of the fact that the Perron-Frobenius and Koopman operators are adjoint, that is, $\langle \mathbb{P}_t \psi,\ \varphi \rangle = \langle \psi,\ \mathbb{U}_t \varphi \rangle$, hence $\langle (\mathbb{P}_t \psi - \psi)/t,\ \varphi \rangle = \langle \psi,\ (\mathbb{U}_t \varphi - \varphi)/t \rangle$. The semigroup $\mathbb{P}_t \psi(\mathbf{x}) = \rho(\mathbf{x}, t)$ can also be obtained as the solution of the following partial differential equation,

$$\frac{\partial \rho}{\partial t} = -\nabla(\rho \cdot \boldsymbol{F}) =: \tilde{L}\rho$$

The infinitesimal generator for the Perron-Frobenius operator, $\tilde{L}$ satisfying,

$$\tilde{L}\rho = \lim_{t \to 0} \frac{\mathbb{P}_t \rho - \rho}{t}$$

2.3 Linear Operator for Continuous-time Stochastic Systems: Fokker Planck Equation

Consider a nonlinear dynamical system perturbed with white noise process

$$\dot{\mathbf{x}} = \boldsymbol{F}(\mathbf{x}) + \boldsymbol{\omega}. \tag{2.5}$$

where $\boldsymbol{\omega}$ is the white noise process with mean $\mu = 0$ and standard deviation $\sigma = 1$. The addition of noise term allows us to use the sample complexity results discovered in Chen and Vaidya (2019) to

determine minimum data requirement for the data-driven approximation of nonlinear dynamics. The following assumption is made on the vector function $\boldsymbol{F}$.

Assumption 7. *Let* $\boldsymbol{F} = (\boldsymbol{F}_1, \dots, \boldsymbol{F}_n)^\top$. *We assume that the functions* $\boldsymbol{F}_i$ $i = 1, \dots n$ *are* $\mathbb{C}^4$ *functions.*

We assume that the distribution of $\mathbf{x}(0)$ is absolutely continuous and has density $\rho_0(\mathbf{x})$. Then we know that $\mathbf{x}(t)$ has a density $\rho(\mathbf{x}, t)$ which satisfies the following Fokker-Planck (F-P) equation also known as Kolomogorov forward equation

$$\frac{\partial \rho(\mathbf{x}, t)}{\partial t} = -\nabla \cdot (\boldsymbol{F}(\mathbf{x})\rho(\mathbf{x}, t)) + \frac{1}{2}\nabla^2 \rho(\mathbf{x}, t). \tag{2.6}$$

Following Assumption 7, we know the solution $\rho(\mathbf{x}, t)$ to F-P equation exists and is differentiable (Theorem 11.6.1 Lasota and Mackey (2013)). Under some regularity assumptions on the coefficients of the F-P equation (Definition 11.7.6 Lasota and Mackey (2013)) it can be shown that the F-P admits a generalized solution. The generalized solution is used in defining stochastic semigroup of operators $\{\mathbb{P}_t\}_{t\geq 0}$ such that

$$[\mathbb{P}_t \rho_0](\mathbf{x}) = \rho(\mathbf{x}, t). \tag{2.7}$$

Furthermore, the right hand side of the F-P equation is the infinitesimal generator for stochastic semigroup of operators $\mathbb{P}_t$ i.e., let ψ be a density function,

$$\mathbb{A}\psi = \lim_{t\to 0} \frac{(\mathbb{P}_t - I)\psi}{t}. \tag{2.8}$$

where

$$\mathbb{A}\psi := -\nabla \cdot ((\boldsymbol{F}(\mathbf{x})\psi)) + \frac{1}{2}\nabla^2 \psi.$$

Let $\varphi(x) \in \mathbb{C}^2(\mathbb{R}^n)$ be an observable. We have

$$\frac{d}{dt}\int \rho(\mathbf{x}, t)\varphi(\mathbf{x})dx = \int \mathbb{A}\rho(\mathbf{x}, t)\varphi(\mathbf{x})d\mathbf{x} = \int \rho(\mathbf{x}, t)\mathbb{A}^*\varphi(\mathbf{x})d\mathbf{x}. \tag{2.9}$$

where $\mathbb{A}^*$ is adjoint to $\mathbb{A}$ and is defined as

$$\mathbb{A}^*\varphi = \boldsymbol{F} \cdot \nabla\varphi + \frac{1}{2}\nabla^2\varphi. \tag{2.10}$$

The semigroup corresponding to the operator $\mathbb{A}^*$ is given by

$$\mathbb{A}^*\varphi = \lim_{t\to 0} \frac{(\mathbb{U}_t - I)\varphi}{t}. \tag{2.11}$$

where

$$[\mathbb{U}_t\varphi](\mathbf{x}) = \mathbb{E}[\varphi(\mathbf{x}(t)) \mid \mathbf{x}(0) = \mathbf{x}]. \tag{2.12}$$

For the deterministic dynamical system $\dot{\mathbf{x}} = \boldsymbol{F}(\mathbf{x})$, i.e., in the absence of noise term, the above definitions of generators and semigroups reduces to Perron-Frobenius and Koopman operators. In particular, the propagation of probability density function capturing uncertainty in initial condition is given by the Perron-Frobenius (P-F) operator and is defined as follows.

Definition 8. *The P-F operator for a deterministic dynamical system $\dot{\mathbf{x}} = \boldsymbol{F}(\mathbf{x})$ is defined as follows*

$$[\mathbb{P}_t\rho_0](\mathbf{x}) = \rho_0(\boldsymbol{S}(-t,\mathbf{x}))\left|\frac{\partial \boldsymbol{S}(-t,\mathbf{x})}{\partial \mathbf{x}}\right|. \tag{2.13}$$

where $\boldsymbol{S}(t,\mathbf{x})$ is the solution of the system (2.2) starting from initial condition $\mathbf{x}$ and at time t, and $|\cdot|$ stands for the determinant.

The infinitesimal generator for the P-F operator is given by

$$\mathbb{A}\psi := -\nabla\cdot(\boldsymbol{F}(\mathbf{x})\psi) = \lim_{t\to 0}\frac{(\mathbb{P}_t - I)\psi}{t}. \tag{2.14}$$

2.4 Spectrum of Linear Operators

The spectrum, i.e., eigenvalues and eigenfunctions, of the linear Koopman and P-F operator carry useful information about the system dynamics. However, given the infinite-dimensional nature of these operators the spectrum of these operators could be very complicated consisting of discrete and continuous part. The spectrum of the Koopman operator is far more complex than the simple point spectrum and could include a continuous spectrum Mezić (2005).

Definition 9 (Koopman eigenfunctions)**.** *The eigenfunction of the Koopman operator is a function ϕ_λ that satisfies*

$$[\mathbb{U}_t\phi_\lambda](\mathbf{x}) = e^{\lambda t}\phi_\lambda(\mathbf{x}). \tag{2.15}$$

for some $\lambda \in \mathbb{C}$. The value λ is the associated eigenvalue of the Koopman eigenfunction.

The eigenfunctions can also be expressed in terms of the infinitesimal generator of the Koopman operator L as follows

$$L\phi_\lambda = \lambda\phi_\lambda.$$

The eigenfunctions of the Koopman operator corresponding to the point spectrum are smooth functions and can be used as coordinates for the linear representation of nonlinear systems.

The spectrum of the Perron-Frobenius operator can also be defined in a similar manner.

Definition 10 (Perron-Frobenius eigenfunctions)**.** *The eigenfunction of the Perron-Frobenius operator is a function $\tilde{\phi}_\lambda$ that satisfies*

$$[\mathbb{P}_t\tilde{\phi}_\lambda](\mathbf{x}) = e^{\lambda t}\tilde{\phi}_\lambda(\mathbf{x}). \tag{2.16}$$

for some $\lambda \in \mathbb{C}$. The value λ is the associated eigenvalue of the Perron-Frobenius eigenfunction.

The eigenfunction with eigenvalue one of the P-F operator captures the steady state dynamics of the system. In particular, the steady state dynamics is supported on eigenfunction or eigenmeasure with eigenvalue one of the P-F operator. Unlike the eigenfunctions of the Koopman operator, the eigenfunctions of the P-F operator are not smooth. In fact the eigenmeasure of the P-F operator will be dirac-delta function when the steady state dynamics is a single point attractor. The connection between the spectral properties of the P-F operator and the stability of dynamical system is explored in Vaidya and Mehta (2008b) and this corresponding connection between Koopman spectrum and stability is explored in Mauroy and Mezic (2013).

CHAPTER 3. DATA-DRIVEN APPROXIMATION OF LINEAR OPERATORS: NATURAL STRUCTURE PRESERVING APPROXIMATION OF LINEAR OPERATORS

In this chapter, we first reviewed some existing approximation methods for the P-F operator and Koopman operator, e.g., Set-oriented method, Dynamic Mode Decomposition(DMD) and Extending DMD. Then we provide a new algorithm for the finite-dimensional approximation of the Koopman and P-F operator that preserves some of the properties of these two operators. In particular, we develop an algorithm that preserves the positivity property of the Koopman operator. Furthermore, the adjoint nature of Koopman and P-F operator is used to impose additional constraints on the entries of the Koopman operator. These structural properties are not considered in the existing algorithms involving DMD and EDMD for the finite-dimensional approximation of the Koopman operator.

We show using examples that preserving these properties leads to a better approximation of eigenfunctions and eigenvalues of the transfer operators, but these features are essential to capture the correct transient behavior of the system. Capturing real transient dynamics is of particular importance to the applications of the transfer operator for data-driven control and estimation problems.

3.1 Set-oriented numerical methods

Set-oriented numerical methods are primarily developed for the finite-dimensional approximation of the Perron-Frobenius operator for the case where system dynamics are known as Dellnitz and Junge (2002); Dellnitz et al. (2001). However, these algorithms can be modified or extended to the case where system information is available in the form of time-series data. The basic idea behind set-oriented numerics is to partition the state space, $\mathbf{X}$, into the disjoint set of boxes D_i such that $\mathbf{X} = \cup_{i=1}^{\infty} D_i$. Consider a finite partition $\mathbf{X}^{'} = \{D_1, \ldots, D_K\}$. Now, instead of a Borel σ-algebra, consider a σ-algebra of all possible subsets of $\mathbf{X}$. A real-valued measure μ_j is defined by ascribing to each element D_j a real number. This allows one to identify the associated measure space with a

finite-dimensional real vector space $\mathbb{R}^K$. A given mapping $\mathbf{T} : \mathbf{X} \to \mathbf{X}$ defines a stochastic transition function $\delta_{\mathbf{T}(\mathbf{x})}(\cdot)$. This function can be used to obtain a coarser representation of P-F operator denoted by $\mathbf{P} : \mathbb{R}^{K\times K} \to \mathbb{R}^{K\times K}$ as follows: For $\mu = (\mu_1, \ldots, \mu_K)$ we define a measure on X as

$$d\mu(\mathbf{x}) = \sum_{k=1}^{K} \mu_k \chi_{D_k}(\mathbf{x}) \frac{dm(\mathbf{x})}{m(D_k)}$$

where $\chi_{D_k}(\mathbf{x})$ is the indicator function of D_k and m is the Lebesgue measure. The finite dimensional approximation of the P-F matrix, $\mathbf{P}$, can now be obtained as follows:

$$\begin{aligned} \nu_i = [\mathbf{P}\mu](D_i) &= \sum_{j=1}^{K} \int_{D_j} \delta_{\mathbf{T}(\mathbf{x})}(D_i)\mu_j \frac{dm(\mathbf{x})}{m(D_j)} \\ = \quad \sum_{j=1}^{K} \mu_k \mathbf{P}_{ij} & \end{aligned} \tag{3.1}$$

where

$$\mathbf{P}_{ij} = \frac{m(\mathbf{T}^{-1}(D_j) \cap D_i)}{m(D_j)}$$

The resulting matrix $\mathbf{P}$ is a Markov matrix and is row stochastic if we consider state μ to be a row vector multiplying from the left of $\mathbf{P}$. The individual entries of this Markov matrix can be obtained by Monte-Carlo approach by running simulation over short time interval starting from different initial conditions. Typically individual boxes D_i will be populated with M uniformly distributed initial conditions. The entry $\mathbf{P}_{ij}$ is then approximated by fraction of initial conditions that are in box D_j in one forward iteration of the mapping $\mathbf{T}$. The Monte Carlo based approach can be extended for computation of the P-F transfer operator from time series data. Let $\{\mathbf{x}_0, \mathbf{T}(\mathbf{x}_0), \ldots, \mathbf{T}^{K-1}(\mathbf{x}_0)\}$ be the time series data set. The number of initial conditions in box i is then given by

$$\sum_{k=0}^{K-1} \chi_i(\mathbf{T}^k(x_0))$$

where χ_i is the indicator function of box i. The (i, j) entry for P-F matrix $\mathbf{P}_{ij}$ is then given by the fraction of these initial conditions from box i that ends up in box j after one iterate of time and is given by following formula.

$$\mathbf{P}_{ij} = \frac{1}{\sum_{k=0}^{K-1} \chi_i(\mathbf{T}^k(x_0))} \sum_{k=0}^{K-1} \chi_i(\mathbf{T}^k(x_0))\chi_j(\mathbf{T}^{k+1}(x_0)).$$

3.2 Dynamic mode decomposition (DMD) and Extending DMD

Dynamic Mode Decomposition method (DMD) has been introduced Schmid (2010) for the dynamical analysis of the fluid flow field data. In the context of this dissertation, DMD can be viewed as a computation algorithm for approximating the spectrum of Koopman operator Rowley et al. (2009). Extension of the DMD is presented in the form of Extending DMD (EDMD) Williams et al. (2015) which does a better job in approximating the spectrum of Koopman operator for both linear and nonlinear underlying system. In the following, we briefly explain the EDMD algorithm and show how the solution of DMD algorithm can be derived as a special case of EDMD. Consider snapshots of data set obtained from simulating a discrete time dynamical system or from an experiment

$$\overline{X} = [\mathbf{x}_1, \mathbf{x}_2, \ldots, \mathbf{x}_M], \quad \overline{Y} = [\mathbf{y}_1, \mathbf{y}_2, \ldots, \mathbf{y}_M] \tag{3.2}$$

where $\mathbf{x}_i \in \mathbf{X}$ and $\mathbf{y}_i \in \mathbf{X}$. The two pair of data sets are assumed to be two consecutive snapshots i.e., $\mathbf{y}_i = \mathbf{T}(\mathbf{x}_i)$. Now let $\mathcal{D} = \{\psi_1, \psi_2, \ldots, \psi_N\}$ be the set of dictionary functions or observables. The dictionary functions are assumed to belong to $\psi_i \in L_2(\mathbf{X}, \mathcal{B}, \mu) = \mathcal{G}$, where μ is some positive measure not necessarily the invariant measure of $\mathbf{T}$. Let $\mathcal{G}_\mathcal{D}$ denote the span of $\mathcal{D}$ such that $\mathcal{G}_\mathcal{D} \subset \mathcal{G}$. The choice of dictionary functions are very crucial and it should be rich enough to approximate the leading eigenfunctions of Koopman operator. Define vector valued function $\mathbf{\Psi} : \mathbf{X} \to \mathbb{C}^N$

$$\mathbf{\Psi}(\mathbf{x}) := \begin{bmatrix} \psi_1(\mathbf{x}) & \psi_2(\mathbf{x}) & \cdots & \psi_N(\mathbf{x}) \end{bmatrix}^\top \tag{3.3}$$

In this application, $\mathbf{\Psi}$ is the mapping from physical space to feature space. Any function $\phi, \hat{\phi} \in \mathcal{G}_\mathcal{D}$ can be written as

$$\phi = \sum_{k=1}^{N} a_k \psi_k = \mathbf{\Psi}^\top \boldsymbol{a}, \quad \hat{\phi} = \sum_{k=1}^{N} \hat{a}_k \psi_k = \mathbf{\Psi}^\top \hat{\boldsymbol{a}} \tag{3.4}$$

for some set of coefficients $\boldsymbol{a}, \hat{\boldsymbol{a}} \in \mathbb{C}^N$. Let

$$\hat{\phi}(\mathbf{x}) = [\mathbb{U}\phi](\mathbf{x}) + r,$$

where $r \in \mathcal{G}$ is a residual function that appears because $\mathcal{G}_\mathcal{D}$ is not necessarily invariant to the action of the Koopman operator. To find the optimal mapping which can minimize this residual, let $\mathbf{K}$ be

the finite dimensional approximation of the Koopman operator. Then the matrix $\mathbf{K}$ is obtained as a solution of least square problem as follows

$$\min_{\mathbf{K}} \parallel \mathbf{G}\mathbf{K} - \mathbf{A} \parallel_F \tag{3.5}$$

$$\begin{aligned} \mathbf{G} &= \frac{1}{M}\sum_{m=1}^{M} \mathbf{\Psi}(\mathbf{x}_m)\mathbf{\Psi}(\mathbf{x}_m)^\top \\ \mathbf{A} &= \frac{1}{M}\sum_{m=1}^{M} \mathbf{\Psi}(\mathbf{x}_m)\mathbf{\Psi}(\mathbf{y}_m)^\top, \end{aligned} \tag{3.6}$$

with $\mathbf{K}, \mathbf{G}, \mathbf{A} \in \mathbb{C}^{N\times N}$. The optimization problem (3.5) can be solved explicitly to obtain following solution for the matrix $\mathbf{K}$

$$\mathbf{K}_{EDMD} = \mathbf{G}^\dagger \mathbf{A} \tag{3.7}$$

where $\mathbf{G}^\dagger$ is the pseudoinverse of matrix $\mathbf{G}$. Hence, under the assumption that the leading Koopman eigenfunctions are nearly contained within $\mathcal{G}_\mathcal{D}$, the subspace spanned by the elements of $\mathcal{D}$. The eigenvalues of $\mathbf{K}$ are the EDMD approximation of Koopman eigenvalues. The right eigenvectors of $\mathbf{K}$ generate the approximation of the eigenfunctions in (3.8). In particular, the approximation of Koopman eigenfunction is given by

$$\phi_j = \mathbf{\Psi}^\top \mathbf{v}_j \tag{3.8}$$

where $\mathbf{v}_j$ is the j-th right eigenvector of $\mathbf{K}$, ϕ_j is the eigenfunction approximation of Koopman operator associated with j-th eigenvalue.

DMD is a particular case of EDMD, and it corresponds to the case where the dictionary functions are chosen to be equal to $\mathcal{D} = \{\mathbf{e}_1^\top, \ldots, \mathbf{e}_N^\top\}$, where $\mathbf{e}_i \in \mathbb{R}^n$ is a unit vector with 1 at i^{th} position and zero elsewhere. With this choice of dictionary function, it can be shown the approximation of the Koopman operator using DMD approach can be written as

$$\mathbf{K}_{DMD} = \overline{Y}\ \overline{X}^\dagger,$$

where $\overline{X}$ and $\overline{Y}$ are dataset as defined in (3.2).

Table 3.1: A table with some commonly used sets of trial functions, and the application where they are most suited.

Name	**Suggested Context**
Hermite Polynomials and Monomials	Problems defined on $\mathbb{R}^n$
Radial Basis Functions	General problems defined on irregular domains
Discontinuous Spectral Elements	Large problems where a block-diagonal $\mathcal{G}$ is beneficial/computationally important

3.3 Naturally Structured Dynamic Mode Decomposition

In our proposed numerical algorithm for finite dimensional approximation of transfer operators from data we start with the choice of dictionary functions $\mathcal{D} = \{\psi_1, \ldots, \psi_N\}$, where $\psi_i(\mathbf{x}) \in \mathcal{G} = L_2(\mathbf{X}, \mathcal{B}, \mu)$. As already stated the choice of dictionary function is crucial and should be rich enough to approximate the Koopman eigenfunctions. Similarly, the data set generated by the dynamics should be rich enough to carry the information about the inherent dynamics of the system. We believe that the proper choice of dictionary function and dataset are intimately connected. Some experimental rules has been summarized in Table. 3.1 based on Williams et al. (2015) and our experience.

We make the following assumptions on the choice of dictionary function.

Assumption 11. *We assume that the dictionary function $\psi_i(\mathbf{x}) \geq 0$ for $i = 1, \ldots, N$ and the inner product Λ of the dictionary functions, $\Lambda = \langle \mathbf{\Psi}(\mathbf{x}), \mathbf{\Psi}(\mathbf{x}) \rangle$ with $[\Lambda]_{ij} = \langle \psi_i, \psi_j \rangle$ is symmetric positive definite matrix.*

Remark 12. *Gaussian radial basis function (RBF) given by $e^{-\frac{\|\mathbf{x}-\mathbf{x}_i\|}{\sigma^2}}$, serves as a good approximation for the choice of dictionary functions satisfying the above assumption.*

Let $\mathcal{G}_\mathcal{D}$ be the span of these dictionary functions. Now consider any function ϕ and $\hat{\phi}$ in $\mathcal{G}_\mathcal{D}$, we can express these functions as

$$\phi = \sum_{k=1}^{N} a_k \psi_k = \mathbf{\Psi}^\top \boldsymbol{a}, \quad \hat{\phi} = \sum_{k=1}^{N} \hat{a}_k \psi_k = \mathbf{\Psi}^\top \hat{\boldsymbol{a}} \tag{3.9}$$

Again function ϕ and $\hat{\phi}$ are related as follows

$$\hat{\phi}(\mathbf{x}) = [\mathbb{U}\phi](\mathbf{x}) + r$$

where $r \in \mathcal{G}$ and represents the error and arise because of the fact that $\mathcal{G}_{\mathcal{D}}$ is not necessarily invariant under the action of Koopman operator. The extending DMD seeks to find the matrix $\mathbf{K} \in \mathbb{R}^{N\times N}$ that does the best job in mapping $\boldsymbol{a}$ to $\hat{\boldsymbol{a}}$. The matrix $\mathbf{K}$ is obtained as a solution of the least square problem as outlined in Eqs. (3.7) and (3.14). Now consider a case where $\phi(\mathbf{x}) \geq 0$. Then under Assumption 11, we know that $a_i \geq 0$. Using the positivity property of the Koopman operator, we know that $[\mathbb{U}\phi](\mathbf{x}) \geq 0$. The vector $\boldsymbol{a}$ is mapped to $\hat{\boldsymbol{a}}$ by the finite dimensional matrix $\mathbf{K}$. To preserve the positivity property of the Koopman operator (i.e., property 4b) we require that coefficient $\hat{a}_i$ are also positive. This, in turn, implies that the mapping $\mathbf{K}$ should satisfy the property

$$\mathbf{K}_{ij} \geq 0, \quad \text{for} \quad i, j = 1, \ldots, N. \tag{3.10}$$

Let $\mathbf{P}$ be the finite dimensional approximation of the P-F operator. Since P-F is Markov operator, its finite dimensional approximation constructed on the dictionary function satisfying Assumption 11 has some properties. In particular, consider any density function, φ, expressed as linear combinations of dictionary functions

$$\varphi = \sum_{k=1}^{N} b_k \psi_k, \quad b_k \geq 0.$$

We have

$$[\mathbb{P}\varphi](\mathbf{x}) = \hat{\varphi}(\mathbf{x}) + r = \sum_{k=1}^{N} \hat{b}_k \psi_k + r,$$

where $r \in \mathcal{G}$ is the residual term which arise because $\mathcal{G}_{\mathcal{D}}$ is not invariant under the action of the P-F operator. The finite dimensional approximation of the P-F operator, $\mathbf{P}$ maps coefficient vector $\boldsymbol{b}$ to $\hat{\boldsymbol{b}}$, i.e., $\hat{\boldsymbol{b}} = \mathbf{P}\boldsymbol{b}$.

We are interested in approximating P-F operator such that the Markov property 4(f) of the infinite dimensional P-F operator is preserved. Since $[\mathbb{P}\varphi](\mathbf{x}) \geq 0$ we have $b_k \geq 0$ for all k. Hence for preserving the Markov property we require that

$$\boldsymbol{b}^\top \mathbb{1} = \hat{\boldsymbol{b}}^\top \mathbb{1}, \tag{3.11}$$

where $\mathbb{1}$ is a vector of all ones.

Based on the adjoint property of Koopman and P-F operators, we have

$$\langle \mathbb{U}\phi, \varphi \rangle = \langle \phi, \mathbb{P}\varphi \rangle$$

Writing φ and ϕ as linear combinations of basis function and using the definition of inner product from Assumption 11, we can approximate the adjoint relationship as follows:

$$\begin{aligned} \langle \mathbb{U}\phi, \varphi \rangle \cong (\mathbf{K}\boldsymbol{a})^\top \boldsymbol{\Lambda} \boldsymbol{b} \quad &, \quad \langle \phi, \mathbb{P}\varphi \rangle \cong \boldsymbol{a}^\top \boldsymbol{\Lambda} \mathbf{P} \boldsymbol{b} \\ \boldsymbol{a}^\top \mathbf{K}^\top \boldsymbol{\Lambda} \boldsymbol{b} \quad &= \quad \boldsymbol{a}^\top \boldsymbol{\Lambda} \mathbf{P} \boldsymbol{b} \end{aligned} \tag{3.12}$$

Since above is true for all $\boldsymbol{a}$ and $\boldsymbol{b}$, we have $\mathbf{K}^\top \boldsymbol{\Lambda} = \boldsymbol{\Lambda} \mathbf{P}$. Combining (3.10), (3.11) and the adjoint property of P-F and Koopman operator (i.e., $\mathbf{P}^\top = \Lambda \mathbf{K} \Lambda^{-1}$), it follows that for the finite-dimensional approximation of the transfer operator to preserve the positivity and Markov properties of its infinite-dimensional counterpart then $\mathbf{K}$ should satisfy following conditions.

$$[\Lambda \mathbf{K} \Lambda^{-1}]_{ij} \geq 0, \quad \sum_{j=1}^{N} [\Lambda \mathbf{K} \Lambda^{-1}]_{ij} = 1, \ i, j = 1, \ldots, N.$$

This leads to the following optimization based formulation for the computation of matrix $\mathbf{K}$

$$\begin{aligned} \min_{\mathbf{K}} \quad & \| \mathbf{G}\mathbf{K} - \mathbf{A} \|_F \\ \text{subject to} \quad & \mathbf{K}_{ij} \geq 0 \\ & [\Lambda \mathbf{K} \Lambda^{-1}]_{ij} \geq 0 \\ & \Lambda \mathbf{K} \Lambda^{-1} \mathbb{1} = \mathbb{1} \end{aligned} \tag{3.13}$$

where $\mathbf{G}$ and $\mathbf{A}$ are defined as follows:

$$\begin{aligned} \mathbf{G} &= \frac{1}{M} \sum_{m=1}^{M} \boldsymbol{\Psi}(\mathbf{x}_m) \boldsymbol{\Psi}(\mathbf{x}_m)^\top \\ \mathbf{A} &= \frac{1}{M} \sum_{m=1}^{M} \boldsymbol{\Psi}(\mathbf{x}_m) \boldsymbol{\Psi}(\mathbf{y}_m)^\top, \end{aligned} \tag{3.14}$$

with $\mathbf{K}, \mathbf{G}, \mathbf{A} \in \mathbb{C}^{N \times N}$ and the data set snapshots $\{x_m, y_m\}$ as defined in (3.2). The optimization problem (3.13) is a convex and can be solved using one of the standard optimization toolbox for solving convex problem.

It is important to emphasize that the matrix $\mathbf{K}$ serves two purposes; a) approximation of Koopman operator if we multiply vector from right; b) approximation to P-F operator if we multiply vector from left.

$$\text{Koopman operator} \ \ \mathbf{v}_{t+1} = \mathbf{K}\mathbf{v}_t$$

$$\text{P} - \text{F operator} \;\; \mathbf{u}_{t+1} = \mathbf{u}_t \mathbf{P}$$

where $\mathbf{P}^\top = \Lambda \mathbf{K} \Lambda^{-1}$, $\mathbf{v}_t \in \mathbb{R}^N$ is column vector and $\mathbf{u}_t \in \mathbb{R}^N$ is row vector, and t is the time index.

Since $\mathbf{P}$ is row stochastic, it is guaranteed to have at least one eigenvalue one. Let, $\bar{\mathbf{u}}_1$ be the left eigenvector with eigenvalue one of the $\mathbf{P}$ matrix. Then the approximation to the invariant density for the dynamical system, $\mathbf{T}$, i.e., $\bar{\varphi}_1(\mathbf{x})$, can be obtained using following formula

$$\bar{\varphi}_1(\mathbf{x}) = \mathbf{\Psi}(\mathbf{x})^\top \bar{\mathbf{u}}_1^\top.$$

Eigenfunction with eigenvalue λ can be obtained as $\bar{\varphi}_\lambda = \mathbf{\Psi}(\mathbf{x})\bar{\mathbf{u}}_\lambda^\top$, where $\bar{\mathbf{u}}_\lambda^\top$ is the left eigenvector with eigenvalue λ of matrix $\mathbf{P}$. Koopman eigenfunction with eigenvalue λ. We will refer to these eigenfunctions obtained using the left eigenvector of the $\mathbf{P}$ matrix as P-F eigenfunction. Similarly, approximate eigenfunctions of Koopman operator can be obtained using the right eigenvector of the $\mathbf{K}$ matrix. Let $\bar{\mathbf{v}}_\lambda$ be the right eigenvector with eigenvalue λ of the $\mathbf{K}$ matrix then the approximate Koopman eigenfunction $\bar{\vartheta}_\lambda$ can be obtained as follows:

$$\bar{\vartheta}_\lambda(\mathbf{x}) = \mathbf{\Psi}(\mathbf{x})^\top \bar{\mathbf{v}}_\lambda.$$

We show that NSDMD preserves the stability property of the original system, and this is one of the main advantages of the proposed algorithm. In particular, that certificate in the form of Lyapunov measure can be computed using the $\mathbf{K}$ matrix. Vaidya and Mehta (2008a) introduced the Lyapunov measure for almost everywhere stability verification of general attractor set in the nonlinear dynamical system. The Lyapunov measure is computed using a transfer operator-based framework. Vaidya and Mehta (2008a) utilized set-oriented numerical methods for the finite-dimensional approximation of the P-F operator from system dynamics. However, a data-driven approach for verifying the stability of the attractor set will involve making use of matrix $\mathbf{K}$ for computing Lyapunov measure. The procedure for calculating the Lyapunov measure will remain the same; the only change is that instead of using the P-F matrix constructed using a set-oriented numerical method, one can use the $\mathbf{K}$ build from time-series data. In the simulation section, we present results for the computation of the stability certificate. Different optimization problems can be formulated based on the main optimization formulation in Eq. (3.13). These different optimization formulations will try to preserve one or all the properties of these two operators. In particular, we have the following different cases.

Case I: With positivity constraint on $\mathbf{K}$ only

$$\begin{aligned} \min_{\mathbf{K}} \quad & \| \mathbf{GK} - \mathbf{A} \|_F \\ \text{subject to} \quad & \mathbf{K}_{ij} \geq 0 \end{aligned} \tag{3.15}$$

Case II: With positivity and Markov constraint on $\mathbf{P}$ only

$$\begin{aligned} \min_{\mathbf{K}} \quad & \| \mathbf{GK} - \mathbf{A} \|_F \\ \text{subject to} \quad & [\Lambda \mathbf{K} \Lambda^{-1}]_{ij} \geq 0 \\ & \Lambda \mathbf{K} \Lambda^{-1} \mathbb{1} = \mathbb{1} \end{aligned} \tag{3.16}$$

Both the optimization formulation (3.15) and (3.16) are convex formulations.

Case III: This case corresponds to combining both Case I and Case II and the optimization formulation corresponding to this case is given in Eq. (3.13).

3.4 Examples and Applications

The simulation results in this section are obtained by solving the optimization problems using GUROBI solver coded in MATLAB.

2D system: For this example we use optimization formulation from **Case I**. A simple 2D nonlinear system is considered first. The differential equation of the system is given as follows,

$$\begin{aligned} \dot{x} &= x - x^3 + y \\ \dot{y} &= 2x - y \end{aligned} \tag{3.17}$$

This continuous time system has 2 stable equilibrium points, located at $(\pm\sqrt{3}, \pm 2\sqrt{3})$ and one saddle point at $(0, 0)$. To generate time-series data of $T = 10$, 1000 initial conditions from $[-5, 5] \times [-5, 5]$ are randomly chosen and propogated using ode23t solver in MATLAB, sampled by $\Delta t = 0.1$. The naturally structured dynamic mode decomposition (NSDMD) algorithm is then implemented with Gurobi solver. The following simulation results are obtained with 500 dictionary functions and $\sigma = 0.45$.

In Fig. 3.1 and Fig. 3.2, we plot the Koopman eigenfunctions associated with eigenvalue 1 using NSDMD algorithm. The eigenfunction with eigenvalue one is clearly shown to separate the two domains of attraction. The separatrix region separating the two domains of attractions is captured by the eigenfunction with the second dominant eigenvalue.

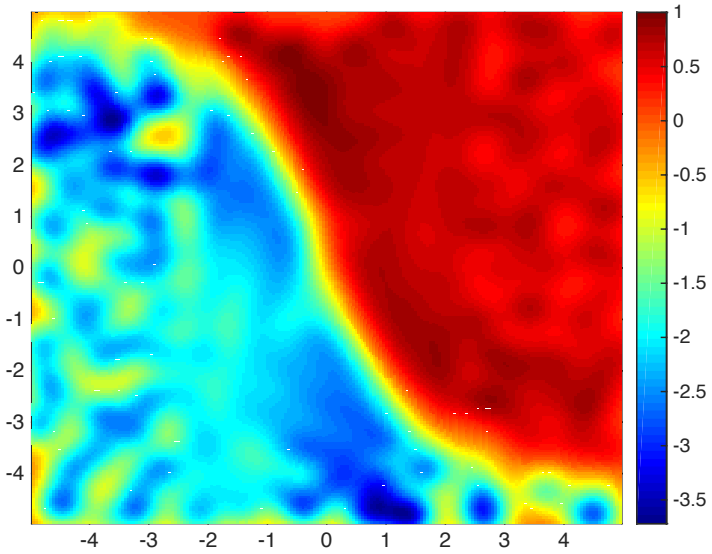

Figure 3.1: CASE-I: Koopman eigenfunction for eigenvalue 1 for system (3.17) using NSDMD

Duffing Oscillator: The simulation results for this example is obtained using formulation of **Case I**. The duffing oscillator is given by following differential equation.

$$\ddot{x} = -0.5\dot{x} - (x^2 - 1)x \tag{3.18}$$

The time step for the continuous-time system is chosen to be equal to $\Delta t = 0.25$ with a total period of $T = 2.5$ and 1000 randomly chosen initial conditions. We solve the differential equation in MATLAB with $ode45$ solver. We use 500 Gaussian radial basis functions to form the dictionary set with $\sigma = 0.1$. In Fig. 3.3 and Fig. 3.4, we plot the first two dominant eigenfunctions of the Koopman operator obtained using NSDMD algorithm. Similar to example 1, we notice the first two dominant Koopman eigenfunctions carry information about the domain of attraction of the two equilibrium points.

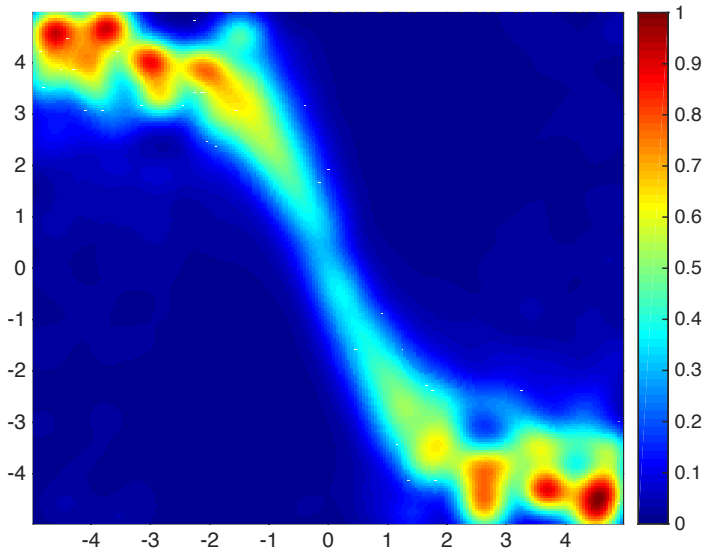

Figure 3.2: CASE-I: Koopman eigenfunction for eigenvalue 0.97 for system (3.17) using NSDMD

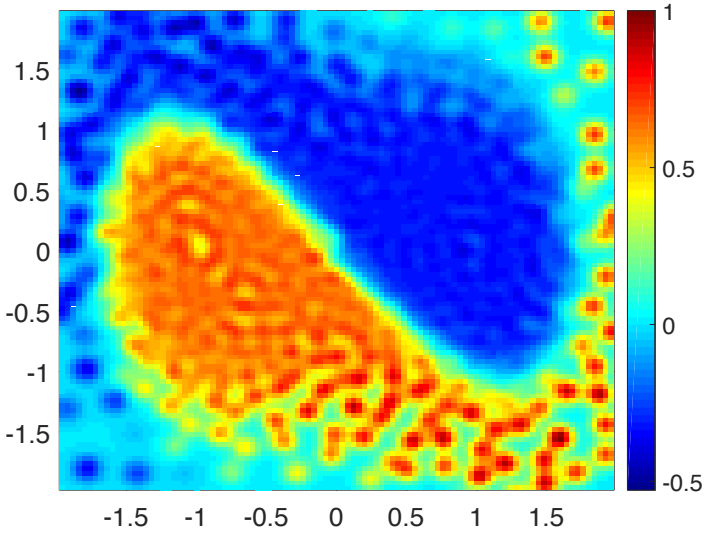

Figure 3.3: CASE-I: Koopman eigenfunction for eigenvalue 1 for Duffing oscillator

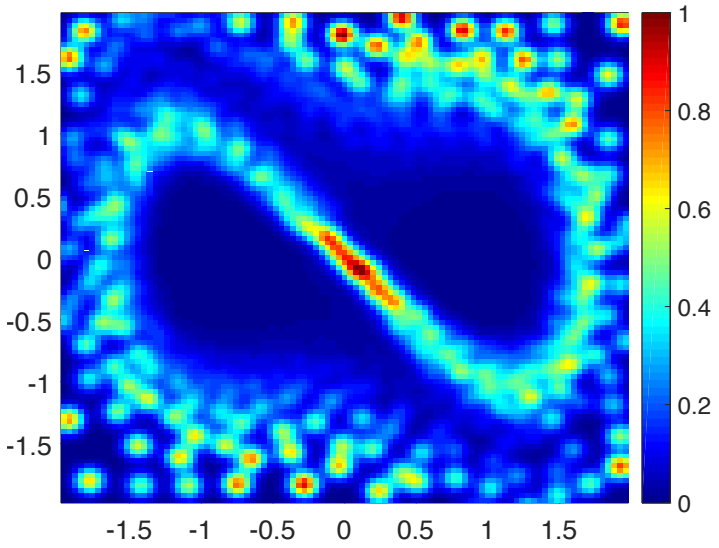

Figure 3.4: CASE-I: Koopman eigenfunction for eigenvalue 0.93 for Duffing oscillator using NSDMD

Henon Map: Consider a following discrete-time system for the Henon map

$$\begin{aligned} x_{t+1} &= 1 - ax_t^2 + y_t \\ y_{t+1} &= bx_t \end{aligned} \tag{3.19}$$

with $a = 1.4$ and $b = 0.3$. Time series data starting from one initial condition over 5000 time step is generated. Dictionary set is constructed using 500 Gaussian radial basis functions. K-means clustering method is used for selecting the centers of these Gaussian radial basis functions over the data set with $\sigma = 0.005$. In Fig. 3.5 we show the eigenfunction with eigenvalue one of the matrix $\mathbf{P}$ capturing the chaotic attractor of Henon map.

Van der Pol Oscillator: The next step of simulation results is performed with Van der Pol Oscillator.

$$\ddot{x} = (1 - x^2)\dot{x} - x. \tag{3.20}$$

Time-domain simulation are performed by using discretization time-step of $\Delta t = 0.1$ over total time period of $T = 10$. The differential equation is solved in MATLAB with $ode45$ solver. Simulation results from 100 different randomly chosen initial conditions are generated. For dictionary set we choose 500 dictionary functions with centers of the dictionary functions determined using k-means clustering algorithm with $\sigma = 0.1$.

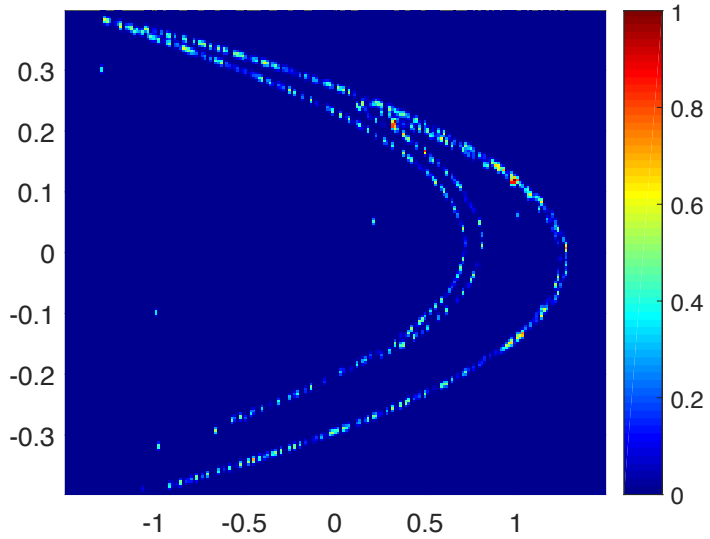

Figure 3.5: CASE-II: P-F eigenfunction for eigenvalue 1 for Henon map using NSDMD

In Fig. 3.6, we show the P-F eigenfunctions corresponding to eigenvalue one of the $\mathbf{P}$ matrix obtained using NSDMD algorithm capturing the limit cycling dynamics of the Vanderpol oscillator.

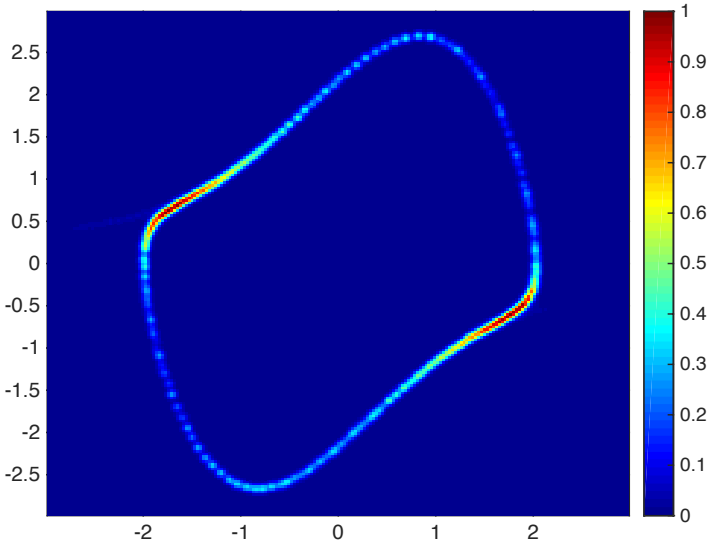

Figure 3.6: CASE-II: P-F eigenfunction $\lambda = 1$ for Van der Pol oscillator using NSDMD

CHAPTER 4. DATA-DRIVEN IDENTIFICATION AND STABILIZATION OF CONTROL DYNAMICAL SYSTEM

In this chapter, we will first give the preliminaries on the feedback stabilization and control lyapunov functions, then we will discuss the application of the linear Operator-theoretic framework for the identification of nonlinear dynamical systems in the Koopman eigenfunctions space. A fully detailed controller design algorithm procedure would be provided and explained step by step.

4.1 Feedback Stabilization and Control Lyapunov Functions

For the simplicity of the presentation, we will consider only the case of single input in this section. All the results carry over to the multi-input case in a straightforward manner. Consider a single input control affine system of the form

$$\dot{\mathbf{x}} = \boldsymbol{F}(\mathbf{x}) + \boldsymbol{G}(\mathbf{x})u, \tag{4.1}$$

where $\mathbf{x}(t) \in \mathbb{R}^n$ denotes the state of the system, $u(t) \in \mathbb{R}$ denotes the single input of the system, and $\boldsymbol{F}, \boldsymbol{G} : \mathbb{R}^n \to \mathbb{R}^n$ are assumed to be continuously differentiable mappings. We assume that $\boldsymbol{F}(\mathbf{0}) = \mathbf{0}$ and the origin is an unstable equilibrium point of the uncontrolled system $\dot{\mathbf{x}} = \boldsymbol{F}(\mathbf{x})$.

The *state feedback stabilization* problem associated with system (4.1) seeks a possible feedback control law of the form

$$u = k(\mathbf{x}).$$

with $k : \mathbb{R}^n \to \mathbb{R}$ such that $\mathbf{x} = \mathbf{0}$ is asymptotically stable within some domain $\mathcal{D} \subset \mathbb{R}^n$ for the closed-loop system

$$\dot{\mathbf{x}} = \boldsymbol{F}(\mathbf{x}) + \boldsymbol{G}(\mathbf{x})k(\mathbf{x}). \tag{4.2}$$

One of the possible approaches for the design of stabilizing feedback controllers for the nonlinear system (4.1) is via control Lyapunov functions that are defined as follows.

Definition 13. *Let $\mathcal{D} \subset \mathbb{R}^n$ be a neighborhood that contains the equilibrium $\mathbf{x} = \mathbf{0}$. A control Lyapunov function (CLF) is a continuously differentiable positive definite function $V : \mathcal{D} \to \mathbb{R}_+$ such that for all $\mathbf{x} \in \mathcal{D} \setminus \{\mathbf{0}\}$ we have*

$$\inf_u \left[\frac{\partial V}{\partial \mathbf{x}} \cdot \boldsymbol{F}(\mathbf{x}) + \frac{\partial V}{\partial \mathbf{x}} \cdot \boldsymbol{G}(\mathbf{x})u\right] := \inf_u \left[V_{\mathbf{x}}\boldsymbol{F}(\mathbf{x}) + V_{\mathbf{x}}\boldsymbol{G}(\mathbf{x})u\right] < 0.$$

It has been shown in Artstein (1983); Sontag (1989) that the existence of a CLF for system (4.1) is equivalent to the existence of a stabilizing control law $u = k(\mathbf{x})$ which is almost smooth everywhere except possibly at the origin $\mathbf{x} = \mathbf{0}$.

Theorem 1 (see Astolfi (2015), Theorem 2)**.** *There exists an almost smooth feedback $u = k(\mathbf{x})$, i.e., k is continuously differentiable for all $\mathbf{x} \in \mathbb{R}^n \setminus \{\mathbf{0}\}$ and continuous at $\mathbf{x} = \mathbf{0}$, which globally asymptotically stabilizes the equilibrium $\mathbf{x} = \mathbf{0}$ for system (4.1) if and only if there exists a radially unbounded CLF $V(\mathbf{x})$ such that*

1. *For all $\mathbf{x} \neq \mathbf{0}$, $V_{\mathbf{x}}\boldsymbol{G}(\mathbf{x}) = 0$ implies $V_{\mathbf{x}}\boldsymbol{F}(\mathbf{x}) < 0$;*
2. *For each $\varepsilon > 0$, there is a $\delta > 0$ such that $\|\mathbf{x}\| < \delta$ implies the existence of a $|u| < \varepsilon$ satisfying $V_{\mathbf{x}}\boldsymbol{F}(\mathbf{x}) + V_{\mathbf{x}}\boldsymbol{G}(\mathbf{x})u < 0$.*

In the theorem above, condition 2) is known as the small control property, and it is necessary to guarantee continuity of the feedback at $\mathbf{x} \neq 0$. If both conditions 1) and 2) hold, an almost smooth feedback can be given by the so-called Sontag's formula

$$k(\mathbf{x}) := \begin{cases} -\frac{V_{\mathbf{x}}\boldsymbol{F} + \sqrt{(V_{\mathbf{x}}\boldsymbol{F})^2 + (V_{\mathbf{x}}\boldsymbol{G})^4}}{V_{\mathbf{x}}\boldsymbol{G}} & \text{if } V_{\mathbf{x}}\boldsymbol{G}(\mathbf{x}) \neq 0 \\ 0 & \text{otherwise.} \end{cases} \tag{4.3}$$

Besides Sontag's formula, we also have several other possible choices to design a stabilizing feedback control law based on the CLF given in Theorem 1. For instance, if we are not constrained to any specifications on the continuity or amplitude of the feedback, we may simply choose

$$k(\mathbf{x}) := -K \operatorname{sign}\left[V_{\mathbf{x}}\boldsymbol{G}(\mathbf{x})\right] \tag{4.4}$$

$$k(\mathbf{x}) := -KV_{\mathbf{x}}\boldsymbol{G}(\mathbf{x}). \tag{4.5}$$

with some constant gain $K > 0$. Then, differentiating the CLF with respect to time along trajectories of the closed-loop (4.2) yields

$$\dot{V} = V_{\mathbf{x}}\boldsymbol{F}(\mathbf{x}) - K\left|V_{\mathbf{x}}\boldsymbol{G}(\mathbf{x})\right|$$
$$\dot{V} = V_{\mathbf{x}}\boldsymbol{F}(\mathbf{x}) - K(V_{\mathbf{x}}\boldsymbol{G}(\mathbf{x}))^2.$$

Hence, by the stabilizability property of condition 1), there must exist some K large enough such that $\dot{V} < 0$ for all $\mathbf{x} \neq \mathbf{0}$, because whenever $V_{\mathbf{x}}\boldsymbol{F}(\mathbf{x}) \geq 0$ we have $V_{\mathbf{x}}\boldsymbol{G}(\mathbf{x}) \neq 0$.

On the other hand, the CLFs also enjoy some optimality property using the principle of inverse optimal control. In particular, consider the following optimal control problem

$$\begin{aligned} \underset{u}{\text{minimize}} \quad & \int_0^\infty (q(\mathbf{x}) + u^\top u)dt \\ \text{subject to} \quad & \dot{\mathbf{x}} = \boldsymbol{F}(\mathbf{x}) + \boldsymbol{G}(\mathbf{x})u \end{aligned} \tag{4.6}$$

for some continuous, positive semidefinite function $q : \mathbb{R}^n \to \mathbb{R}$. Then the modified Sontag's formula

$$k(\mathbf{x}) := \begin{cases} -\frac{V_{\mathbf{x}}\boldsymbol{F} + \sqrt{(V_{\mathbf{x}}\boldsymbol{F})^2 + q(x)(V_{\mathbf{x}}\boldsymbol{G})^2}}{V_{\mathbf{x}}\boldsymbol{G}} & \text{if } V_{\mathbf{x}}\boldsymbol{G}(\mathbf{x}) \neq 0 \\ 0 & \text{otherwise.} \end{cases} \tag{4.7}$$

builds a strong connection with the optimal control. In particular, if the CLF has level curves that agree in shape with those of the value function associated with cost (4.6), then the modified Sontag's formula (4.7) will reduce to the optimal controller Freeman and Primbs (1996); Primbs et al. (1999).

4.2 Infinite Dimensional Bilinear Representation

Consider the control dynamical system perturbed by stochastic noise process

$$\dot{\mathbf{x}} = \boldsymbol{F}(\mathbf{x}) + \boldsymbol{G}(\mathbf{x})u + \boldsymbol{\omega}, \tag{4.8}$$

where $\boldsymbol{\omega} \in \mathbb{R}^n$ is the white noise process. As already discussed the presence of noise term will allow us to use sample complexity bounds from Chen and Vaidya (2019) to determine data requirement for the approximation. Sample complexity bounds can also be discovered without the additive noise term and is the topic of our current investigation.

Assumption 14. *Let* $\boldsymbol{F} = (\boldsymbol{F}_1, \ldots, \boldsymbol{F}_n)^\top$ *and* $\boldsymbol{G} = (\boldsymbol{G}_1, \ldots, \boldsymbol{G}_n)^\top$. *We assume that the functions* $\boldsymbol{F}_i$ *and* $\boldsymbol{G}_i$ *for* $i = 1, \ldots n$ *are* $\boldsymbol{C}^4$ *functions.*

The objective is to identify the nonlinear vector fields $\boldsymbol{F}$ and $\boldsymbol{G}$ using the time-series data generated by the control dynamical system and arrive at a continuous-time dynamical system of the form

$$\dot{\mathbf{z}} = \boldsymbol{\Lambda}\mathbf{z} + uB\mathbf{z}, \tag{4.9}$$

where $\mathbf{z} \in \mathbb{R}^N$ with $N \geq n$. We now make the following assumption on the control dynamical system (4.8).

Assumption 15. *We assume that all the trajectories of the control dynamical system (4.8) starting from different initial conditions for control input* $u = 0$ *and for constant input remain bounded.*

Remark 16. *This assumption is essential to ensure that the control dynamical system can be identified from the time-series data generated by the system for two different input signals.*

The goal is to arrive at a continuous-time bilinear representation of the nonlinear control system (4.8). Towards this goal we assume that the time-series data from the continuous time dynamical system (4.8) is available for two different control inputs namely zero input and constant input. The discrete time-series data is generated from the continuous time dynamical system with sufficiently small discretization time step Δt and this time-series data is represented as

$$(\mathbf{x}^s_{k+1}, \mathbf{x}^s_k). \tag{4.10}$$

The subscript s signifies that the data is generated by a dynamical system of the form

$$\dot{\mathbf{x}} = \boldsymbol{F}(\mathbf{x}) + \boldsymbol{G}(\mathbf{x})s + \boldsymbol{\omega}. \tag{4.11}$$

so that $s = 0$ and $s = 1$ corresponds to the case of zero input and constant input respectively. Let

$$\boldsymbol{\Psi} = [\psi_1, \ldots, \psi_N]^\top$$

be the set of observables with $\psi_i : \mathbb{R}^n \to \mathbb{R}$. The time evolution of these observables under the continuous time control dynamical system with no noise can be written as

$$\begin{aligned} \frac{d\boldsymbol{\Psi}}{dt} &= \boldsymbol{F}(\mathbf{x}) \cdot \nabla\boldsymbol{\Psi} + u\boldsymbol{G}(\mathbf{x}) \cdot \nabla\boldsymbol{\Psi} \\ &= \mathcal{A}\boldsymbol{\Psi} + u\mathcal{B}\boldsymbol{\Psi}, \end{aligned} \tag{4.12}$$

where $\mathcal{A}$ and $\mathcal{B}$ are linear operators. The objective is to construct the finite dimensional approximation of these linear operators, $\mathcal{A}$ and $\mathcal{B}$ respectively from time-series data to arrive at a finite dimensional approximation of control dynamical system as in Eq. (4.9).

With reference to Eq. (2.10), let $\mathbb{A}_1^*$ and $\mathbb{A}_0^*$ be the generator corresponding to the control dynamical system with constant input i.e., $s = 1$ and $s = 0$ respectively in Eq. (4.11). We have

$$(\mathbb{A}_1^* - \mathbb{A}_0^*)\psi = \boldsymbol{G}(\mathbf{x}) \cdot \nabla\psi. \tag{4.13}$$

Under the assumption that the sampling time Δt between the two consecutive time-series data point is sufficiently small, the generators $\mathbb{A}_s^*$ can be approximated as

$$\mathbb{A}_s^* \approx \frac{\mathbb{U}_{\Delta t}^s - I}{\Delta t}. \tag{4.14}$$

Substituting for $s = 1$ and $s = 0$ in (4.14) and using (4.13), we obtain

$$\frac{\mathbb{U}_{\Delta t}^1 - \mathbb{U}_{\Delta t}^0}{\Delta t} \approx \boldsymbol{G}(\mathbf{x}) \cdot \nabla = \mathcal{B}. \tag{4.15}$$

and

$$\frac{\mathbb{U}_{\Delta t}^0 - I}{\Delta t} \approx \boldsymbol{F}(\mathbf{x}) \cdot \nabla = \mathcal{A}. \tag{4.16}$$

Using the time-series data generated from dynamical system (4.11) for $s = 0$ and $s = 1$, it is possible to construct the finite dimensional approximation of the operators $\mathbb{U}_{\Delta t}^0$ and $\mathbb{U}_{\Delta t}^1$ respectively thereby approximating the operators $\mathcal{A}$ and $\mathcal{B}$ respectively. In the following we explain the extending dynamic mode decomposition-based procedure for the approximation of these operators from time-series data.

4.3 Finite Dimensional Approximation

We use Extending Dynamic Mode Decomposition (EDMD) algorithm for the approximation of $\mathbb{U}_{\Delta t}^1$ and $\mathbb{U}_{\Delta t}^0$ thereby approximating $\mathcal{A}$ and $\mathcal{B}$ in Eqs. (4.14) and (4.15) respectively Williams et al. (2015). For this purpose let the time-series data generated by the dynamical system (4.11) be given by

$$\overline{\boldsymbol{X}} = [\mathbf{x}_1^s, \mathbf{x}_2^s, \ldots, \mathbf{x}_M^s], \quad \overline{\boldsymbol{Y}} = [\mathbf{y}_1^s, \mathbf{y}_2^s, \ldots, \mathbf{y}_M^s]. \tag{4.17}$$

where $\mathbf{y}_k^s = \mathbf{x}_{k+1}^s$ with $s = 0$ or $s = 1$ i.e., zero input and constant input. Furthermore, let $\mathcal{H} = \{\psi_1, \psi_2, \ldots, \psi_N\}$ be the set of dictionary functions or observables and $\mathcal{G}_\mathcal{H}$ be the span of $\mathcal{H}$. The choice of dictionary functions is very crucial and it should be rich enough to approximate the leading eigenfunctions of the Koopman operator. Define vector-valued function $\mathbf{\Psi} : X \to \mathbb{C}^N$

$$\mathbf{\Psi}(\mathbf{x}) := \begin{bmatrix} \psi_1(\mathbf{x}) & \psi_2(\mathbf{x}) & \cdots & \psi_N(\mathbf{x}) \end{bmatrix}^\top. \tag{4.18}$$

In this application, $\mathbf{\Psi}$ is the mapping from state space to function space. Any two functions f and $\hat{f} \in \mathcal{G}_\mathcal{H}$ can be written as

$$f = \sum_{k=1}^{N} a_k \psi_k = \mathbf{\Psi}^\top \boldsymbol{a}, \quad \hat{f} = \sum_{k=1}^{N} \hat{a}_k \psi_k = \mathbf{\Psi}^\top \hat{\boldsymbol{a}}. \tag{4.19}$$

for some coefficients $\boldsymbol{a}$ and $\hat{\boldsymbol{a}} \in \mathbb{C}^N$. Let

$$\hat{f}(\mathbf{x}) = [\mathbb{U}_{\Delta t}^s f](\mathbf{x}) + r,$$

where r is a residual function that appears because $\mathcal{G}_\mathcal{H}$ is not necessarily invariant to the action of the Koopman operator. To find the optimal mapping which can minimize this residual, let $\mathbf{K}$ be the finite dimensional approximation of the Koopman operator $U_{\Delta t}^s$. Then the matrix $\mathbf{K}^s$ is obtained as a solution of least-squares problem as follows

$$\underset{\mathbf{K}^s}{\text{minimize}} \quad \|\boldsymbol{G}^s \mathbf{K}^s - \boldsymbol{A}^s\|_F \tag{4.20}$$

where

$$\boldsymbol{G}^s = \frac{1}{M} \sum_{m=1}^{M} \mathbf{\Psi}(\mathbf{x}_m^s) \mathbf{\Psi}(\mathbf{x}_m^s)^\top, \quad \boldsymbol{A}^s = \frac{1}{M} \sum_{m=1}^{M} \mathbf{\Psi}(\mathbf{x}_m^s) \mathbf{\Psi}(\boldsymbol{y}_m^s)^\top \tag{4.21}$$

with $\mathbf{K}^s, \boldsymbol{G}^s, \boldsymbol{A}^s \in \mathbb{C}^{N \times N}$. The optimization problem (4.20) can be solved explicitly with a solution in the following form

$$\mathbf{K}^s = (\boldsymbol{G}^s)^\dagger \boldsymbol{A}^s. \tag{4.22}$$

where $(\boldsymbol{G}^s)^\dagger$ denotes the pseudoinverse of matrix $\boldsymbol{G}^s$.

Under the assumption that the leading Koopman eigenfunctions are contained within $\mathcal{G}_\mathcal{H}$, the eigenvalues of $\mathbf{K}$ are approximations of the Koopman eigenvalues. The right eigenvectors of $\mathbf{K}^{s=0}$

can be used then to generate the approximation of Koopman eigenfunctions. In particular, the approximation of Koopman eigenfunction is given by

$$\phi_j = \mathbf{\Psi}^\top \mathbf{v}_j, \quad j = 1, \ldots, N \tag{4.23}$$

where $\mathbf{v}_j$ is the j-th right eigenvector of $\mathbf{K}^0$, and ϕ_j is the approximation of the eigenfunction of Koopman operator corresponding to the j-th eigenvalue, $\lambda_j \in \mathbb{C}$.

The bilinear representation of nonlinear control dynamical system can be constructed either in the space of basis function $\mathbf{\Psi}$ or the eigenfunctions of the Koopman operator $\mathbf{\Phi}$, where

$$\mathbf{\Phi}(\mathbf{x}) := [\phi_1(\mathbf{x}), \ldots, \phi_N(\mathbf{x})]^\top.$$

In this work, we constructed the bilinear representation in the Koopman eigenfunctions coordinates Sootla et al. (2018); Mauroy and Mezić (2016) Towards this goal, we define

$$\hat{\mathbf{\Phi}}(\mathbf{x}) := [\hat{\phi}_1(\mathbf{x}), \ldots, \hat{\phi}_N(\mathbf{x})]^\top.$$

where $\hat{\phi}_i := \phi_i$ if ϕ_i is a real-valued eigenfunction and $\hat{\phi}_i := 2\mathrm{Re}(\phi)$, $\hat{\phi}_{i+1} := -2\mathrm{Im}(\phi_i)$, if i and $i+1$ are complex conjugate eigenfunction pairs. Consider now the transformation $\hat{\mathbf{\Phi}} : \mathbb{R}^n \to \mathbb{R}^N$ as

$$\mathbf{z} = \hat{\mathbf{\Phi}}(\mathbf{x}).$$

Then in this new coordinates system Eq. (4.1) takes the following form

$$\dot{\mathbf{z}} = \mathbf{\Lambda}\mathbf{z} + u\mathbf{B}\mathbf{z}. \tag{4.24}$$

where the matrix $\mathbf{\Lambda}$ has a block diagonal form where the block corresponding to the eigenvalue $\hat{\lambda}_i$, such that $\mathbf{\Lambda}_{(i,i)} = \hat{\lambda}_i$ if ϕ_i is real, and

$$\begin{bmatrix} \mathbf{\Lambda}_{(i,i)} & \mathbf{\Lambda}_{(i,i+1)} \\ \mathbf{\Lambda}_{(i+1,i)} & \mathbf{\Lambda}_{(i+1,i+1)} \end{bmatrix} = |\lambda_i| \begin{bmatrix} \cos(\angle\hat{\lambda}_i) & \sin(\angle\hat{\lambda}_i) \\ -\sin(\angle\hat{\lambda}_i) & \cos(\angle\hat{\lambda}_i) \end{bmatrix}. \tag{4.25}$$

if ϕ_i and ϕ_{i+1} are complex conjugate pairs. The value $\hat{\lambda}_i$ associated with the continuous time system dynamics. The relationship between discrete-time Koopman eigenvalues λ_i and continuous time $\hat{\lambda}_i$ can be written as $\hat{\lambda}_i = \log(\lambda_i)/\Delta t$.

Similarly data generated using constant input for the control dynamical system is used to generate time-series data $\{\mathbf{x}_k^1\}$ and for the approximation of $\mathbf{K}^1$. The approximation of the operator $\mathcal{B}$ in the coordinates of basis functions, $\mathbf{\Psi}(\mathbf{x})$ denoted by $\bar{B}$, and the eigenfunction coordinates $\hat{\mathbf{\Phi}}(\mathbf{x})$ denoted by $\mathbf{B}$ can be obtained as follows:

$$\bar{\mathbf{B}} = \frac{\mathbf{K}^1 - \mathbf{K}^0}{\Delta t}, \qquad B = V^\top \bar{B} (V^\top)^{-1} \tag{4.26}$$

where each column of V, v_j is the jth eigenvector of $\mathbf{K}^0$.

There exist two sources of error in the approximation of Koopman operator and its spectrum, and both of them will be reflected in the bilinear representation of nonlinear system, namely $\mathbf{\Lambda}$ and B matrices. The first source of error is due to a finite number of basis functions used in the approximation of the Koopman operator. Under the assumption that the choice of basis functions is sufficiently rich and N is large, this approximation error is expected to be small. However, the selection of basis functions is an active research topic with no agreement on the best choice of basis functions for general nonlinear systems. The second source of error, which is more relevant to this work, arise due to the finite length of data used in the approximation of the Koopman operator. Sample complexity results for nonlinear stochastic dynamics using linear operator theory is developed in Chen and Vaidya (2019). These results provide error bounds for the approximation of the Koopman operator as the function of finite data length under the assumption that the action of the Koopman operator is closed on the space of finite basis functions. In particular, for any given $\epsilon > 0$ and $T > 2M + 2$, with probability at least $1 - \epsilon$, the least square estimator $\mathbf{K}^s$ in (4.22) will reconstructs the true Koopman operator $\mathbf{K}_{\text{true}}$ with following error bound

$$\|\mathbf{K}^s - \mathbf{K}^s_{\text{true}}\|_F \leq \frac{c}{\epsilon\sqrt{T}} \sqrt{\mathbb{E}\{\text{Tr}(\boldsymbol{G}^s)\}\mathbb{E}\{\|(\boldsymbol{G}^s)^{-1}\|_F^2\}}. \tag{4.27}$$

where c is constant and is a function of the additive noise variance, and $\|\cdot\|_F$ stands for Frobenius norm. These sample complexity results are used to determine the data required to achieve the desired level of accuracy of the approximation.

4.4 Feedback Controller Design

The control Lyapunov function provides a powerful tool for the design of a stabilizing feedback controller, which also enjoys some optimality property using the principle of inverse optimality. However, one of the main challenges is to provide a systematic procedure to find CLFs. For a general nonlinear system finding a CLF remains a challenging problem. We exploit the bilinear structure of the nonlinear system in the Koopman eigenfunction space to provide a systematic procedure for computing control Lyapunov function. We restrict the search for the control Lyapunov function to the class of quadratic Lyapunov function of the form $V(\mathbf{z}) = \mathbf{z}^\top P\mathbf{z}$. It is important to emphasize that although the Lyapunov function is restricted to be quadratic in Koopman eigenfunctions space $\mathbf{z}$, the Lyapunov function contains higher-order nonlinearities in the original state space $\mathbf{x}$. Theorem 2 can be stated for the quadratic stabilization of the following bilinear control system

$$\dot{\mathbf{z}} = \mathbf{\Lambda}\mathbf{z} + u\mathbf{B}\mathbf{z}. \tag{4.28}$$

In the sequel, if there exists a quadratic CLF for the bilinear system (4.28), then we will say that the system (4.28) is *quadratic stabilizable*.

Theorem 2. *System (4.28) is quadratic stabilizable if and only if there exists an $N \times N$ symmetric positive definite $\mathbf{P}$[1] such that for all non-zero $\mathbf{z} \in \mathbb{R}^N$ with $\mathbf{z}^\top(\mathbf{P}\mathbf{\Lambda}+\mathbf{\Lambda}^\top\mathbf{P})\mathbf{z} \geq 0$, we have $\mathbf{z}^\top(\mathbf{P}\mathbf{B}+\mathbf{B}^\top\mathbf{P})\mathbf{z} \neq 0$.*

Proof. Sufficiency ($\Leftarrow$): Suppose there is a symmetric, positive definite P that satisfies the condition of Theorem 2. We can use it to construct $V(\mathbf{z}) = \mathbf{z}^\top\mathbf{P}\mathbf{z}$ as our Lyapunov candidate function, and the derivative of V with respect to time along trajectories of (4.28) is given by

$$\begin{aligned}\dot{V} &= \mathbf{z}^\top\mathbf{P}\dot{\mathbf{z}} + \dot{\mathbf{z}}^\top\mathbf{P}\mathbf{z} \\ &= \mathbf{z}^\top(\mathbf{P}\mathbf{\Lambda} + \mathbf{\Lambda}^\top\mathbf{P})\mathbf{z} + u\mathbf{z}^\top(\mathbf{P}\mathbf{B} + \mathbf{B}^\top\mathbf{P})\mathbf{z}.\end{aligned}$$

[1] *In this Chapter 4 and Chapter 5, the notation $\mathbf{P}$ is used to denote the positive definite matrix used in the construction of quadratic Lyapunov function. The notation is not to be confused with the same notation, $\mathbf{P}$ used for the finite dimensional matrix representation of the P-F operator in Chapter 3.*

Since for all $\mathbf{z} \neq 0$ we have $\mathbf{z}^\top(\mathbf{PB}+\mathbf{B}^\top\mathbf{P})\mathbf{z} \neq 0$ when $\mathbf{z}^\top(\mathbf{P\Lambda}+\mathbf{\Lambda}^\top\mathbf{P})\mathbf{z} \geq 0$, we can always find a control input $u(\mathbf{z})$ such that

$$\dot{V} < 0, \quad \forall \mathbf{z} \in \mathbb{R}^N \setminus \{0\}.$$

Therefore, $V(\mathbf{z})$ is indeed a CLF for system (4.28).

Necessity ($\Rightarrow$): We will prove this by contradiction. Suppose that system (4.28) has a CLF in the form of $V(\mathbf{z}) = \mathbf{z}^\top\mathbf{P}\mathbf{z}$, where $\mathbf{P}$ does not satisfy the condition of Theorem 2. That is, there exists some $\bar{\mathbf{z}} \neq 0$ such that $\bar{\mathbf{z}}^\top(\mathbf{P\Lambda}+\mathbf{\Lambda}^\top\mathbf{P})\bar{\mathbf{z}} \geq 0$ but $\bar{\mathbf{z}}^\top(\mathbf{PB}+\mathbf{B}^\top\mathbf{P})\bar{\mathbf{z}} = 0$. In this case, we have

$$\dot{V}(\bar{\mathbf{z}}) = \bar{\mathbf{z}}^\top(\mathbf{P\Lambda}+\mathbf{\Lambda}^\top\mathbf{P})\bar{\mathbf{z}} \geq 0.$$

for any input u, which contradicts the definition of a CLF. This completes the proof. □

The following convex optimization formulation can be formulated to search for quadratic Lyapunov function for bilinear system without uncertainty in Eq. (4.28)

$$\begin{aligned} \underset{t>0,\ \mathbf{P}=\mathbf{P}^\top}{\text{minimize}} \quad & t - \gamma \text{Trace}(\mathbf{PB}) \\ \text{subject to} \quad & tI - (\mathbf{P\Lambda}+\mathbf{\Lambda}^\top\mathbf{P}) \succeq 0 \\ & c^{\max} I \succeq \mathbf{P} \succeq c^{\min} I \end{aligned} \tag{4.29}$$

where $c^{\max} > c^{\min} > 0$, respectively, are two given positive scalars forming bounds for the largest and the smallest eigenvalues of P. The variable t here represents an epigraph form for the largest eigenvalue of $\mathbf{P\Lambda}+\mathbf{\Lambda}^\top\mathbf{P}$.

Optimization (4.29) has combined two objectives. On the one hand, we minimize the largest eigenvalue of $\mathbf{P\Lambda}+\mathbf{\Lambda}^\top\mathbf{P}$. On the other hand, we try to maximize the smallest singular value of $\mathbf{PB}+\mathbf{B}^\top\mathbf{P}$ at the same time. Noticing that it may be difficult to maximize the smallest singular value of $\mathbf{PB}+\mathbf{B}^\top\mathbf{P}$ directly, we maximize the trace of $\mathbf{PB}$ instead and employ a parameter $\gamma > 0$ to balance these two objectives.

Remark 17. *When an optimal $\mathbf{P}^\star$ is solved from (4.29), we still need to check whether it satisfies the condition of Theorem 2 or not. So if a matrix $\mathbf{P}^\star$ fails the condition check, then we may tune the parameter γ and solve the above optimization again until we obtain a correct $\mathbf{P}^\star$. Nevertheless, we*

observe from simulations (see the multiple examples in our simulation section) that when we choose a value $\gamma = 2$, optimization (4.29) will always yield an optimal $P^\star$ that satisfies the condition of Theorem 2.

Remark 18. *We also need to point out that, compared to searching for a nonlinear CLF for the original nonlinear system (4.1), the procedure for seeking a quadratic CLF for the bilinear system (4.28) becomes quite easier and more systematic. Furthermore, a quadratic CLF for the bilinear system is, in fact, non-quadratic (i.e., contains higher-order nonlinear terms) for the system (4.1).*

Once a quadratic control Lyapunov function $V(\mathbf{z}) = \mathbf{z}^\top \mathbf{P}\mathbf{z}$ is found for bilinear system (4.28), we have several choices for designing a stabilizing feedback control law. For instance, applying the control law (4.4) or (4.5) we can construct

$$k(\mathbf{z}) = -\beta_k \operatorname{sign}\left[\mathbf{z}^\top(\mathbf{P}\mathbf{B} + \mathbf{B}^\top\mathbf{P})\mathbf{z}\right]. \tag{4.30}$$

$$k(\mathbf{z}) = -\beta_k \mathbf{z}^\top(\mathbf{P}\mathbf{B} + \mathbf{B}^\top\mathbf{P})\mathbf{z}. \tag{4.31}$$

Moreover, given a positive semidefinite cost $q(\mathbf{z}) \geq 0$, we may also apply the inverse optimality property to design an optimal control via Sontag's formula (4.7) to obtain

$$k(\mathbf{z}) = \begin{cases} -\frac{\mathbf{z}^\top(\mathbf{P}\mathbf{\Lambda}+\mathbf{\Lambda}^\top\mathbf{P})\mathbf{z}+\sqrt{(\mathbf{z}^\top(\mathbf{P}\mathbf{\Lambda}+\mathbf{\Lambda}^\top\mathbf{P})\mathbf{z})^2+q(\mathbf{x})(\mathbf{z}^\top(\mathbf{P}\mathbf{B}+\mathbf{B}^\top\mathbf{P})\mathbf{z})^2}}{\mathbf{z}^\top(\mathbf{P}\mathbf{B}+\mathbf{B}^\top\mathbf{P})\mathbf{z}} & \text{if } \mathbf{z}^\top(\mathbf{P}\mathbf{B}+\mathbf{B}^\top\mathbf{P})\mathbf{z} \neq 0 \\ 0 & \text{otherwise.} \end{cases} \tag{4.32}$$

The controller design framework is outlined in Algorithm 1 for the design of stabilizing feedback controller from time-series data.

4.5 Simulation results

In this section, we look at three different applications of our proposed operator-theoretic data-driven stabilizing controller design framework. One application is in the 2D duffing oscillator system, where we studied the spectrum of identified Koopman and P-F operator to capture the invariant set of the nonlinear system and demonstrate how the closed-loop trajectories globally stabilized to the origin by the designed controller. In the second example, we pick the 3D chaotic system, Lorenz attractor,

Algorithm 1: Data-Driven Stabilizing Controller Design Framework

Data: Given open-loop time-series data $\{\mathbf{x}_k^0\} = \{\mathbf{x}_0^0, \mathbf{x}_1^0, \ldots, \mathbf{x}_M^0\}$, and $\{\mathbf{x}_k^1\}$ with $s = 1$ in (4.11) both with Gaussian process noise added

Result: Feedback control $u = k(\mathbf{z})$

Phase I: Modeling and Identification

Choose N dictionary functions $\mathbf{\Psi}(\mathbf{x}) := \begin{bmatrix}\psi_1(\mathbf{x}) & \psi_2(\mathbf{x}) & \cdots & \psi_N(\mathbf{x})\end{bmatrix}^\top$.

for $\mathbf{x}_i,\ i = 0, 1, 2, \ldots, M$ **do**

$\mathbf{\Psi}(\mathbf{x}_i) := \begin{bmatrix}\psi_1(\mathbf{x}_i) & \psi_2(\mathbf{x}_i) & \cdots & \psi_N(\mathbf{x}_i)\end{bmatrix}^\top$

end

Obtain $\boldsymbol{G}^0$ and $\boldsymbol{A}^0$ matrices $\boldsymbol{G}^0 = \frac{1}{M}\sum_{m=1}^{M} \mathbf{\Psi}(\mathbf{x}_m)\mathbf{\Psi}(\mathbf{x}_m)^\top$; $\boldsymbol{A}^0 = \frac{1}{M}\sum_{m=0}^{M-1} \mathbf{\Psi}(\mathbf{x}_m)\mathbf{\Psi}(\mathbf{x}_{m+1})^\top$.

Compute $\mathbf{K}^0 = (\boldsymbol{G}^0)^\dagger \boldsymbol{A}^0$, and its eigenfunctions $\phi_j = \mathbf{\Psi}^\top v_j$, where v_j is the jth eigenvector of $\mathbf{K}^0$ with respect to eigenvalue λ_j, $j = 1, 2, \ldots, N$.

Convert to continuous time eigenvalues $\hat{\lambda}_i = \log(\lambda_i)/\Delta t$

Get $\mathit{\Lambda} = diag(\hat{\lambda}_1, \hat{\lambda}_2, \ldots, \hat{\lambda}_N)$ by block diagonalization of eigenvalues λ_i, use (4.25) if i, $i+1$ complex conjugate.

Obtain the new eigenfuntion $\hat{\mathbf{\Phi}}(\mathbf{x})$ similarly, where $\hat{\phi}_i := \phi_i$ if ϕ_i is a real-valued and $\hat{\phi}_i := 2\mathrm{Re}(\phi)$, $\hat{\phi}_{i+1} := -2\mathrm{Im}(\phi_i)$, if i and $i+1$ are complex conjugate.

Replace the dictionary function $\mathbf{\Psi}(\mathbf{x})$ with $\mathbf{z} = \hat{\mathbf{\Phi}}(\mathbf{x})$ and repeat Step 2 to 7 with the datasets $\{\mathbf{x}_k^0\}$ and $\{\mathbf{x}_k^1\}$ to get $\bar{\boldsymbol{U}}^0$ and $\bar{\boldsymbol{U}}^1$.

Get $\mathbf{B} = (\bar{\boldsymbol{U}}^1 - \bar{\boldsymbol{U}}^0)/\Delta t$

end

Phase II: Optimization

Solve the following convex problem for optimal $\mathbf{P}*$ with $\mathbf{\Lambda}$ and $\mathbf{B}$,

$$\begin{aligned} \underset{t>0,\ \mathbf{P}=\mathbf{P}^\top}{\text{minimize}} \quad & t - \gamma \mathrm{Trace}(\mathbf{PB}) \\ \text{subject to} \quad & tI - (\mathbf{P\Lambda} + \mathbf{\Lambda}^\top \mathbf{P}) \succeq 0 \\ & c^{\max} I \succeq \mathbf{P} \succeq c^{\min} I \end{aligned}$$

where $c^{\max} > c^{\min} > 0$, $\gamma > 0$ are chosen properly.

end

Feedback control $u = k(\mathbf{z}) = -\beta_k \mathbf{z}^\top(\mathbf{PB} + \mathbf{B}^\top\mathbf{P})\mathbf{z}$ or modified Sontag's formula,

$$k(\mathbf{z}) = \begin{cases} -\frac{\mathbf{z}^\top(\mathbf{P\Lambda}+\mathbf{\Lambda}^\top\mathbf{P})\mathbf{z} + \sqrt{(\mathbf{z}^\top(\mathbf{P\Lambda}+\mathbf{\Lambda}^\top\mathbf{P})\mathbf{z})^2 + q(\mathbf{x})(\mathbf{z}^\top(\mathbf{PB}+\mathbf{B}^\top\mathbf{P})\mathbf{z})^2}}{\mathbf{z}^\top(\mathbf{PB}+\mathbf{B}^\top\mathbf{P})\mathbf{z}} & \text{if } \mathbf{z}^\top(\mathbf{PB}+\mathbf{B}^\top\mathbf{P})\mathbf{z} \neq 0 \\ 0 & \text{otherwise.} \end{cases}$$

and use the designed controller to stabilize the system to one of the attractors. In the third example, we use the developed framework to implement the nonlinear stabilization of the IEEE 9bus system.

4.5.1 Application to 2D Duffing Oscillator

The first example we present is the stabilization of Duffing oscillator. The controlled Duffing oscillator equation is written as follows.

$$\begin{aligned} \dot{x}_1 &= x_2 \\ \dot{x}_2 &= (x_1 - x_1^3) - 0.5x_2 + u. \end{aligned} \tag{4.33}$$

The uncontrolled equation for Duffing oscillator consists of three equilibrium points, two of the equilibrium points at $(\pm 1, 0)$ are stable, and one equilibrium point at the origin is unstable. For identification of the control system dynamics, we excite the system with white noise with zero mean and 0.01 variance. The continuous time control equation is discretized with a sampling time of $\Delta t = 0.25s$. In Fig. 4.2a, we show the sampling complexity plot for the approximation error as the function of data length. As proved in Chen and Vaidya (2019), the error for the approximation of the $\mathbf{\Lambda}$ and $\mathbf{B}$ matrix decreases as $\frac{1}{\sqrt{T}}$, where T is a data length. The error plot in Fig. 4.2a satisfies this rate of decay. The sample complexity results in Fig. 4.2a are obtained using ten randomly chosen initial conditions and generating time-series data over the different lengths of time ranging from six-time steps to 30-time steps. For each fixed time step we compute the $\mathbf{\Lambda}$ and $\mathbf{B}$ matrices. The error $\parallel \mathbf{\Lambda} - \bar{\mathbf{\Lambda}} \parallel_2$ and $\parallel \mathbf{B} - \bar{\mathbf{B}} \parallel_2$ is computed at each fixed time step where $\bar{\mathbf{\Lambda}}$ and $\bar{\mathbf{B}}$ are computed using data collected over 50 time steps. The dictionary function used in the approximation of the Koopman operator has a maximum degree of five, i.e., 21 basis functions, $N = 21$. In particular, the following choice of dictionary function is made in the approximation

$$\mathbf{\Psi}(\mathbf{x}) = [1,\ x_1,\ x_2,\ x_1x_2,\ \ldots,\ x_1^5,\ x_1^4x_2,\ x_1^3x_2^2,\ x_1^2x_2^3,\ x_1x_2^4,\ x_2^5].$$

For control design, we use an approximation of $\mathbf{\Lambda}$ and $\mathbf{B}$ matrices computed over 30 time steps. The controller is designed using the Algorithm 2. For this Duffing oscillator example, we use a control design formula in Eq. (4.31). To verify the effectiveness of the designed controller we simulate the closed-loop system with the `ode15s` solver in **MATLAB** starting from 10 randomly chosen initial

conditions within the region $[-1.5, 1.5] \times [-1, 1]$. In Fig. 4.2d, we show the closed-loop trajectories in red starting from different initial conditions overlaid on the open-loop trajectories in blue. We notice that the controller forces the trajectories of the closed-loop system along the stable manifold of the open-loop system before the trajectories slide to the origin. The time trajectories and control plots from different initial conditions are shown in Fig. 4.2b and Fig. 4.2c, respectively.

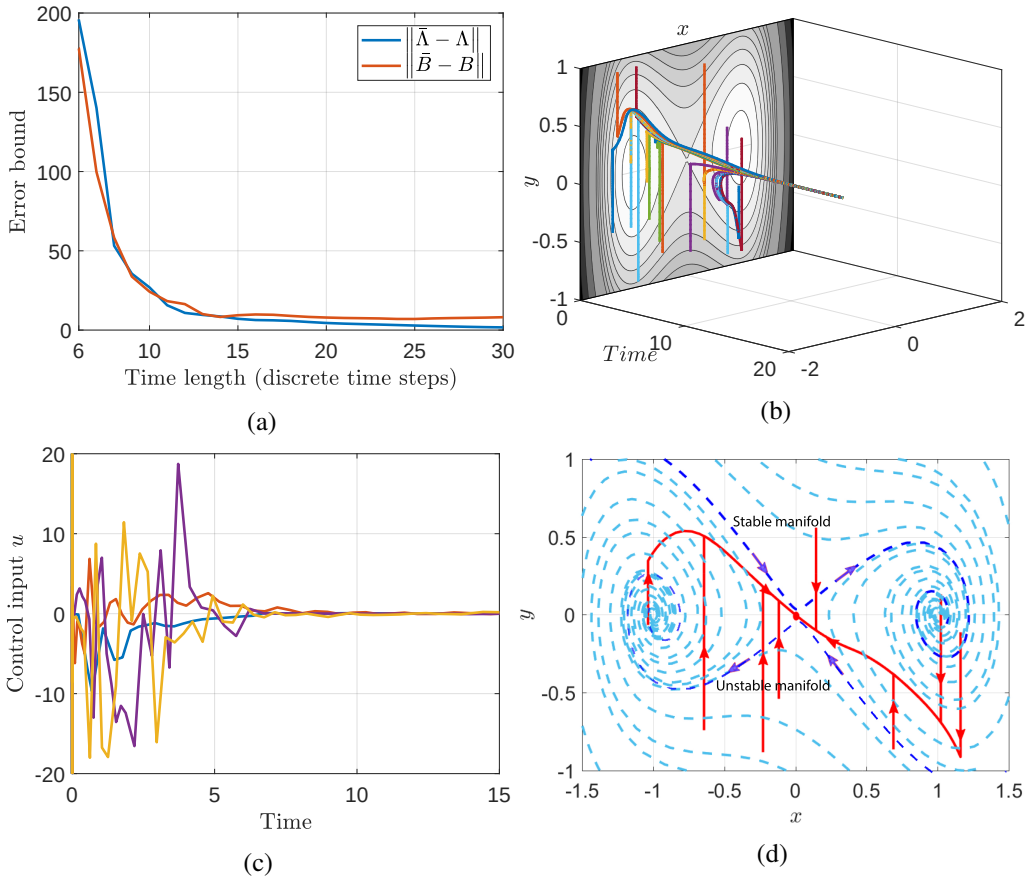

Figure 4.2: Data-driven stabilization of Duffing oscillator. a) Sample complexity error bounds for the approximation of $\mathbf{\Lambda}$ and $\mathbf{B}$ matrices as the function of data length; b) Closed-loop trajectories vs time from multiple initial conditions; c) Control value vs time from different initial conditions; d) Comparison of closed loop and open loop trajectories in state space.

4.5.2 Application to 3D Lorenz System

The second example we pick is that of Lorenz system. The control Lorenz system can be written as follows

$$\begin{aligned} \dot{x}_1 &= \sigma(x_2 - x_1) \\ \dot{x}_2 &= x_1(\rho - x_3) - x_2 + u \\ \dot{x}_3 &= x_1 x_2 - \beta x_3. \end{aligned} \tag{4.34}$$

where $\boldsymbol{x} \in \mathbb{R}^3$ and $u \in \mathbb{R}$ is the single input. With the parameter values $\rho = 28$, $\sigma = 10$, $\beta = \frac{8}{3}$, and control input $u = 0$ the Lorenz system exhibits chaotic behavior. In this 3D example, we generated the time-series data from 1000 random chosen initial conditions and propagate each of them for $T_{final} = 10s$ with sampling time $\Delta t = 0.001s$. For the purpose of identification the system is excited with white noise input with zero mean and 0.01 variance. The dictionary functions $\Psi(\mathbf{x})$ consist of 20 monomials of most degree $D = 3$

$$\mathbf{\Psi}(\mathbf{x}) = [1,\ x_1,\ x_2,\ x_3,\ \ldots,\ x_1^3,\ x_1^2 x_2,\ x_1^2 x_3,\ x_1 x_2 x_3,\ \ldots\ x_3^3].$$

The objective is to stabilize one of the critical points $(\sqrt{\beta(\rho-1)}, \sqrt{\beta(\rho-1)}, \rho - 1)$ of the Lorenz system. The system is stabilized using the control formula in Eq. (4.31). To validate the closed-loop control designed using the Algorithm 2, we perform the closed-loop simulation with five randomly chosen initial conditions in the domain $[-5, 5] \times [-5, 5] \times [0, 10]$ and solve the closed-loop system with `ode15s` solver in **MATLAB**. In Fig. 4.4a, we show the open-loop and closed-loop trajectories starting from five different initial conditions, and the closed-loop trajectories are converging to the critical point. The time trajectories in Fig. 4.4(b-d) shows that all the initial conditions can be stabilized to the desired point within 4s.

4.5.3 Application to Power System

In the last example, we consider the IEEE 9 bus system, the line diagram of which is shown in Fig. 4.6a. The model we are using is based on the modified nine bus test system in Sauer and Pai (1997). The system consists of 3 synchronous machines(generators) with IEEE type-I exciters,

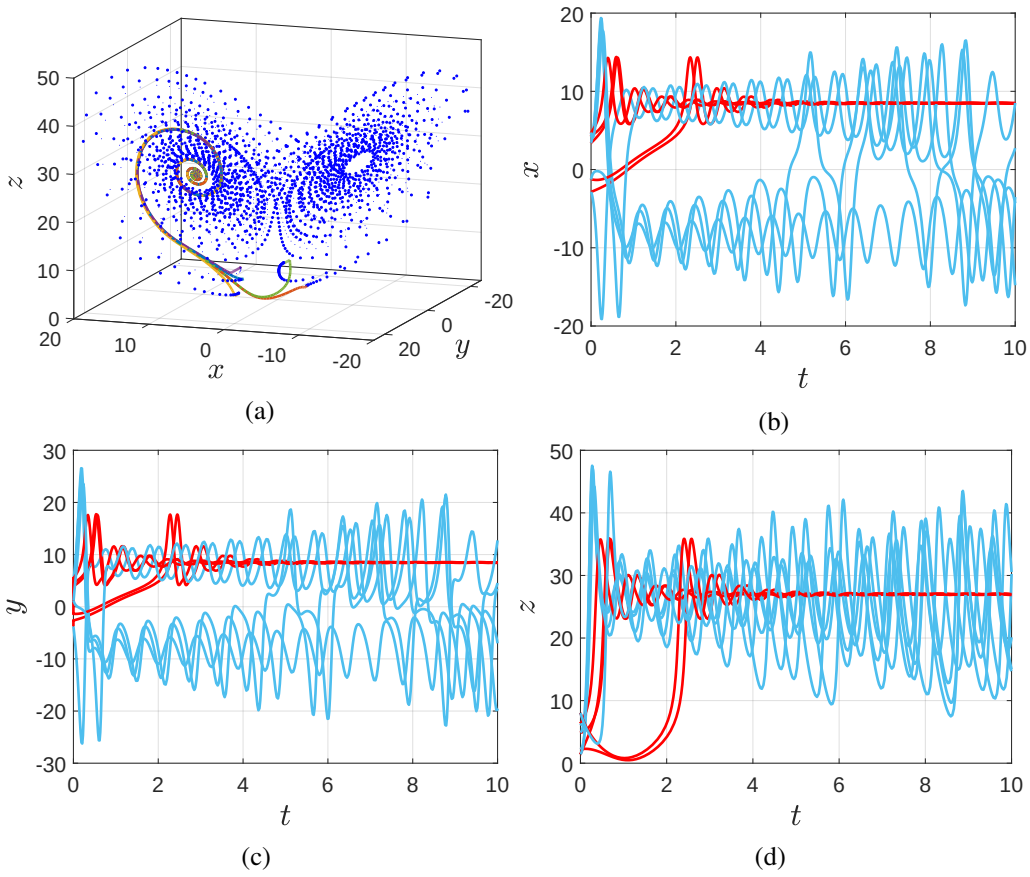

Figure 4.4: Feedback Stabilization of Lorenz system. a) Comparison of open loop and closed loop trajectories in state space; b) $x(t)$ vs time, open loop (blue) and closed loop (red); c) $y(t)$ vs time, open loop (blue) and closed loop (red); d) $z(t)$ vs time, open loop (blue) and closed loop (red).

Table 4.1: 9 bus system: Bus data at base case loading

Bus Number	V_0 p.u.	P_{L0} MW	Q_{L0} MVar	P_{G0} MW	V_{max} p.u.	V_{min} p.u.
1	1.04	0	0	71.61	1.1	0.9
2	1.025	0	0	163	1.1	0.9
3	1.025	0	0	85	1.1	0.9
4	1	0	0	0	1.1	0.9
5	1	125	50	0	1.1	0.9
6	1	90	30	0	1.1	0.9
7	1	0	0	0	1.1	0.9
8	1	100	35	0	1.1	0.9
9	1	0	0	0	1.1	0.9

loads, and transmission lines. The synthetic data is generated using PST (Power System Toolbox) in MATLAB Chow and Cheung (1992). The 9 bus power system network can be described by a set of differential algebraic equations (DAE). Consider a power system model with n_g generator buses and n_l load buses, the closed-loop generator dynamics for the ith generator bus can be represented as a 2^{nd} order dynamical model with the control u:

$$\begin{aligned} \frac{d\delta_i}{dt} &= \omega_i - \omega_s \\ \frac{d\omega_i}{dt} &= \frac{1}{M_i}\left(P_{m_i} - \sum_{j\in\mathcal{N}_i}\frac{E_iE_j}{X_{ij}}\sin(\delta_i-\delta_j) - D_i(\omega_i-\omega_s)\right) + u_i. \end{aligned} \tag{4.35}$$

where δ_i, ω_i are the dynamic states of the generator and correspond to the generator rotor angle and the angular velocity of the rotor. The values for the other parameters are chosen as follows: $\omega_s = 1$, the generator mass $M_i = 23.64,\ 6.4,\ 3.1$, the internal damping $D_i = 0.05,\ 0.95,\ 0.05$, the generator power $P_{m_i} = 0.719,\ 1.63,\ 0.85$ for $i = 1, 2, 3$. The values of X_{ij} are taken from the PST in MATLAB.

The 3 generator, 9 bus system's parameters are summarized in the Table. 4.1 and Table. 4.2.

For the approximation of Koopman operator and eigenfunctions, the time-series data are generated from 100 initial conditions. Each initial condition is propagated for $T_{final} = 10s$ and $\Delta t = 0.01s$. The dictionary functions $H(\mathbf{x})$ in this example are chosen as 84 monomials of most degree $D = 3$. The data-driven stabilizing control is designed using modified Sontag's formula control in Eq. (4.7), where $q(\mathbf{x}) = 10\mathbf{x}^\top\mathbf{x}$. The simulation results for this example are shown in Fig. 4.6. We notice that

Table 4.2: 9 bus system: Line data at base case loading

Bus Number From	**Bus Number To**	R p.u.	X p.u.	B p.u.
1	4	0	0.0576	0
2	7	0	0.0625	0
4	6	0.017	0.092	0.158
5	4	0.01	0.085	0.176
7	5	0.032	0.161	0.306
7	8	0.0085	0.072	0.149
8	9	0.0119	0.1008	0.209
9	3	0	0.0576	0
9	6	0.039	0.17	0.358

the open-loop system is marginally stable with sustained oscillations. The objective of the stabilizing controller is to stabilize to frequencies to $\omega_s = 1$, and the point for the stabilization of δ dynamics is determined by P_{m_i}. Simulation results in Fig. 4.6c and 4.6d show that the data-driven stabilizing controller is successful in stabilizing the power system dynamics.

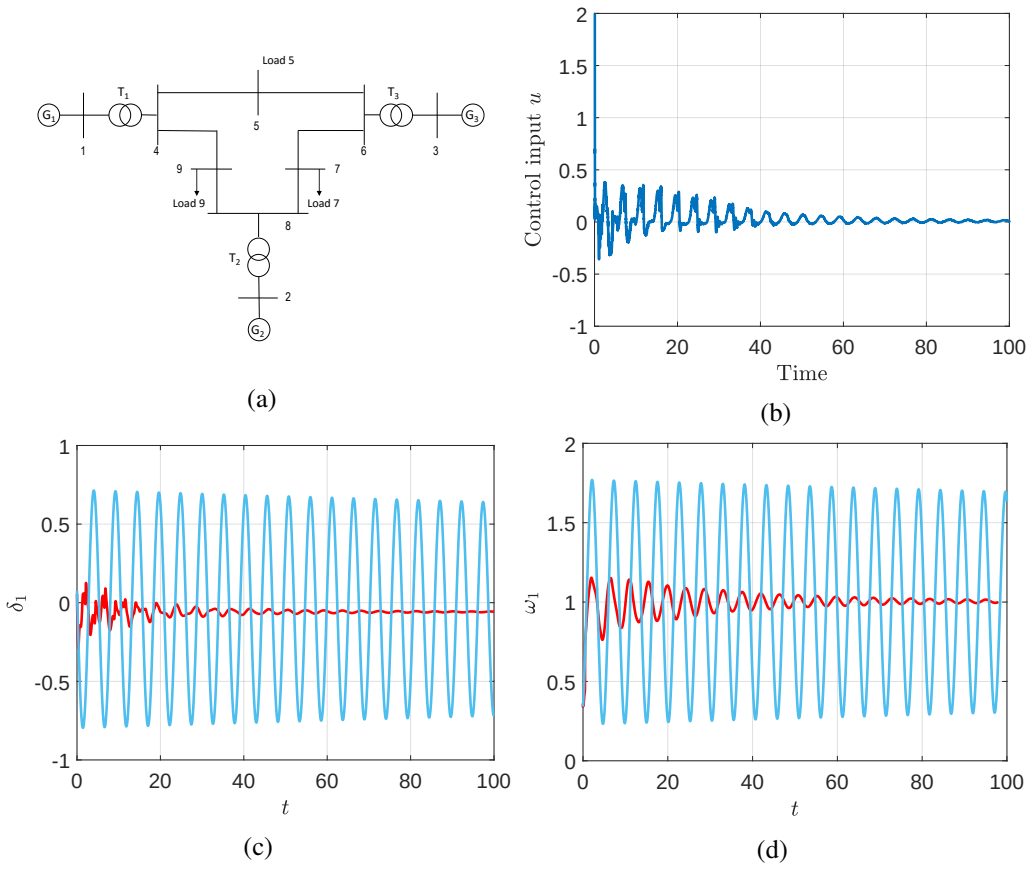

Figure 4.6: Stabilization of IEEE nine bus system. a) Line diagram for IEEE nine bus system; b) Control value vs time; c) Comparison of open loop and closed loop trajectory for phase angle $\delta_1(t)$ of generator 1; d) Comparison of open loop and closed loop trajectory for frequency $\omega_1(t)$ of generator 1.

CHAPTER 5. OPTIMAL QUADRATIC REGULATION OF NONLINEAR SYSTEM USING KOOPMAN OPERATOR

In this chapter, we study the optimal quadratic regulation problem for nonlinear systems. The optimal quadratic regulation problem for nonlinear system is formulated in terms of the finite-dimensional approximation of the bilinear system. A convex optimization-based approach is proposed for solving the quadratic regulator problem for bilinear system.

Consider a following single input nonlinear dynamics

$$\dot{\mathbf{x}} = \mathbf{F}(\mathbf{x}) + \mathbf{G}(\mathbf{x})u. \tag{5.1}$$

where $\mathbf{x} \in \mathbb{R}^n$ is the state and $u \in \mathbb{R}^p$ is control input. For the simplicity of presentation we discuss results for the single input case i.e., $p = 1$. Let $\psi_t(\mathbf{x})$ be the solution of autonomous (uncontrolled) dynamical system,

$$\dot{\mathbf{x}} = \mathbf{F}(\mathbf{x}). \tag{5.2}$$

5.1 Control System Representation in Koopman Eigenfunction Space

The eigenfunctions of Koopman operator corresponding to the point spectrum are smooth functions and can be used as coordinates for linear representation of nonlinear systems. Let

$$\mathbf{\Phi}(\mathbf{x}) = [\phi_1(\mathbf{x}), \ldots, \phi_N(\mathbf{x})]^\top$$

be the first N dominant Koopman eigenfunctions with associated eigenvalues $\lambda_i \in \mathbb{C}$ for $i = 1, \ldots, N$ and hence ϕ_i's are in general complex-valued functions. Utilizing the technique from Surana and Banaszuk (2016), we can transform these complex eigenfunctions to real as follows. Define

$$\hat{\mathbf{\Phi}}(\mathbf{x}) := [\hat{\phi}_1(\mathbf{x}), \ldots, \hat{\phi}_N(\mathbf{x})]^\top$$

where $\hat{\phi}_i := \phi_i$ if ϕ_i is a real-valued eigenfunction and $\hat{\phi}_i := 2\mathrm{Re}(\phi)$, $\hat{\phi}_{i+1} := -2\mathrm{Im}(\phi_i)$, if i and $i+1$ are complex conjugate eigenfunction pairs. Consider now the transformation as $\hat{\mathbf{\Phi}} : \mathbb{R}^n \to \mathbb{R}^N$

as

$$\mathbf{z} = \hat{\mathbf{\Phi}}(\mathbf{x}).$$

Then in this new coordinates system Eq. (5.1) takes the following form

$$\dot{\mathbf{z}} = \mathbf{\Lambda}\mathbf{z} + \frac{\partial \hat{\mathbf{\Phi}}}{\partial \mathbf{x}}\mathbf{G}(\mathbf{x})u. \tag{5.3}$$

where the matrix $\mathbf{\Lambda}$ has following form: in bilinear system (5.3), $\mathbf{\Lambda} \in \mathbb{R}^{N\times N}$ can be written as a block diagonal matrix of Koopman eigenvalues $\lambda_1, \lambda_2, \ldots, \lambda_N$ such that $\mathbf{\Lambda}_{(i,i)} = \lambda_i$ if ϕ_i is real, and

$$\begin{bmatrix} \mathbf{\Lambda}_{(i,i)} & \mathbf{\Lambda}_{(i,i+1)} \\ \mathbf{\Lambda}_{(i+1,i)} & \mathbf{\Lambda}_{(i+1,i+1)} \end{bmatrix} = |\lambda_i| \begin{bmatrix} \cos(\angle\lambda_i) & \sin(\angle\lambda_i) \\ -\sin(\angle\lambda_i) & \cos(\angle\lambda_i) \end{bmatrix}$$

if ϕ_i and ϕ_{i+1} are complex conjugate pairs. Next we assume that the control input u in (5.1) is of the form

$$u = \alpha^\top(t)\mathbf{z} = \sum_{k=1}^{N} \alpha_k(t)\hat{\phi}_k(\mathbf{x}). \tag{5.4}$$

Note that although the control input is assumed to be linear in eigenfunction coordinates, it is in fact nonlinear as the function of state variable $\mathbf{x}$.

Remark 19. *By assuming the above form of control input u, the new effective control is $\alpha_k(t)$. Furthermore, by assumption, the above form of the input, we are restricting the new control input to be either time-dependent or constant in time, i.e., parametric input. In this chapter, we are interested in solving infinite horizon problems, and hence the choice of α_k is restricted to be parametric and hence constant.*

Substituting for the control input u into (5.3), we obtain

$$\dot{\mathbf{z}} = \mathbf{\Lambda}\mathbf{z} + \sum_k \alpha_k(t)\frac{\partial \hat{\mathbf{\Phi}}}{\partial \mathbf{x}}\mathbf{G}(\mathbf{x})\hat{\phi}_k(\mathbf{x})$$

We now make the following assumption.

Assumption 20. *We assume that $\frac{\partial \hat{\mathbf{\Phi}}}{\partial \mathbf{x}}\mathbf{G}(\mathbf{x})\hat{\phi}_k(\mathbf{x})$ lies in the span of $\hat{\mathbf{\Phi}}(\mathbf{x})$ i.e., there exists a matrix $\mathbf{B}_k \in \mathbb{R}$*

$$\frac{\partial \hat{\mathbf{\Phi}}}{\partial \mathbf{x}}\mathbf{G}(\mathbf{x})\hat{\phi}_k(\mathbf{x}) = \mathbf{B}_k\hat{\mathbf{\Phi}}(\mathbf{x}). \tag{5.5}$$

Remark 21. *In general, Assumption 20 may or may not hold true and will depend upon the specific structure of function* $\mathbf{G}$ *and the choice of basis functions used in the approximation of the Koopman operator. More generally, one can also consider functions other than* $\hat{\phi}_k$ *in the determination of matrix* $\mathbf{B}_k$ *in Eq. (5.5). For the case where the Assumption 20 is not true, a least-squares problem can be formulated for the approximation of matrix* $\mathbf{B}_k$ *as we do in Section 5.3.*

Using Assumption 20, the system (5.3) is transformed to system of the form

$$\dot{\mathbf{z}} = \mathbf{\Lambda}\mathbf{z} + \sum_k \alpha_k(t)\mathbf{B}_k\mathbf{z} \tag{5.6}$$

$\alpha_k(t)$ are restricted to be function of time or static value but are not allowed to be function of state $\mathbf{z}$.

5.2 Optimal Quadratic Regulation

The quadratic cost function for the single input nonlinear system (5.1) can be written as

$$\int_0^\infty \mathbf{x}^\top(t)\bar{\mathbf{Q}}\mathbf{x}(t) + ru^2(t)dt \tag{5.7}$$

The quadratic in control and state cost function in state space can be approximated in the Koopman eigenfunction space as follows. Transforming the quadratic cost function associated with control from state space to Koopman eigenfunction space is straight forward. In particular, using (5.4), we have

$$ru(t)^\top u(t) = r\mathbf{z}^\top(t)\alpha(t)\alpha^\top(t)\mathbf{z}(t).$$

To transform the cost associated with the state, we let $\mathbf{\Psi}$ be the choice of basis functions used in the approximation of the Koopman eigenfunctions, $\mathbf{z} = \hat{\mathbf{\Phi}}(\mathbf{x})$. We have following relation between $\mathbf{\Psi}(\mathbf{x})$ and $\hat{\mathbf{\Phi}}(\mathbf{x})$, $\mathbf{z} := \hat{\mathbf{\Phi}} = \mathbf{V}^\top\mathbf{\Psi}$, where $\mathbf{V} = [\mathbf{v}_1, \ldots, \mathbf{v}_N]$ with $\mathbf{v}_i$ is the i^{th} right eigenvector of the finite dimensional approximation of the Koopman operator. We discuss more on this in Section 5.3 on finite dimensional approximation of Koopman eigenfunction. Under the assumption that the choice of basis function $\mathbf{\Psi}$ is of the form $\psi_1(\mathbf{x}) = 1$ and $\psi_2(\mathbf{x}) = \mathbf{x}$, we can write $\mathbf{x}^\top\bar{\mathbf{Q}}\mathbf{x} = \mathbf{\Psi}^\top\mathbf{Q}\mathbf{\Psi}$, where matrix $\mathbf{Q}$ is of the form

$$\mathbf{Q} = \text{diag}\{0, \bar{\mathbf{Q}}, 0, \ldots, 0\}$$

Now combining $\hat{\mathbf{\Phi}} = \mathbf{V}^\top \mathbf{\Psi}$, $\mathbf{\Psi} = (\mathbf{V}^\top)^{-1}\hat{\mathbf{\Phi}}$, and $\mathbf{x}^\top \bar{\mathbf{Q}}\mathbf{x} = \mathbf{\Psi}^\top \mathbf{Q}\mathbf{\Psi}$, we obtain

$$\mathbf{x}^\top \mathbf{Q}\mathbf{x} = \hat{\mathbf{\Phi}}\mathbf{V}^{-1}\mathbf{Q}(\mathbf{V}^\top)^{-1}\hat{\mathbf{\Phi}} \tag{5.8}$$

With the above transformation, we have following infinite horizon optimal quadratic regulation problem in Koopman eigenfunction space.

$$\begin{aligned} \min_{\alpha \in \mathbb{R}^n} J &:= \int_0^\infty \mathbf{z}(\tau)^\top \Big(\mathbf{V}^{-1}\mathbf{Q}(\mathbf{V}^\top)^{-1} + \alpha\alpha^\top \Big) \mathbf{z}(\tau) d\tau \\ \text{subject to} \dot{\mathbf{z}} &= \Big(\mathbf{A} + \sum_{i=1}^n \alpha_i \mathbf{B}_i \Big) \mathbf{z} := \mathbf{A}_{\text{c}}(\alpha)\mathbf{z} \\ \mathbf{z}(0) &= \mathbf{z}_0 \end{aligned} \tag{5.9}$$

where $\mathbf{Q} = \mathbf{Q}^\top \succ 0$ is a given positive definite matrix and $\mathbf{A}_{\text{c}}(\alpha)$ denotes the closed-loop system as a function of the control input $\alpha \in \mathbb{R}^n$.

Assumption 22. *We assume that problem (5.9) is feasible and has a finite optimal cost.*

Suppose that $\alpha \in \mathbb{R}^n$ is any feasible point to problem (5.9). In other words, α stabilizes the closed-loop system. Then the integral cost J evaluated at α equals to

$$J = \mathbf{z}_0^\top \mathbf{P}\mathbf{z}_0$$

for some symmetric positive definite $\mathbf{P} = \mathbf{P}^\top \succ 0$[1] which satisfies the Lyapunov equation

$$\mathbf{A}_{\text{c}}(\alpha)^\top \mathbf{P} + \mathbf{P}\mathbf{A}_{\text{c}}(\alpha) + \mathbf{Q} + \alpha\alpha^\top = 0. \tag{5.10}$$

$$\mathbf{A}^\top \mathbf{P} + \mathbf{P}\mathbf{A} + \sum_i \alpha_i (\mathbf{B}_i^\top \mathbf{P} + \mathbf{P}\mathbf{B}_i) + \mathbf{Q} + \alpha\alpha^\top = 0 \tag{5.11}$$

To see this, let us express the state trajectory $\mathbf{z}(t)$ of the closed-loop system as $\mathbf{z}(t) = e^{\mathbf{A}_{\text{c}}(\alpha)t}\mathbf{z}_0$. Substituting it into the integral cost J yields

$$J = \mathbf{z}_0^\top \left[\int_0^\infty e^{\mathbf{A}_{\text{c}}^\top(\alpha)\tau} \Big(\mathbf{Q} + \alpha\alpha^\top \Big) e^{\mathbf{A}_{\text{c}}(\alpha)\tau} d\tau \right] \mathbf{z}_0.$$

[1] In this chapter $\mathbf{P}$ denotes the quadratic matrix for Lyapunov function only.

Let us further define

$$\mathbf{P} := \int_0^\infty e^{\mathbf{A}_c^\top(\alpha)\tau}\Big(\mathbf{Q} + \alpha\alpha^\top\Big)e^{\mathbf{A}_c(\alpha)\tau}d\tau$$

then it is easy to show that $\mathbf{P}$ satisfies

$$\mathbf{A}_c(\alpha)^\top\mathbf{P} + \mathbf{P}\mathbf{A}_c(\alpha) = -\mathbf{Q} - \alpha\alpha^\top.$$

According to the argument above, the optimal control (5.9) can be equivalently rewritten as

$$\begin{aligned} \underset{\alpha,\mathbf{P}=\mathbf{P}^\top}{\text{minimize}} \quad & \mathbf{z}_0^\top\mathbf{P}\mathbf{z}_0 \\ \text{subject to} \quad & \mathbf{P} \succ 0 \text{ and (5.10)}. \end{aligned} \tag{5.12}$$

We notice that problem (5.12) is non-convex due to the equality constraint (5.10), which contains quadratic terms in both α and $\mathbf{P}$. Below, we will design an ADMM-like iterative algorithm to solve problem (5.12).

Let us define the augmented Lagrangian associated with problem (5.12) as

$$\begin{aligned} L_\rho(\alpha,\mathbf{P},\mathbf{W}) := {} & \mathbf{z}_0^\top\mathbf{P}\mathbf{z}_0 + I_{\text{pd}}(\mathbf{P}) \\ & + \text{tr}\left\{\mathbf{W}\left[\mathbf{A}_c(\alpha)^\top\mathbf{P} + \mathbf{P}\mathbf{A}_c(\alpha) + \mathbf{Q} + \alpha\alpha^\top\right]\right\} \\ & + \frac{\rho}{2}\left\|\mathbf{A}_c(\alpha)^\top\mathbf{P} + \mathbf{P}\mathbf{A}_c(\alpha) + \mathbf{Q} + \alpha\alpha^\top\right\|_{\text{fro}}^2 \end{aligned} \tag{5.13}$$

where $\rho > 0$ is a given parameter that scales the augmented term, $\mathbf{W} = \mathbf{W}^\top$ is the matrix Lagrange multiplier associated with equality constraint (5.10), and $\|\cdot\|_{\text{fro}}$ denotes the matrix Frobenius norm. Moreover, the indicator function $I_{\text{pd}}(\cdot)$ is defined as

$$I_{\text{pd}}(Z) := \begin{cases} 0 & \text{if } Z = Z^\top \succ 0 \\ \infty & \text{otherwise.} \end{cases}$$

Then we propose the iterative algorithm in Algorithm 2.

We present below the details about how to implement steps 1) and 2) in Algorithm 2.

For step 1), we note that even when $\mathbf{P_k}$ and $\mathbf{W_k}$ are fixed, $L_\rho(\alpha,\mathbf{P_k},\mathbf{W_k})$ is not convex in α. Therefore, we propose the following relaxation problem to search for an "argmin" of L_ρ with respect

Algorithm 2: An iterative algorithm for problem (5.12)

initialize $(\alpha_{\mathbf{0}}, \mathbf{P_0}, \mathbf{W_0})$ with $\mathbf{P_0} = \mathbf{P_0}^\top \succ 0$, $\mathbf{W_0} = \mathbf{W_0}^\top$, $\rho > 0$, and a tolerance $\varepsilon > 0$
repeat for $\mathbf{k} = 0, 1, 2, \cdots$
  1) $\alpha_{\mathbf{k+1}} := \underset{\alpha \in \mathbb{R}^n}{\operatorname{argmin}} L_\rho(\alpha, \mathbf{P_k}, \mathbf{W_k})$
  2) $\mathbf{P_{k+1}} := \underset{\mathbf{P}=\mathbf{P}^\top}{\operatorname{argmin}} L_\rho(\alpha_{\mathbf{k+1}}, \mathbf{P}, \mathbf{W_k})$
  3) $\mathbf{W_{k+1}} := \mathbf{W_k} + \rho\big[\mathbf{A}_{\mathrm{c}}(\alpha_{\mathbf{k+1}})^\top \mathbf{P_{k+1}} + \mathbf{P_{k+1}}\mathbf{A}_{\mathrm{c}}(\alpha_{\mathbf{k+1}})$
    $+ \mathbf{Q} + \alpha_{\mathbf{k+1}}\alpha_{\mathbf{k+1}}^\top\big]$
quit if $\|(\alpha_{\mathbf{k+1}}, \mathbf{P_{k+1}}, \mathbf{W_{k+1}}) - (\alpha_{\mathbf{k}}, \mathbf{P_k}, \mathbf{W_k})\| < \varepsilon$.

to α, which is

$$\begin{aligned} \underset{\alpha,\ Z=Z^\top}{\text{minimize}} \quad & \operatorname{tr}(\mathbf{W_k} Z) + \frac{\rho}{2}\|Z\|_{\mathrm{fro}}^2 \\ \text{subject to} \quad & \mathbf{A}_{\mathrm{c}}(\alpha)^\top \mathbf{P_k} + \mathbf{P_k}\mathbf{A}_{\mathrm{c}}(\alpha) + \mathbf{Q} + \alpha\alpha^\top \preceq Z \end{aligned} \tag{5.14}$$

where constraint (5.14) can be further rewritten as an LMI

$$\begin{bmatrix} Z - \mathbf{A}_{\mathrm{c}}(\alpha)^\top \mathbf{P_k} - \mathbf{P_k}\mathbf{A}_{\mathrm{c}}(\alpha) - \mathbf{Q} & \alpha \\ \alpha^\top & 1 \end{bmatrix} \succeq 0. \tag{5.15}$$

For step 2), fortunately, we observe that $L_\rho(\alpha_{\mathbf{k+1}}, \mathbf{P}, \mathbf{W_k})$ is convex in $\mathbf{P}$ when $\alpha_{\mathbf{k+1}}$ and $\mathbf{W_k}$ are both given. Hence, the "argmin" of L_ρ with respect to $\mathbf{P}$ can be computed by

$$\begin{aligned} \underset{\mathbf{P}=\mathbf{P}^\top}{\text{minimize}} \quad & L_\rho(\alpha_{\mathbf{k+1}}, \mathbf{P}, \mathbf{W_k}) \\ \text{subject to} \quad & \mathbf{P} \succ 0. \end{aligned} \tag{5.16}$$

We would like to point out that when we are solving problem (5.16), we can ignore the indicator function $I_{\mathrm{pd}}(\cdot)$ since we have already focused our search of $\mathbf{P}$ within the positive definite cone $\mathbf{P} = \mathbf{P}^\top \succ 0$. Under these circumstances, the indicator function always turns out to be zero.

5.3 Approximation of Koopman eigenfunctions

In this section, we will use Extending Dynamic Mode Decomposition (EDMD) algorithm for the approximation of Koopman eigenfunctions Williams et al. (2015). Given the continuous time system,

$\dot{\mathbf{x}} = f(\mathbf{x})$, one can generate the time-series data from the simulation or the experiment as follows

$$\overline{\mathbf{X}} = [\mathbf{x}_1, \mathbf{x}_2, \ldots, \mathbf{x}_M], \quad \overline{\mathbf{Y}} = [\mathbf{y}_1, \mathbf{y}_2, \ldots, \mathbf{y}_M] \tag{5.17}$$

where $\mathbf{x}_i \in \mathbf{X}$ and $\mathbf{y}_i = T(\mathbf{x}_i) = f(\mathbf{x}_i)\Delta t + \mathbf{x}_i \in \mathbf{X}$. Now let $\mathcal{H} = \{\psi_1, \psi_2, \ldots, \psi_N\}$ be the set of dictionary functions or observables. The dictionary functions are assumed to belong to $\psi_i \in L_2(\mathbf{X}, \mathcal{B}, \mu) = \mathcal{G}$, where μ is some positive measure, not necessarily the invariant measure of T. Let $\mathcal{G}_\mathcal{H}$ denote the span of $\mathcal{H}$ such that $\mathcal{G}_\mathcal{H} \subset \mathcal{G}$. The choice of dictionary functions is very crucial and it should be rich enough to approximate the leading eigenfunctions of the Koopman operator. Define vector-valued function $\mathbf{\Psi} : \mathbf{X} \to \mathbb{C}^N$

$$\mathbf{\Psi}(\mathbf{x}) := \begin{bmatrix} \psi_1(\mathbf{x}) & \psi_2(\mathbf{x}) & \cdots & \psi_N(\mathbf{x}) \end{bmatrix}^\top. \tag{5.18}$$

$$\phi = \sum_{k=1}^{N} a_k \psi_k = \mathbf{\Psi}^\top \boldsymbol{a}, \quad \hat{\phi} = \sum_{k=1}^{N} \hat{a}_k \psi_k = \mathbf{\Psi}^\top \hat{\boldsymbol{a}} \tag{5.19}$$

for some coefficients $\boldsymbol{a}$ and $\hat{\boldsymbol{a}} \in \mathbb{C}^N$. Let $\hat{\phi}(\mathbf{x}) = [\mathbb{U}_{\Delta t}\phi](\mathbf{x}) + r$, where $r \in \mathcal{G}$ is a residual function that appears because $\mathcal{G}_\mathcal{H}$ is not necessarily invariant to the action of the Koopman operator. To find the optimal mapping which can minimize this residual, let $\mathbf{K}$ be the finite dimensional approximation of the Koopman operator $\mathbb{U}_{\Delta t}$. Then the matrix $\mathbf{K}$ is obtained as a solution of least square problem as follows

$$\underset{\mathbf{K}}{\text{minimize}} \quad \|\mathbf{G}\mathbf{K} - \mathbf{A}\|_F \tag{5.20}$$

$$\mathbf{G} = \frac{1}{M}\sum_{m=1}^{M} \mathbf{\Psi}(\mathbf{x}_m)\mathbf{\Psi}(\mathbf{x}_m)^\top, \; \mathbf{A} = \frac{1}{M}\sum_{m=1}^{M} \mathbf{\Psi}(\mathbf{x}_m)\mathbf{\Psi}(\mathbf{y}_m)^\top.$$

with $\mathbf{K}, \mathbf{G}, \mathbf{A} \in \mathbb{C}^{N\times N}$. The optimization problem (5.20) can be solved explicitly with a solution in the following form

$$\mathbf{K}_{EDMD} = \mathbf{G}^\dagger \mathbf{A} \tag{5.21}$$

where $\mathbf{G}^\dagger$ denotes the psedoinverse of matrix $\mathbf{G}$[2]. The eigenvalues of $\mathbf{K}$ are approximations of the Koopman eigenvalues. The right eigenvectors of $\mathbf{K}$ can be used then to generate the approximation

[2]With some abuse of notations, here $\mathbf{G}$ is different from the control matrix $\mathbf{G}(\mathbf{x})$

of Koopman eigenfunctions. In particular, the approximation of Koopman eigenfunction is given by

$$\phi_j = \mathbf{\Psi}^\top \mathbf{v}_j, \quad j = 1, \dots, N \tag{5.22}$$

where $\mathbf{v}_j$ is the j-th right eigenvector of $\mathbf{K}$, and ϕ_j is the approximation of the eigenfunction of Koopman operator corresponding to the j-th eigenvalue λ_j. $\mathbf{\Lambda} \in \mathbb{R}^{N \times N}$ can be written as a block diagonal matrix of Koopman eigenvalues depending upon real or complex conjugate pair of eigenvalues.

For the computation of $\mathbf{B}_k$ matrix in (5.6), we formulate a least-square problem based on the assumption 20. Suppose that from the time-series data we can evaluate

$$\boldsymbol{J} := \left[\left.\frac{\partial \hat{\Phi}}{\partial \mathbf{x}}\right|_{\mathbf{x}_1} \cdot \boldsymbol{G}(\mathbf{x}_1) \quad \left.\frac{\partial \hat{\Phi}}{\partial \mathbf{x}}\right|_{\mathbf{x}_2} \cdot \boldsymbol{G}(\mathbf{x}_2) \quad \cdots \quad \left.\frac{\partial \hat{\Phi}}{\partial \mathbf{x}}\right|_{\mathbf{x}_M} \cdot \boldsymbol{G}(\mathbf{x}_M) \right]$$

$$\text{and} \quad \boldsymbol{H} := \left[\hat{\Phi}(\mathbf{x}_1) \;\; \hat{\Phi}(\mathbf{x}_2) \;\; \cdots \;\; \hat{\Phi}(\mathbf{x}_M) \right] \in \mathbb{R}^{N \times M}$$

at the points $\mathbf{x}_1, \mathbf{x}_2, \cdots, \mathbf{x}_M$, then the least-squares problem for the estimation of the B matrix can be formulated as

$$\underset{\mathbf{B} \in \mathbb{R}^{N \times N}}{\text{minimize}} \quad \|\boldsymbol{J} - \mathbf{B}\boldsymbol{H}\|_F.$$

The error in the approximation of the $\mathbf{B}$ matrix can be explicitly accounted for by formulating a robust optimization problem for optimal control. The formulation of robust optimization problem for optimal control where the error from the B matrix approximation as well as error due to finite data length Chen and Vaidya (2019) is beyond the scope of this dissertation.

5.4 Simulation Results

In this section, we will present the simulation results for the Koopman-based optimal quadratic regulation for affine in input control system.

5.4.1 2D linear system

Consider a controlled 2D unstable linear system given as follows

$$\begin{aligned} \dot{x}_1 &= -x_1 + 2x_2 \\ \dot{x}_2 &= 0.1x_2 + u \end{aligned} \tag{5.23}$$

where $\mathbf{x} \in \mathbb{R}^2$ and $u \in \mathbb{R}$ is the single input. The nonlinear system without control has a unique unstable equilibrium point at the origin. In this example, we will use the the proposed Koopman-based quadratic regulation (KQR) controller design algorithm to find the optimal controller within the neighborhood of $(0, 0)$. By choosing the monomial basis function of the most degree less than or equal to 5, one can shift the state space to the 21-dimensional monomial basis space, as follows,

$$\mathbf{\Psi}(\mathbf{x}) = [1, x_1, x_2, x_1^2, x_1x_2, x_2^2, \ldots, x_1x_2^4, x_2^5].$$

The Koopman eigenfunction approximation $\mathbf{\Lambda}$, B_k matrices are obtained from 10s time series data, which are generated using 100 random initial conditions within $[-2, 2] \times [-2, 2]$.

For the closed-loop simulation, we choose initial point at $(1, 2)$ and solve the closed-loop system with `ode45` solver in **MATLAB**. To verify the optimality of the proposed controller, we compare the closed-loop simulation result with the infinite horizon Linear quadratic regulator (LQR) controller. For the infinite horizon LQR controller, $J(\mathbf{x}) = \int_0^\infty \Big(\mathbf{x}(\tau)^\top \bar{\mathbf{Q}}\mathbf{x}(\tau) + u^\top Ru\Big)d\tau$, where both $\bar{\mathbf{Q}}$ and $\mathbf{R}$ matrices have been chosen as identity matrix, hence the designed feedback gain $K = [0.3815,\ 1.3394]$.

In Fig. 5.1 $\sim$ Fig. 5.3, the closed-loop trajectories with both controllers are converging to the origin, In the Fig.5.1, it can be observed that the proposed KQR controller follows a similar shape of converging path while the LQR control consumes the minimum energy.

5.4.2 Van der Pol oscillator

The first example, we choose the Van der Pol oscillator to obtain the time series dataset. The nonlinear dynamics of the Van der Pol oscillator, $\mathbf{F}(\mathbf{x})$, is shown in equation (5.24).

$$\begin{aligned} \dot{x}_1 &= x_2 \\ \dot{x}_2 &= (1 - x_1^2)x_2 - x_1 + u \end{aligned} \tag{5.24}$$

In order to obtain a good approximation of the Koopman eigenfunction associated with the nonlinear system, we generate the time series data with ten randomly chosen initial conditions within $[-2,\ 2] \times [-4,\ 4]$, and each trajectory has a length of $T = 10s, \Delta t = 0.01s$.

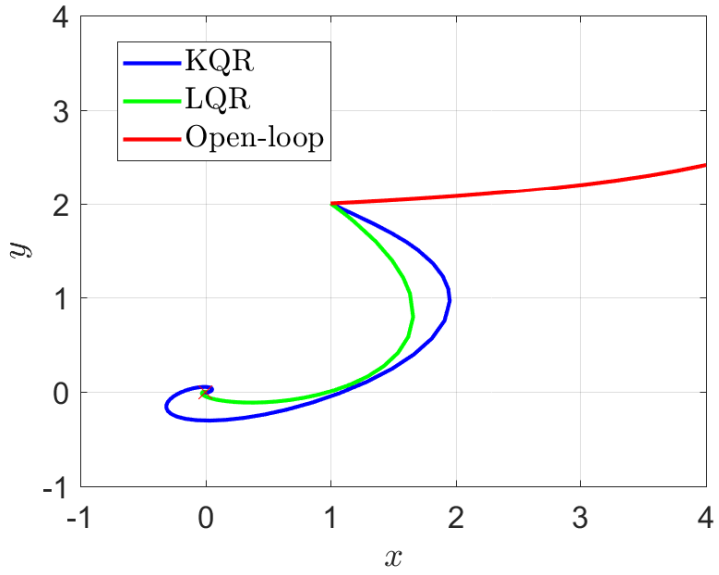

Figure 5.1: Koopman-based quadratic regulation controller(KQR) and LQR controller closed-loop and open-loop trajectories for the 2D linear system

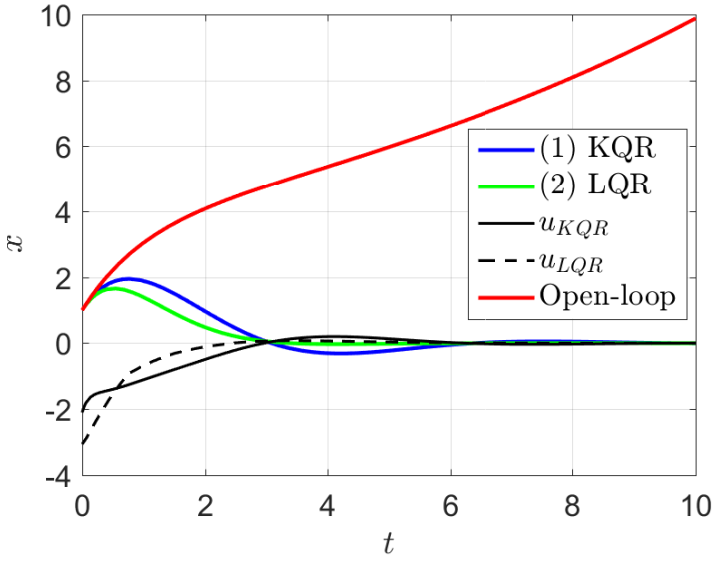

Figure 5.2: Closed-loop(blue, green) and open-loop(red) time trajectories of state x_1, and control input u(black) for the 2D linear system

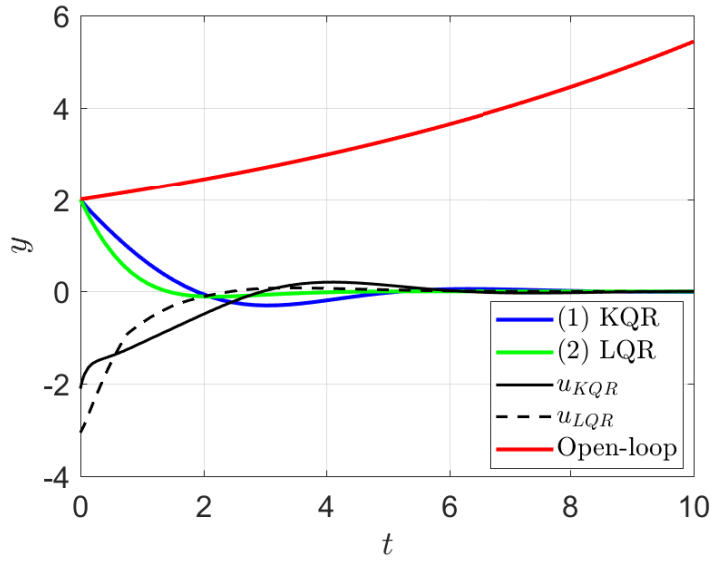

Figure 5.3: Closed-loop(blue, green) and open-loop(red) time trajectories of state x_2, and control input u(black) for the 2D linear system

The 21 monomial basis function of the most degree less than or equal to 5 will again be chosen as the basis function for the Koopman eigenfunction. For the Koopman-based quadratic regulation control, we still use the same quadratic regulation cost, such that the $\bar{\mathbf{Q}}$ and $\mathbf{R}$ to be identity. By applying Algorithm 2 to the optimization (5.12) with 527 iteration steps, one can get the optimal solution and apply the optimal $u^* = \alpha^* \mathbf{z}$ to the Van der Pol oscillator.

To start with, we apply the designed Koopman-based quadratic regulation (KQR) controller to the closed-loop system with one initial condition $(x_0, y_0) = (9, -2)$. To verify the improvement of the proposed controller, we compare the closed-loop simulation result with the infinite horizon Linear quadratic regulator (LQR) controller using the model linearized at the origin. With $\bar{\mathbf{Q}}$ to be identify and $R = 1$, the optimal feedback gain $K = [0.4142 \ \ 2.6818]$. The closed-loop simulation results from $t = 0$ to $t = 50s$ are shown in Fig. 5.4 $\sim$ Fig. 5.5. It can be observed that the Koopman-based controller is stabilizing the trajectories to the origin within the 20s, while the LQR control trajectories are following the open-loop trajectories for the first 10s, and takes more than 30s to converge to the origin. Furthermore, the controller designed using our proposed approach can obviously be as data-driven control, whereas the control based on linearization requires the knowledge of system dynamics.

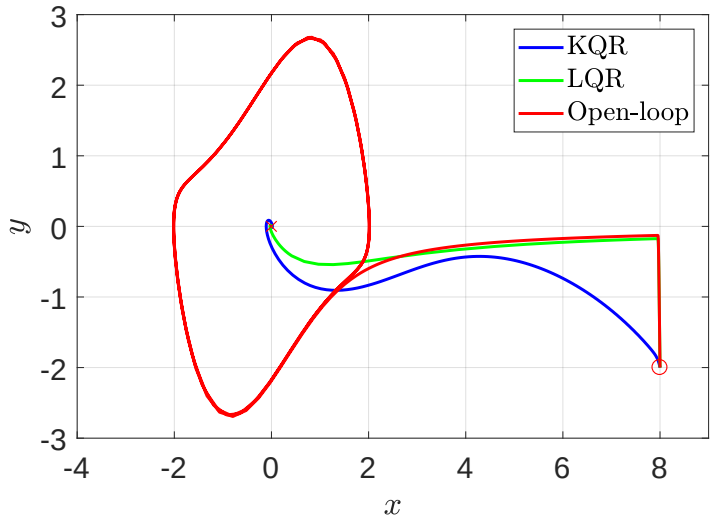

Figure 5.4: Closed-loop and open-loop trajectories for the Van der Pol oscillator

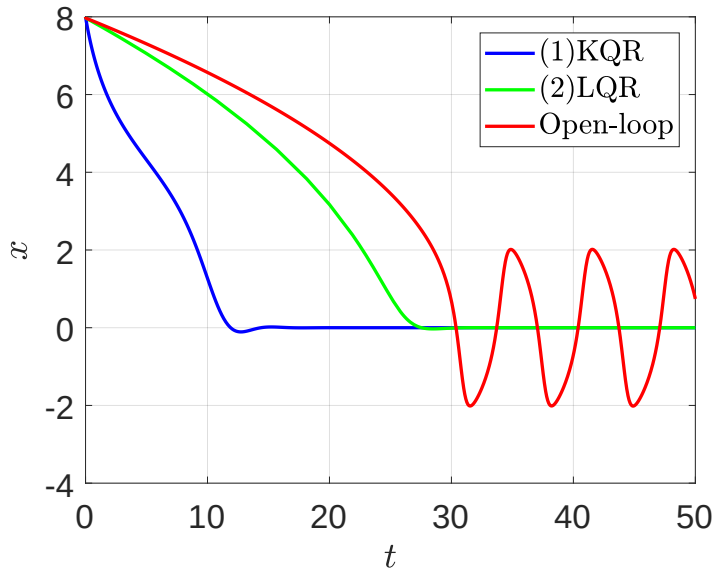

Figure 5.5: Closed-loop(blue, green) and open-loop(red) time trajectories of state x_1 for the Van der Pol oscillator

5.4.3 Duffing oscillator

Another prototype of 2D nonlinear dynamics is the duffing oscillator. The corresponding differential equation with the control input u is written as follows

$$\begin{aligned} \dot{x}_1 &= x_2 \\ \dot{x}_2 &= (x_1 - x_1^3) - 0.5x_2 + u. \end{aligned} \tag{5.25}$$

The open-loop system has two stable equilibrium points $(\pm 1, 0)$ and one unstable equilibrium point at the origin. For the approximation we are using 1000 randomly chosen initial conditions where $x_0 \in [-2,\ 2]$ and $y_0 \in [-5,\ 5]$, and each trajectory has length of $T = 10s, \Delta t = 0.025s$. The 21 monomials of most degree $D = 5$ are chosen as the basis functions. For control cost function, we use $\bar{\mathbf{Q}}$ to be identity and $R = 1$.

To solve the quadratic regulation control problem formulated in (5.12), we apply the algorithm (2) with 684 iteration steps to get the optimal solution α^* and $\mathbf{P}$.

Starting from the initial point at $(x_0, y_0) = (2, 1)$, the closed-loop simulation results from $t = 0$ to $t = 10s$ are shown in Fig. 5.6 $\sim$ Fig. 5.8. Even the open-loop trajectory has crossed the $\mathbf{x} = 0$ and arrived at the other equilibrium point $(-1, 0)$, the closed-loop trajectory using KQR control can still converge to the origin within 4s. For the comparison with the LQR controller designed based on the linearized model around the origin, which generates the feedback gain $K = [2.4142\ 1.9654]$. From Fig. 5.6, we can observe that the control path using KQR is shorter than the LQR, and also the control effort u_{KQR} has shorter time integral than u_{LQR}, which is showing improvement of the data-driven controller than the classic LQR control.

In this section, the simulation results show the effectiveness of the developed optimal control strategy. In the next chapter, the results of the comprehensive controller design framework will be demonstrated in detail and applied to some industrial examples.

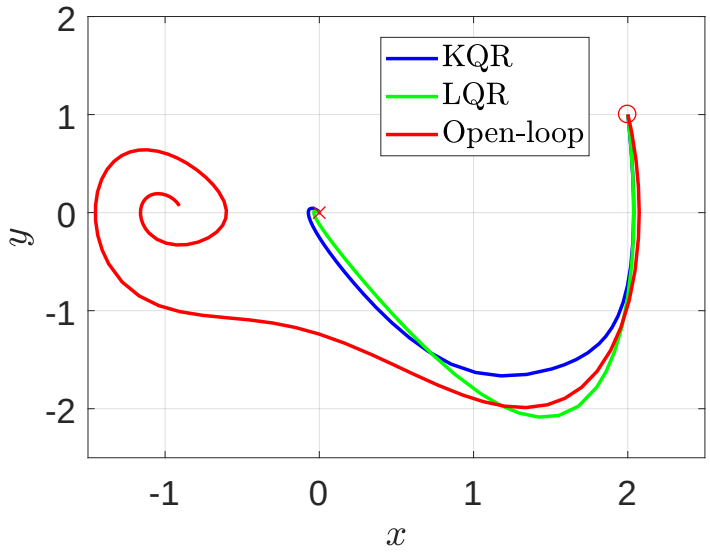

Figure 5.6: Closed-loop and open-loop trajectories for the Duffing oscillator

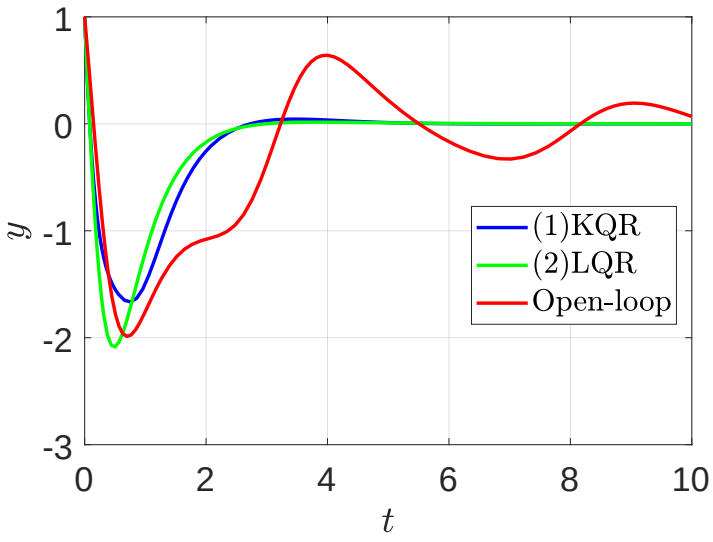

Figure 5.7: Closed-loop(blue, green) and open-loop(red) time trajectories of state x_2 for the Duffing oscillator

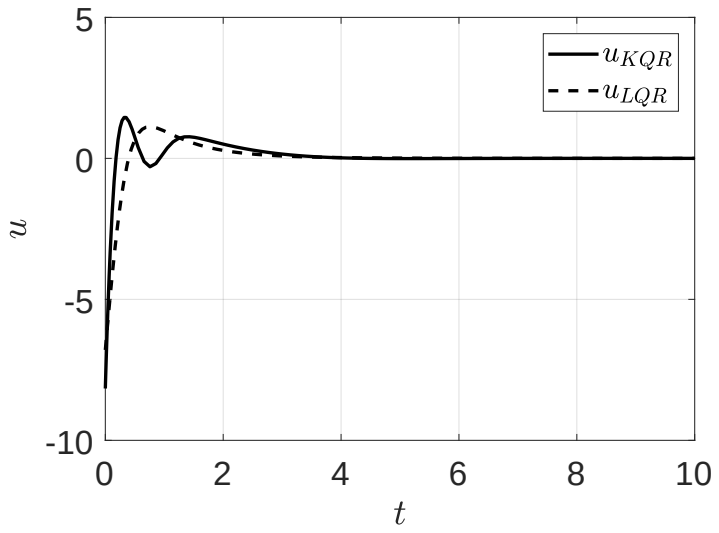

Figure 5.8: Control input u trajectories using KQR and LQR for the Duffing oscillator

CHAPTER 6. A CONVEX APPROACH TO DATA-DRIVEN OPTIMAL CONTROL VIA PERRON-FROBENIUS AND KOOPMAN OPERATOR

Bowen Huang and Umesh Vaidya

Department of Electrical and Computer Engineering, Iowa State University

Modified from a manuscript submitted to in IEEE Transactions on Automatic Control

6.1 Abstract

The paper is about the data-driven computation of optimal control for a class of control affine deterministic nonlinear system. We assume that the control dynamical system model is not available, and the only information about the system dynamics is available in the form of time-series data. We provide a convex formulation for the optimal control problem of the nonlinear system. The convex formulation relies on the duality result in the stability theory of a dynamical system involving density function and Perron-Frobenius operator. The optimal control problem is formulated as an infinite-dimensional convex optimization program. The finite-dimensional approximation of the optimization problem relies on the recent advances made in the data-driven computation of the Koopman operator, which is dual to the Perron-Frobenius operator. Simulation results are presented to demonstrate the application of the developed framework.

6.2 Introduction

The data-driven control of the dynamical system is a problem that has attracted tremendous interest from various research communities. The interest is partly due to easy access to the data and increased complexity of engineered systems where analytical models are challenging to obtain or unknown. The optimal control problem (OCP) is particularly difficult when the underlying system dynamics is nonlinear even for the case where the underlying system models are known. The solution to the OCP involves solving an infinite-dimensional nonlinear partial differential equation, namely

Hamilton Jacobi Bellman (HJB) equation. The HJB equation is also at the heart of the variety of reinforcement learning (RL) algorithm, one of the popular approaches for solving data-driven OCP Sutton and Barto (2018). The nonlinear and infinite-dimensional nature of the HJB equation makes the OCP challenging. There have been increased research efforts towards the extension of systematic model-based methods for controlling linear and nonlinear systems to a data-driven setting.

Progress is made for a class of linearly solvable OCP using alternate Kullback-Leibler (KL) based formulation of OCP for stochastic dynamical system and path integral-based numerical scheme Kappen (2007); Todorov (2009); Theodorou et al. (2010); Williams et al. (2017). In this paper, we provide a convex approach for the data-driven optimal control for a class of control affine deterministic nonlinear system using a linear operator theoretic framework involving Perron-Frobenius (P-F) and Koopman operators. For designing the data-driven optimal control, it is assumed that the analytical model of the system dynamics is not known, and the only information about the system dynamics is available in the form of time-series data from single or multiple trajectories. In particular, we assume that data can be collected from the control dynamical system for zero input and unit step input.

The linear P-F and Koopman operators are used to lift nonlinear dynamics from state space to linear, albeit infinite-dimensional, dynamics in the space of functions. More recently, the data-driven approach for the approximation of Koopman operator has attracted a lot of attention for the analysis of nonlinear systems with applications to power systems Susuki et al. (2016); Sharma et al. (2019b), fluid dynamics Mezić (2013), and robotics system Bruder et al. (2019). There have also been efforts for the use of Koopman operator for control Kaiser et al. (2017); Huang et al. (2018); Arbabi et al. (2018); Ma et al. (2019); Korda and Mezic (2020); Mauroy and Mezic (2013); Huang et al. (2020). However, unlike an autonomous dynamical system, lifting of control affine nonlinear system leads to a bilinear control system, which is hard to control. On the other hand, the application of linear P-F operator for nonlinear control was proposed in Vaidya et al. (2010a); Raghunathan and Vaidya (2013). The P-F based control makes use of duality in the stability theory result discovered in Rantzer (2001) and later generalize using linear operator theoretic framework in Vaidya and Mehta (2008b); Rajaram et al. (2010b). At the heart of the P-F control result is the convexity property enjoyed in the co-design problem of jointly finding the dual stability certificate in the form of density function or Lyapunov

measure and the controller Prajna et al. (2004); Vaidya et al. (2010a). This convexity property is exploited for the design of data-driven stabilization control in Choi et al. (2020). The proposed convex formulation for the OCP also draws some parallel with the dual formulation involving occupation measure for the OCP Henrion and Korda (2013); Korda (2016); Korda et al. (2017). The detailed comparison between these two approaches is beyond the scope of this paper.

In this paper, we discover a systematic framework based on the linear operator theory for the data-driven optimal control of a class of control affine deterministic nonlinear systems. The computation framework itself exploits the recent advances in the data-driven approximation of the Koopman operator and the duality between Koopman and P-F operator for the finite-dimensional approximation of the P-F operator and its generator. In particular, the computational framework makes use of the Naturally Structured Dynamic Mode Decomposition (NSDMD)Huang and Vaidya (2018) algorithm for the approximation preserving positivity and Markov properties of the linear operators. Time-series data from single or multiple trajectories corresponding to a system with zero input and unit step input are used in the training process for the approximation. The theoretical framework relies on the P-F operator and the density-based formulation of the OCP in the dual density space. In the density-based approach, the nonlinear control system is lifted using a P-F operator. The P-F lifting is instrumental in the convex formulation of the OCP in the dual space. There are two main contributions of this paper. First, it provides convex formulation to the OCP in the dual density space. The second main contribution is in providing a computational framework for the data-driven approximation of optimal control using linear P-F and Koopman operators.

The paper is organized as follows. In Section 6.3, we present some preliminaries on the linear operator theory and NSDMD algorithm for the finite-dimensional approximation of the Koopman and P-F operators. The main results on the formulation of the convex optimization problem for optimal control are presented in Section 6.4. The computational framework for the finite-dimensional approximation of the OCP is presented in Section 6.5. Simulation results are presented in Section 6.6 followed by remark and conclusion in Section 6.7.

6.3 Preliminaries and Notations

In this section, we discuss some preliminaries and introduce some notations, which are used in deriving the main results on data-driven optimal control. Consider a dynamical system

$$\dot{\mathbf{x}} = \mathbf{f}(\mathbf{x}), \quad \mathbf{x} \in \mathbf{X} \subseteq \mathbb{R}^n. \tag{6.1}$$

We denote by $\phi_t(\mathbf{x})$ the solution of the system (6.1) and $\mathcal{N}$ be the neighborhood of the equilibrium point at the origin. Let $\mathcal{M}(\mathbf{X})$ be the space of measure supported on $\mathbf{X}$, $\mathcal{F}$ be the space of scalar valued functions from $\mathbf{X} \to \mathbb{R}$, and $\mathcal{L}_1(\mathbf{X})$ the space of integrable functions on $\mathbf{X}$. The inner product between functions will be denoted by $\langle \varphi, \psi \rangle_{\mathbf{X}} := \int_{\mathbf{X}} \varphi(\mathbf{x})\psi(\mathbf{x})d\mathbf{x}$.

Definition 23 (Equivalent Measures)**.** *Two measures μ_1 and μ_2 are said to be equivalent i.e., $\mu_1 \approx \mu_2$ provided $\mu_1(B) = 0$ if and only if $\mu_2(B) = 0$ for all set $B \subset \mathbf{X}$.*

6.3.1 Perron-Frobenius and Koopman Operator

One can associate two linear operators with (6.1) namely Perron-Frobenius and Koopman operators. These two operators lift the nonlinear dynamics from the finite dimensional state space to the infinite dimensional space of functions.

Definition 24 (Koopman Operator)**.** *$\mathbb{U}_t : \mathcal{F} \to \mathcal{F}$ is defined as*

$$[\mathbb{U}_t\varphi](\mathbf{x}) = \varphi(\phi_t(\mathbf{x})) \tag{6.2}$$

Definition 25 (Perron-Frobenius Operator)**.** *$\mathbb{P}_t : \mathcal{F} \to \mathcal{F}$ is defined as*

$$[\mathbb{P}_t\psi](\mathbf{x}) = \psi(\phi_{-t}(\mathbf{x})) \left| \frac{\partial \phi_{-t}(\mathbf{x})}{\partial \mathbf{x}} \right| \tag{6.3}$$

where $|\cdot|$ stands for determinant.

These two operators are dual to each other and the duality is expressed as

$$\int_{\mathbb{R}^n} [\mathbb{U}_t \varphi](\mathbf{x}) \psi(\mathbf{x}) d\mathbf{x} = \int_{\mathbb{R}^n} [\mathbb{P}_t \psi](\mathbf{x}) \varphi(\mathbf{x}) d\mathbf{x} \tag{6.4}$$

The generator for the P-F operator is defined as

$$\lim_{t \to 0} \frac{(\mathbb{P}_t - I)\psi}{t} = -\nabla \cdot (\mathbf{f}(\mathbf{x})\psi(\mathbf{x})) =: \mathcal{P}_{\mathbf{f}} \psi \tag{6.5}$$

The generator for the Koopman operator is given by

$$\lim_{t \to 0} \frac{(\mathbb{U}_t - I)\varphi}{t} = \mathbf{f}(\mathbf{x}) \cdot \nabla \varphi(\mathbf{x}) =: \mathcal{K}_{\mathbf{f}} \varphi \tag{6.6}$$

Property 26. *These two operators enjoy positivity and Markov properties which are used in the approximation.*

1. *Positivity: The P-F and Koopman operators are positive operators i.e., for any* $0 \leq \varphi(\mathbf{x}) \in \mathcal{F}$ *and* $0 \leq \psi(\mathbf{x}) \in \mathcal{F}$*, we have*

$$[\mathbb{P}_t \psi](\mathbf{x}) \geq 0, \quad [\mathbb{K}_t \varphi](\mathbf{x}) \geq 0, \quad \forall t \geq 0 \tag{6.7}$$

2. *Markov Property: The P-F operator satisfies Markov property i.e.,*

$$\int_{\mathbf{X}} [\mathbb{P}_t \psi](\mathbf{x}) d\mathbf{x} = \int_{\mathbf{X}} \psi(\mathbf{x}) d\mathbf{x} \tag{6.8}$$

6.3.2 Almost everywhere stability and stabilization

The formulation for the OCP we present in the dual space is intimately connected to density function and Lyapunov measure introduced for verifying the almost everywhere notion of stability defined below.

Definition 27. *The equilibrium point at* $x = 0$ *is said to be almost everywhere stable w.r.t. measure,* μ*, if*

$$\mu\{\mathbf{x} \in \mathbf{X} : \lim_{t \to \infty} \phi_t(\mathbf{x}) \neq 0\} = 0$$

Following theorem from Rantzer (2001) provide condition for almost eveywhere stability with respect to (w.r.t.) Lebesgue measure.

Theorem 28. *Given the system* $\dot{\mathbf{x}} = \mathbf{f}(\mathbf{x})$*, where* $\mathbf{f}$ *is continuous differentiable and* $\mathbf{f}(0) = 0$*, suppose there exists a nonnegative* ρ *is continuous differentiable for* $\mathbf{x} \neq 0$ *such that* $\rho(\mathbf{x})\mathbf{f}(\mathbf{x})/|\mathbf{x}|$ *is integrable on* $\{\mathbf{x} \in \mathbb{R}^n \,:\, |\mathbf{x}| \geq 1\}$ *and*

$$[\nabla \cdot (\rho \mathbf{f})](\mathbf{x}) > 0 \text{ for almost all } \mathbf{x}. \tag{6.9}$$

Then, for almost all initial states $\mathbf{x}(0)$*, the trajectory* $\mathbf{x}(t)$ *tends to zero as* $t \to \infty$*.*

The density ρ serves as a stability certificate and can be viewed as a dual to the Lyapunov function Rantzer (2001). Applying Theorem 28 to control system, $\dot{\mathbf{x}} = \mathbf{f}(\mathbf{x}) + \mathbf{g}(\mathbf{x})\mathbf{u}$, we arrive at

$$\nabla \cdot (\rho(\mathbf{f} + \mathbf{g}\mathbf{u})) > 0 \text{ for almost all } \mathbf{x}. \tag{6.10}$$

The control synthesis problem becomes searching for a pair $(\rho, \mathbf{u})$ such that (6.10) holds. Even though (6.10) is again bilinear, it becomes linear in terms of $(\rho, \rho\mathbf{u})$. Thus, the density function based method for control synthesis is a convex problem.

6.3.3 Data-Driven Approximation: Naturally Structured Dynamic Mode Decomposition

Naturally structured dynamic mode decomposition (NSDMD) is a modification of Extended Dynamic Mode Decomposition (EDMD) algorithm Williams et al. (2015), one of the popular algorithm for Koopman approximation from data. The modifications are introduced to incorporate the natural properties of these operators namely positivity and Markov. For the continuous-time dynamical system (6.1), consider snapshots of data set obtained as time-series data from single or multiple trajectories

$$\mathcal{X} = [\mathbf{x}_1, \mathbf{x}_2, \ldots, \mathbf{x}_M], \quad \mathcal{Y} = [\mathbf{y}_1, \mathbf{y}_2, \ldots, \mathbf{y}_M] \tag{6.11}$$

where $\mathbf{x}_i \in \mathbf{X}$ and $\mathbf{y}_i \in \mathbf{X}$. The pair of data sets are assumed to be two consecutive snapshots i.e., $\mathbf{y}_i = \phi_{\Delta t}(\mathbf{x}_i)$, where $\phi_{\Delta t}$ is solution of (6.1). Let $\mathbf{\Psi} = [\psi_1, \ldots, \psi_N]^\top$ be the choice of basis func-

tions. The popular Extended Dynamic Mode Decomposition algorithm provides the finite dimensional approximation of the Koopman operator as the solution of the following least square problem.

$$\min_{\mathbf{K}} \| \mathbf{GK} - \mathbf{A} \|_F \tag{6.12}$$

where

$$\mathbf{G} = \frac{1}{M}\sum_{m=1}^{M} \mathbf{\Psi}(\mathbf{x}_m)\mathbf{\Psi}(\mathbf{x}_m)^\top, \mathbf{A} = \frac{1}{M}\sum_{m=1}^{M} \mathbf{\Psi}(\mathbf{x}_m)\mathbf{\Psi}(\mathbf{y}_m)^\top \tag{6.13}$$

with $\mathbf{K}, \mathbf{G}, \mathbf{A} \in \mathbb{R}^{N\times N}$, $\|\cdot\|_F$ stands for Frobenius norm. The above least square problem admits an analytical solution

$$\mathbf{K}_{EDMD} = \mathbf{G}^\dagger \mathbf{A}. \tag{6.14}$$

In this paper, we work with Gaussian Radial basis function (RBF) for the finite dimensional approximation of the linear operators. Under the assumption that the basis functions are positive, like the Gaussian RBF, the NSDMD algorithm propose following convex optimization problem for the approximation of the Koopman operator that preserves positivity and Markov property in Property 26.

$$\begin{aligned} &\min_{\mathbf{K}} \| \mathbf{GK} - \mathbf{A} \|_F \\ \text{s.t.} \quad &[\mathbf{\Lambda K \Lambda^{-1}}]_{ij} \geq 0, \quad \mathbf{\Lambda K \Lambda^{-1}} \mathbb{1} = \mathbb{1} \end{aligned} \tag{6.15}$$

where $\mathbf{\Lambda} = \int_{\mathbf{X}} \mathbf{\Psi}\mathbf{\Psi}^\top d\mathbf{x}$ is a constant matrix, $\mathbb{1}$ is a vector of all ones, and $\mathbf{G}$, $\mathbf{A}$ are as defined in Eq. (6.13). The first and second constraints in (6.15) ensure that finite-dimensional approximation preserves the positivity property and Markov property respectively. The approximation for the P-F operator and its generator is given by

$$\mathbb{P}_{\Delta t} \approx \mathbf{\Lambda}^{-1}\mathbf{K}^\top\mathbf{\Lambda} =: \mathbf{P}, \qquad \mathcal{P}_{\mathbf{F}} \approx \frac{\mathbf{P}-\mathbf{I}}{\Delta t} =: \mathbf{M} \tag{6.16}$$

Since the basis function are assumed to be positive Gaussian, the constant $\mathbf{\Lambda}$ matrix can be computed explicitly as

$$\Lambda_{i,j} = (\frac{\pi\sigma^2}{2})^{n/2} e^{\frac{-\|c_i - c_j\|^2}{2\sigma^2}}, i, j = 1, 2, \ldots, N$$

6.4 Convex Formulation of Optimal Control Problem

We consider optimal control problem for control affine system of the form

$$\dot{\mathbf{x}} = \mathbf{f}(\mathbf{x}) + \mathbf{g}(\mathbf{x})\mathbf{u} \tag{6.17}$$

where, $\mathbf{x} \in \mathbf{X} \subset \mathbb{R}^n$ is the state, $\mathbf{u} \in \mathbb{R}^p$ is the control input and $\mathbf{g}(\mathbf{x}) = (\mathbf{g}_1(\mathbf{x}), \ldots, \mathbf{g}_p(\mathbf{x}))$ with $\mathbf{g}_i \in \mathbb{R}^n$ is the input vector field. We make following assumption for (6.17).

Assumption 29. *We assume that the system (6.17) has locally stable equilibrium point at the origin when $\mathbf{u} = 0$. We denote by $\mathcal{N}$ the local domain of attraction of the stable equilibrium point at the origin. Furthermore, the linearization of system dynamics at the origin is assumed to be controllable i.e., pair $(\frac{\partial \mathbf{f}}{\partial \mathbf{x}}(0), \mathbf{g}(0))$ is controllable.*

Remark 30. *The assumption 29 is not restrictive. The local stabilizing controller can be designed again using data if the equilibrium point for the uncontrolled system is not stable to begin with. In fact we outline a procedure for the design of data-driven locally optimal control for all the simulation examples, where the assumption is not satisfied.*

We denote by $\mathbf{X}_1 := \mathbf{X} \setminus \mathcal{N}$, where $\mathcal{N}$ is the neighborhood of the origin (Definition 29). In the following, we assume that the measure $\mu \in \mathcal{M}(\mathbf{X})$ is equivalent to Lebesgue and that there exists a density function $0 < h(\mathbf{x}) \in \mathcal{L}_1(\mathbf{X})$ such that $\frac{d\mu}{d\mathbf{x}} = h(\mathbf{x})$. Consider the cost function of the form

$$J(\mu) = \int_{\mathbf{X}_1} \int_0^\infty q(\mathbf{x}) + \mathbf{u}^\top \mathbf{R}\mathbf{u} \, dt d\mu(\mathbf{x}) \tag{6.18}$$

The $q : \mathbf{X} \to \mathbb{R}^+$ is a positive function such that $q(0) = 0$ and $\mathbf{R} > 0$ is positive definite. The objective is to minimize the cost starting from all initial condition $\mathbf{x} \in \mathbf{X}_1$ and weighted by measure $d\mu$. The reason for restricting the initial condition to set $\mathbf{X}_1$ will be clarified later in Section 6.4.1. We now make following assumption on the optimal control.

Assumption 31. *We assume that the optimal control input is feedback i.e., $\mathbf{u} = \mathbf{k}(\mathbf{x})$ and system (6.17) with feedback control input is almost everywhere stable w.r.t. μ, (Definition 27).*

We next prove a theorem, the proof of which can be derived using results reported in Vaidya and Mehta (2008b); Rajaram et al. (2010b), however we prove it here for the sake of completeness.

Lemma 32. *If the feedback control system* $\dot{\mathbf{x}} = \mathbf{f}(\mathbf{x}) + \mathbf{g}(\mathbf{x})\mathbf{k}(\mathbf{x}) =: \mathbf{f}_c(\mathbf{x})$ *satisfies Assumption 31 then*

$$\lim_{t\to\infty} [\mathbb{P}_t^c h](\mathbf{x}) = 0 \tag{6.19}$$

where, $h = \frac{d\mu}{d\mathbf{x}}$ *and* $\mathbb{P}_t^c$ *is P-F operator for system* $\dot{\mathbf{x}} = \mathbf{f}_c(\mathbf{x})$.

Proof. For any set $B \subset \mathbf{X}_1$, let $B_t := \{\mathbf{x} \in \mathbf{X} : \phi_t(\mathbf{x}) \in B\}$, then

$$\chi_{B_t}(\mathbf{x}) = \chi_B(\phi_t(\mathbf{x})) = [\mathbb{K}_t \chi_B](\mathbf{x}).$$

Furthermore,

$$0 = \lim_{t\to\infty} \chi_{B_t}(\mathbf{x}) = \lim_{t\to\infty} \chi_B(\phi_t(\mathbf{x})) = \lim_{t\to\infty} [\mathbb{K}_t \chi_B](\mathbf{x})$$

for all point $\mathbf{x}$ such that $\phi_t(\mathbf{x}) \to 0$. Since the system is a.e. stable w.r.t. measure $d\mu(\mathbf{x}) = h(\mathbf{x})d\mathbf{x}$, we have

$$0 = \int_{\mathbf{X}} \lim_{t\to\infty} [\mathbb{K}_t \chi_B](\mathbf{x}) h(\mathbf{x}) d\mathbf{x} = \int_{\mathbf{X}} \chi_B(\mathbf{x}) \lim_{t\to\infty} [\mathbb{P}_t h](\mathbf{x}) d\mathbf{x}.$$

The above is true for arbitrary set $B \subset \mathbf{X}_1$, hence we have $\lim_{t\to\infty} [\mathbb{P}_t h](\mathbf{x}) = 0$.

Remark 33. *The condition in Eq. (6.19) is also sufficient for almost everywhere stability. However, to prove the main result, we only use necessity. In fact, the main result of this paper on the convex formulation of the OCP can be proven without Assumption 31. However, given the data-driven computational focus of this paper, we will present the more technical results with less restrictive assumptions in later publication.*

□

With the assumed feedback form of the control input, the OCP can be written as

$$\begin{aligned} \min_{\mathbf{k}} \quad & \int_{\mathbf{X}_1} \left[\int_0^\infty q(\mathbf{x}) + \mathbf{k}(\mathbf{x})^\top \mathbf{R}\mathbf{k}(\mathbf{x})\, dt\right] d\mu(\mathbf{x}) \\ \text{s.t.} \quad & \dot{\mathbf{x}} = \mathbf{f}(\mathbf{x}) + \mathbf{g}(\mathbf{x})\mathbf{k}(\mathbf{x}) \end{aligned} \tag{6.20}$$

We now state the main theorem on the convex formulation of the OCP.

Theorem 34. *Under the Assumption 31, the OCP (6.20) can be written as following infinite dimensional convex optimization problem*

$$\begin{aligned} \min_{\rho\geq 0,\bar{\boldsymbol{\rho}}} \quad & \int_{\mathbf{X}_1} q(\mathbf{x})\rho(\mathbf{x}) + \frac{\bar{\boldsymbol{\rho}}(\mathbf{x})^\top \mathbf{R}\bar{\boldsymbol{\rho}}(\mathbf{x})}{\rho} d\mathbf{x} \\ & \text{s.t.} \quad \nabla\cdot(\mathbf{f}\rho + \mathbf{g}\bar{\boldsymbol{\rho}}) = h \end{aligned} \tag{6.21}$$

and the optimal feedback control input recovered from the solution of the above linear program as

$$\mathbf{k}(\mathbf{x}) = \frac{\bar{\boldsymbol{\rho}}(\mathbf{x})}{\rho(\mathbf{x})} \tag{6.22}$$

Proof. With the feedback control input the cost can be written as

$$J(\mu) = \int_{\mathbf{X}_1}\int_0^\infty q(\mathbf{x}(t)) + \mathbf{k}(\mathbf{x}(t))^\top \mathbf{R}\mathbf{k}(\mathbf{x}(t)) dt d\mu \tag{6.23}$$

where $x(t)$ is the solution of feedback control system

$$\dot{\mathbf{x}} = \mathbf{f}(\mathbf{x}) + \mathbf{g}(\mathbf{x})\mathbf{k}(\mathbf{x}) =: \mathbf{f}_c(\mathbf{x}). \tag{6.24}$$

Let $\mathbb{K}_t^c$ and $\mathbb{P}_t^c$ be the Koopman and P-F semigroup for the feedback control system (6.24). The cost function can be written in terms of the Koopman operator as

$$J(\mu) = \textstyle\int_{\mathbf{X}_1}\int_0^\infty [\mathbb{K}_t^c(q + \mathbf{k}^\top\mathbf{R}\mathbf{k})](\mathbf{x})\ dt d\mu \tag{6.25}$$

$$= \textstyle\int_0^\infty \left\langle \mathbb{K}_t^c(q + \mathbf{k}^\top\mathbf{R}\mathbf{k}), h\right\rangle_{\mathbf{X}_1} dt \tag{6.26}$$

where $\langle\cdot,\cdot\rangle_{\mathbf{X}_1}$ stands for inner product between functions and we have used the fact that $d\mu = hd\mathbf{x}$. Using the duality property between the P-F and Koopman operator, we obtain

$$J = \int_0^\infty \left\langle q + \mathbf{k}^\top\mathbf{R}\mathbf{k}, \mathbb{P}_t^c h\right\rangle_{\mathbf{X}_1} dt = \left\langle q + \mathbf{k}^\top\mathbf{R}\mathbf{k}, \rho\right\rangle_{\mathbf{X}_1}$$

where we have exchanged the integral over time with integral over space and defined

$$\rho(\mathbf{x}) := \int_0^\infty [\mathbb{P}_t^c h](\mathbf{x}) dt, \quad \mathbf{x}\in\mathbf{X}_1 \tag{6.27}$$

It follows that $\rho(\mathbf{x})$ is a solution to the following equation

$$\nabla\cdot(\mathbf{f}_c(\mathbf{x})\rho(\mathbf{x})) = h(\mathbf{x}), \quad x\in\mathbf{X}_1 \tag{6.28}$$

Substituting (6.27) in (6.28), we obtain

$$\begin{aligned} \nabla \cdot (\mathbf{f}_c(\mathbf{x})\rho(\mathbf{x})) &= \int_0^\infty \nabla \cdot (\mathbf{f}_c(\mathbf{x})[\mathbb{P}_t^c h](\mathbf{x}))dt \\ = \int_0^\infty -\frac{d}{dt}[\mathbb{P}_t^c h](\mathbf{x})dt &= -[\mathbb{P}_t^c h](\mathbf{x})\Big|_{t=0}^{\infty} = h(\mathbf{x}) \end{aligned} \tag{6.29}$$

where we have used the infinitesimal generator property of P-F operator Eq. (6.5) and the fact that $\lim_{t\to\infty}[\mathbb{P}_t^c h](\mathbf{x}) = 0$ from Lemma 32. Furthermore, since $h > 0$, it follows that $\rho > 0$ from the positivity property of P-F semigroup $\mathbb{P}_t^c$. The OCP can then be written as

$$\begin{aligned} \min_{\mathbf{k},\rho\geq 0} \quad & \int_{\mathbf{X}_1} (q(\mathbf{x}) + \mathbf{k}(\mathbf{x})^\top \mathbf{R}\mathbf{k}(\mathbf{x}))\rho(\mathbf{x})d\mathbf{x} \\ s.t. \quad & \nabla \cdot ((\mathbf{f} + \mathbf{g}\mathbf{k})\rho) = h. \end{aligned} \tag{6.30}$$

Using the fact that $\rho > 0$, we can write above problem as

$$\begin{aligned} \min_{\bar{\boldsymbol{\rho}},\rho\geq 0} & \int_{\mathbf{X}_1} q(\mathbf{x})\rho(\mathbf{x}) + \frac{\bar{\boldsymbol{\rho}}^\top \mathbf{R}\bar{\boldsymbol{\rho}}}{\rho} d\mathbf{x} \\ s.t. \quad & \nabla \cdot (\mathbf{f}\rho + \mathbf{g}\bar{\boldsymbol{\rho}}) = h \end{aligned} \tag{6.31}$$

where $\bar{\boldsymbol{\rho}}(\mathbf{x}) = \mathbf{k}(\mathbf{x})\rho(\mathbf{x})$. Once we solve for $\bar{\boldsymbol{\rho}}$ and ρ, $\mathbf{k}$ can be recovered as $\mathbf{k}(\mathbf{x}) = \frac{\bar{\boldsymbol{\rho}}(\mathbf{x})}{\rho(\mathbf{x})}$ □

We next consider the optimization problem with $\mathcal{L}_1$ norm on control input.

$$\begin{aligned} \min_{\mathbf{k}} \quad & \textstyle\int_{\mathbf{X}_1} \left[\int_0^\infty q(\mathbf{x}) + \beta|\mathbf{k}(\mathbf{x})|\, dt\right] d\mu(\mathbf{x}) \\ \text{s.t.} \quad & \dot{\mathbf{x}} = \mathbf{f}(\mathbf{x}) + \mathbf{g}(\mathbf{x})\mathbf{k}(\mathbf{x}) \end{aligned} \tag{6.32}$$

The solution to the above optimization problem can be obtained by solving the following infinite-dimensional linear program.

Theorem 35. *Under the Assumption 31, the OCP (6.32) can be written as following infinite dimensional linear optimization problem*

$$\begin{aligned} \min_{\rho\geq 0,\bar{\boldsymbol{\rho}}} \quad & \int_{\mathbf{X}_1} q(\mathbf{x})\rho(\mathbf{x}) + |\bar{\boldsymbol{\rho}}(\mathbf{x})|d\mathbf{x} \\ \text{s.t.} \quad & \nabla \cdot (\mathbf{f}\rho + \mathbf{g}\bar{\boldsymbol{\rho}}) = h \end{aligned} \tag{6.33}$$

and the optimal feedback control input recovered from the solution of the above linear program as $\mathbf{k}(\mathbf{x}) = \frac{\bar{\boldsymbol{\rho}}(\mathbf{x})}{\rho(\mathbf{x})}$.

Proof. The proof of this theorem follows along the lines of proof of Theorem 34. □

6.4.1 Local Optimal Controller

The density function ρ for the solution of optimization problem satisfy

$$\rho(\mathbf{x}) = \int_0^\infty [\mathbb{P}_t^c h](\mathbf{x}) dt$$

where $\mathbb{P}_t^c$ is the P-F operator for the closed-loop system $\dot{\mathbf{x}} = \mathbf{f}(\mathbf{x}) + \mathbf{g}(\mathbf{x})\mathbf{k}(\mathbf{x})$ and hence ρ serves as an occupancy measure i.e., $\int_A \rho(\mathbf{x}) d\mathbf{x} = \left\langle \int_0^\infty [\mathbb{K}_t \chi_A] dt, h \right\rangle$ signifies the amount of time closed-loop system trajectories spend in the set A with initial condition supported on measure μ. Because of this, $\rho(\mathbf{x})$ has singularity at the equilibrium point stabilized by the closed-loop system. Due to this singularity at the origin, we need to exclude the small neighborhood around the origin for the proper parameterization of the density function ρ in the computation of optimal control. In particular, the optimization problem (6.40) and (6.41) is solved excluding the small neighborhood around the origin. To ensure optimality at the origin, we design local optimal control based on the data-driven identification of linear dynamics around the origin. The data-driven procedure for local control is outlined in Section 6.5.1.

6.4.2 Nonlinear Stabilization Using Density Function

The constraints in the optimization problem can be used for the designing of stabilizing feedback controller. In particular, almost everywhere stabilizing feedback controller, $\mathbf{u} = \mathbf{k}(\mathbf{x})$, for system $\dot{\mathbf{x}} = \mathbf{f}(\mathbf{x}) + \mathbf{g}(\mathbf{x})\mathbf{u}$, can be obtained by solving following linear inequalities for ρ and $\bar{\boldsymbol{\rho}}$

$$\nabla \cdot (\mathbf{f}\rho + \mathbf{g}\bar{\boldsymbol{\rho}}) > 0. \tag{6.34}$$

The stabilizing feedback controller can be recovered as $\mathbf{k}(\mathbf{x}) = \frac{\bar{\boldsymbol{\rho}}(\mathbf{x})}{\rho(\mathbf{x})}$. On the other hand solving following equation

$$\nabla \cdot (\mathbf{f}\rho + \mathbf{g}\bar{\boldsymbol{\rho}}) = h. \tag{6.35}$$

for some positive function h leads to the design of almost everywhere stabilizing feedback controller w.r.t. measure μ with density function h i.e., $d\mu = h(\mathbf{x})d\mathbf{x}$.

6.5 Data Driven Approximation of Optimal Control

For the data-driven computation of optimal control, we need to provide finite dimensional approximation of the infinite dimensional linear program (6.21) and (6.33). Towards this goal we need the data-driven approximation of the generator corresponding to vector field $\mathbf{f}$ and $\mathbf{g}$ i.e., $\nabla \cdot (\mathbf{f}\rho)$ and $\nabla \cdot (\mathbf{g}\bar{\boldsymbol{\rho}})$.

Assumption 36. *We assume that the basis functions, $\psi_k(\mathbf{x})$ for $k = 1, \ldots, N$ are positive and let*

$$\boldsymbol{\Psi}(\mathbf{x}) = [\psi_1(\mathbf{x}), \ldots, \psi_N(\mathbf{x})]^\top.$$

Remark 37. *In this paper, we use Gaussian RBF to obtain all the simulation results i.e., $\psi_k(\mathbf{x}) = \exp^{-\frac{\|\mathbf{x}-\mathbf{c}_k\|}{\sigma^2}}$. where $\mathbf{c}_k$ is the center of the k^{th} Gaussian RBF.*

Let $\mathbf{K}_0 \in \mathbb{R}^{N\times N}$ be the finite-dimensional approximation of the Koopman operator corresponding to uncontrolled dynamical system $\dot{\mathbf{x}} = \mathbf{f}(\mathbf{x})$. Similarly, let $\mathbf{K}_j$ for $j = 1, \ldots, p$ be the Koopman operator for the system with unit step applied to i^{th} input with all other inputs zero i.e., $\mathbf{u} = \mathbf{e}_j$ and $\dot{\mathbf{x}} = \mathbf{f}(\mathbf{x}) + \mathbf{g}(\mathbf{x})\mathbf{e}_j$. These Koopman operator are obtained using NSDMD algorithm from section 6.3.3 with time series data generated from the dynamical system with discretization time-step of Δt. Corresponding to these Koopman operator, we can compute the P-F operator as

$$\mathbf{P}_j = \boldsymbol{\Lambda}^{-1}\mathbf{K}_j^\top\boldsymbol{\Lambda}, \quad j = 0, 1, \ldots, p. \tag{6.36}$$

The $\boldsymbol{\Lambda}$ matrix can be computed explicitly since the basis functions are chosen to be Gaussian RBF, with entires $\Lambda_{i,j} = (\frac{\pi\sigma^2}{2})^{n/2} e^{\frac{-\|\mathbf{c}_i-\mathbf{c}_j\|^2}{2\sigma^2}}$, $i, j = 1, 2, \ldots, N$. The approximation of the P-F generator corresponding to the vector field $\mathbf{f}$ is

$$\mathcal{P}_{\mathbf{f}} \approx \frac{1}{\Delta t}(\mathbf{P}_0 - \mathbf{I}) =: \mathbf{M}_0 \tag{6.37}$$

Using linearity property of the generator it follows that

$$\mathcal{P}_{\mathbf{g}_j} = \mathcal{P}_{\mathbf{f}+\mathbf{g}_j} - \mathcal{P}_{\mathbf{f}} \approx \frac{\mathbf{P}_j - \mathbf{P}_0}{\Delta t} = \mathbf{M}_j, j = 1, \ldots, p \tag{6.38}$$

Let $\rho(\mathbf{x})$, and $\bar{\boldsymbol{\rho}}(\mathbf{x})$ be expressed in terms of the basis function

$$\rho(\mathbf{x}) \approx \boldsymbol{\Psi}(\mathbf{x})^\top\mathbf{v}, \quad \bar{\rho}_j(\mathbf{x}) \approx \boldsymbol{\Psi}(\mathbf{x})^\top\mathbf{w}_j, \ j = 1, \ldots, p \tag{6.39}$$

With the above approximation of the generators $\mathcal{P}_{\mathbf{f}}$ and $\mathcal{P}_{\mathbf{g}_i}$ and $\rho, \bar{\boldsymbol{\rho}}$ we can approximate the equality constraints in the optimization problem (6.21) as finite dimensional equality constraints.

$$-\boldsymbol{\Psi}(\mathbf{x})^\top \left(\mathbf{M}_0 \mathbf{v} + \sum_{j=1}^{p} \mathbf{M}_j \mathbf{w}_j \right) = \boldsymbol{\Psi}(\mathbf{x})^\top \mathbf{m}$$

We now proceed with the approximation of the cost function.

$$\int_{\mathbf{X}_1} q(\mathbf{x}) \rho(\mathbf{x}) d\mathbf{x} \approx \int_{\mathbf{X}} q(\mathbf{x}) \boldsymbol{\Psi}^\top d\mathbf{x} \mathbf{v} = \mathbf{d}^\top \mathbf{v}$$

where the vector $\mathbf{d} := \int_X q(\mathbf{x}) \boldsymbol{\Psi} d\mathbf{x}$ can be pre-computed.

Remark 38. *We now assume that the Gaussian radial basis functions have essentially disjoint support. This will be true if the centers for the Gaussian RBF are chosen such that their centers are* 3σ *distance apart.*

With this assumption we can approximate $\frac{\bar{\boldsymbol{\rho}}_j}{\rho} = \boldsymbol{\Psi}^\top \frac{\mathbf{w}_j}{\mathbf{v}}$, where we assume element-wise division, hence

$$\frac{\bar{\boldsymbol{\rho}}^\top \mathbf{R} \bar{\boldsymbol{\rho}}}{\rho} = \sum_i \sum_j r_{ij} \bar{\boldsymbol{\rho}}_i \frac{\bar{\boldsymbol{\rho}}_j}{\rho} \approx \sum_{i,j} r_{ij} \mathbf{w}_i^\top \boldsymbol{\Psi} \boldsymbol{\Psi}^\top \frac{\mathbf{w}_j}{\mathbf{v}}$$

where $r_{ij} = r_{ji}$.

$$\int_{\mathbf{X}_1} \frac{\bar{\boldsymbol{\rho}}^\top \mathbf{R} \bar{\boldsymbol{\rho}}}{\rho} d\mathbf{x} \approx \sum_{i,j} \mathbf{w}_i^\top \mathbf{D}_{ij} \frac{\mathbf{w}_j}{\mathbf{v}}$$

where, $\mathbf{D}_{ij} = \int_{\mathbf{X}_1} r_{ij} \boldsymbol{\Psi} \boldsymbol{\Psi}^\top d\mathbf{x}$. We have the following approximation to the optimization problem (6.21)

$$\begin{aligned} &\min_{\boldsymbol{\Psi}^\top \mathbf{v} \geq 0, \mathbf{w}_j} \mathbf{d}^\top \mathbf{v} + \textstyle\sum_{ij} r_{ij} \mathbf{w}_i^\top \mathbf{D}_{ij} \frac{\mathbf{w}_j}{\mathbf{v}} \\ &\text{s.t. } -\boldsymbol{\Psi}(\mathbf{x})^\top \left(\mathbf{M}_0 \mathbf{v} + \sum_{j=1}^{p} \mathbf{M}_j \mathbf{w}_j \right) = \boldsymbol{\Psi}(\mathbf{x})^\top \mathbf{m} \end{aligned}$$

Since the basis functions are assumed to be positive, (Assumption 36), the approximation for the ρ and $\bar{\boldsymbol{\rho}}$ in (6.39) can be obtained by solving following finite-dimensional problem.

$$\begin{aligned} &\min_{\mathbf{v} \geq 0, \mathbf{w}_j} \mathbf{d}^\top \mathbf{v} + \textstyle\sum_{ij} r_{ij} \mathbf{w}_i^\top \mathbf{D}_{ij} \frac{\mathbf{w}_j}{\mathbf{v}} \\ &\text{s.t. } -\left(\mathbf{M}_0 \mathbf{v} + \sum_{j=1}^{p} \mathbf{M}_j \mathbf{w}_j \right) = \mathbf{m} \end{aligned} \tag{6.40}$$

The optimal control is then approximated as $\mathbf{u} = \mathbf{\Psi}^\top(\mathbf{x})\frac{\mathbf{w}}{\mathbf{v}}$, where the division is element-wise. Similarly, the finite dimensional approximation of the OCP (6.33) corresponding to $\mathcal{L}_1$ norm on control is given by

$$\begin{aligned} &\min_{\mathbf{v}\geq 0, \mathbf{w}_j} \mathbf{d}^\top \mathbf{v} + \beta c \sum_{j=1}^{p} |\mathbf{w}_j| \\ &\text{s.t. } -\left(\mathbf{M}_0\mathbf{v} + \sum_{j=1}^{p} \mathbf{M}_j \mathbf{w}_j\right) = \mathbf{m} \end{aligned} \tag{6.41}$$

where $c = \int_{\mathbf{X}_1} \psi_i(\mathbf{x})d\mathbf{x} = \int_{\mathbf{X}_1} \psi_j(\mathbf{x})d\mathbf{x}$ is a positive constant.

6.5.1 Computation of Local Optimal Controller

For the computation of local optimal controller, we identify local linearized dynamics from data. For the identification of the linearized dynamics, we again use the same time series data used in the approximation of the global P-F except that the basis functions are chosen to be identity function i.e., $\mathbf{\Psi}(\mathbf{x}) = \mathbf{x}$ and instead of using NSDMD algorithm we use EDMD algorithm for the Koopman approximation. In particular, let $\mathbf{A}$ and $\mathbf{B} = [\mathbf{b}_1, \ldots, \mathbf{b}_p]$ are the identified matrix, then following (6.12)-(6.14)-(6.37)-(6.38), we have

$$\mathbf{A} = \frac{\mathbf{K}_0^\top - \mathbf{I}}{\Delta t}, \quad \mathbf{b}_j = \frac{\mathbf{K}_j^\top - \mathbf{K}_j^\top}{\Delta t}, \quad j = 1, \ldots, p \tag{6.42}$$

where $\mathbf{K}_j$ for $j = 0, 1, \ldots, p$ are the Koopman approximation obtained using EDMD algorithm with $\mathbf{\Psi}(\mathbf{x}) = \mathbf{x}$ basis function and for control input zero and unit step input $\mathbf{e}_j$ respectively. Once we have the above local approximation of the system matrices, the linear quadratic regulator based local controller is obtained using MATLAB command $\mathrm{lqrd}(\mathbf{A}, \mathbf{B}, \mathbf{Q}, \mathbf{R})$. The existence of local optimal controller is guaranteed based on Assumption 29. The detailed algorithm is summarized in Algorithm 3.

6.6 Simulation results

All the simulation results in this paper are obtained using Gaussian RBF. Following the rule of thumb are abided in the selection of centers and σ parameters for the Gaussian RBF. The centers of the RBF are chosen to be uniformly distributed in the state space at distance d. The σ for the Gaussian

RBF is chosen such that $d \leq 3\sigma \leq 1.5d$. The number of basis functions along each dimension is chosen to be 15×15 for 2D example and $8 \times 10 \times 10$ for 3D examples.

6.6.1 Controlled Van der Pol oscillator

$$\dot{x}_1 = x_2, \quad \dot{x}_2 = (1 - x_1^2)x_2 - x_1 + u \tag{6.43}$$

where $x \in \mathbb{R}^2$ and $u \in \mathbb{R}$ is the single input. For this example we consider the OCP with quadratic cost on state, $q(\mathbf{x}) = \mathbf{x}^\top \mathbf{x}$ and quadratic cost on control. The finite dimensional optimization formulation in Eq. (6.40) is applied for the design of optimal control.

For the approximation of P-F operator, we applied NSDMD algorithm using one-step time-series data with 10000 initial conditions, $\Delta t = 0.01$ (i.e., 10^4 time-series data samples). In this example, we are using 225 Gaussian radial basis functions as the basis functions $\mathbf{\Psi}(\mathbf{x})$, with the radius $\sigma = 0.2$, and the centers of basis functions are distributed uniformly within the range of $[-2,\ 2] \times [-3,\ 3]$. In Fig. 6.2 and Fig. 6.3 we show the successful simulation results for the comparison of the open loop and closed trajectories starting from five different initial conditions in the domain $[-2, 2] \times [-2, 2]$.

6.6.2 *Controlled Lorenz system*

The control Lorenz system can be written as follows

$$\begin{aligned} \dot{x}_1 &= \sigma(x_2 - x_1) \\ \dot{x}_2 &= x_1(\rho - x_3) - x_2 + u \\ \dot{x}_3 &= x_1 x_2 - \beta x_3. \end{aligned} \tag{6.44}$$

where $\mathbf{x} \in \mathbb{R}^3$ and $u \in \mathbb{R}$ is the single input. With the parameter values $\rho = 28$, $\sigma = 10$, $\beta = \frac{8}{3}$, and control input $u = 0$ the Lorenz system exhibits chaotic behavior. In this 3D example, we generated the time-series data from 50000 random chosen initial conditions from $[-15, 15] \times [-20, 20] \times [0, 40]$ and propagate each of them for one time step with sampling time $\Delta t = 0.01s$. For this example, we consider optimal control formulation given in Eq. (6.32) with state cost $q(\mathbf{x}) = \mathbf{x}^\top \mathbf{x}$ and 1-norm cost

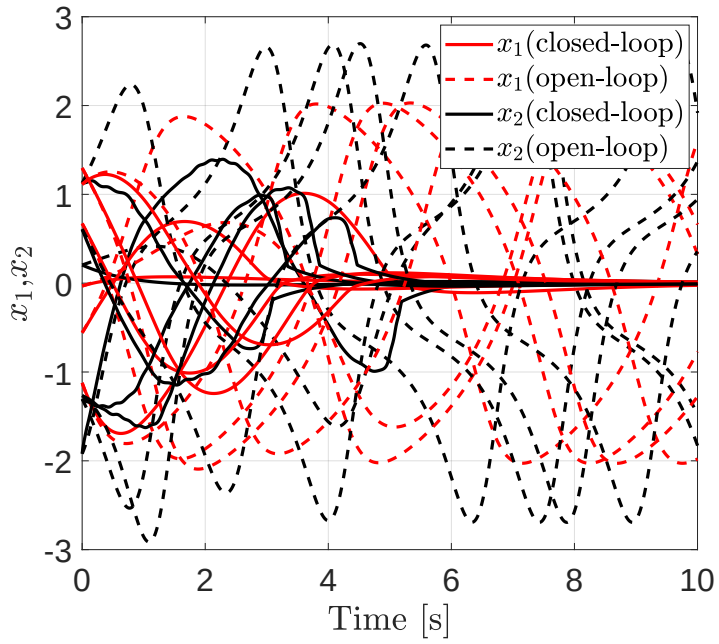

Figure 6.2 $x_{1\sim2}$ vs t

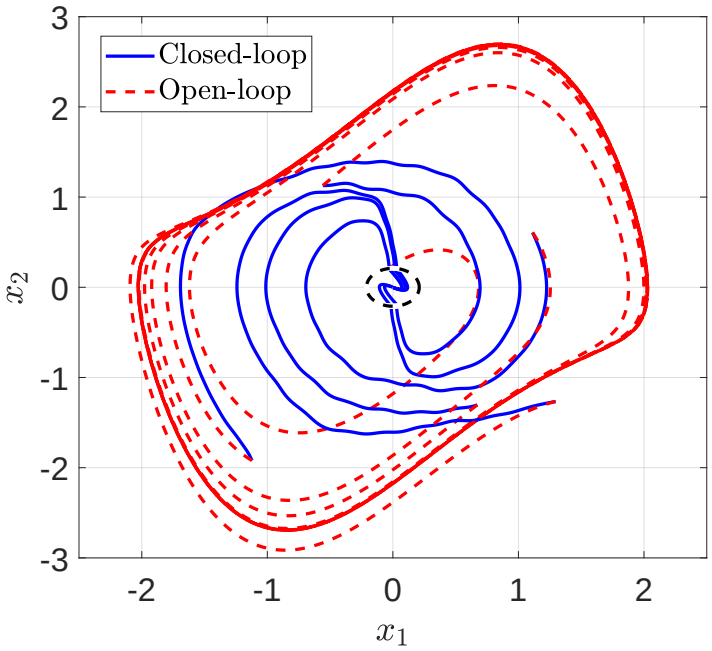

Figure 6.3 Trajectories in 2-D space

Figure 6.4: Van der Pol oscillator optimal control

on control. The finite dimensional approximation for this case is given in Eq. (6.41). We are using 800 Gaussian radial basis functions $\mathbf{\Psi}(\mathbf{x})$, with $\sigma = 2.5$. To validate the closed-loop control designed using the Algorithm 3, we perform the closed-loop simulation with $\mathcal{L}_1$ norm control cost in (6.32). In Fig. 6.6 and Fig. 6.7, we show the open-loop and closed-loop trajectories starting from five different initial conditions and the closed-loop trajectories are converging to the origin, The time trajectories in Fig. 6.6 show that all the initial conditions can be stabilized to the origin within 3s with a minimized control and state-dependent cost.

6.6.3 *3-D integrator system*

The next example is an unstable 3-D integrator. The control 3-D system can be written as follows

$$\begin{aligned} \dot{x}_1 &= x_1^2 - x_1^3 + x_2 \\ \dot{x}_2 &= x_3 \\ \dot{x}_3 &= u. \end{aligned} \tag{6.45}$$

where $\mathbf{x} \in \mathbb{R}^3$ and $u \in \mathbb{R}$ is the single input. With the control input $u = 0$ the system will go to infinity obviously. In the 3-D integrator example, we generated the time-series data from 30000 random chosen initial conditions from $[-5, 5] \times [-5, 5] \times [-5, 5]$ and propagate each of them for 1 time step with sampling time $\Delta t = 0.01s$.

From the optimal control side, we want to see if the controller will be able to stabilize the strongly unstable system to the origin. We are using 800 Gaussian radial basis functions as the basis functions $\mathbf{\Psi}(\mathbf{x})$, with the radius $\sigma = 0.5$, and the centers of basis functions are distributed uniformly within the range of $[-5,\ 5] \times [-5,\ 5] \times [-5, 5]$. In this example, we still use the quadratic cost $q(\mathbf{x}) = \mathbf{x}^\top \mathbf{x}$ on the state and 1-norm cost on the control.

For the validation of the closed-loop optimal control designed using the Algorithm 3, we perform the closed-loop simulation with five randomly chosen initial conditions in the domain $[-5, 5] \times [-5, 5] \times [-1, 1]$. In Fig. 6.10 and Fig. 6.11, since the open-loop system dynamics are known to be strongly unstable, we show only the closed-loop trajectories starting from five different initial conditions, and all the trajectories are converging to the origin, The time trajectories in Fig. 6.10 shows that all the initial conditions can be stabilized to the origin within 20s successfully.

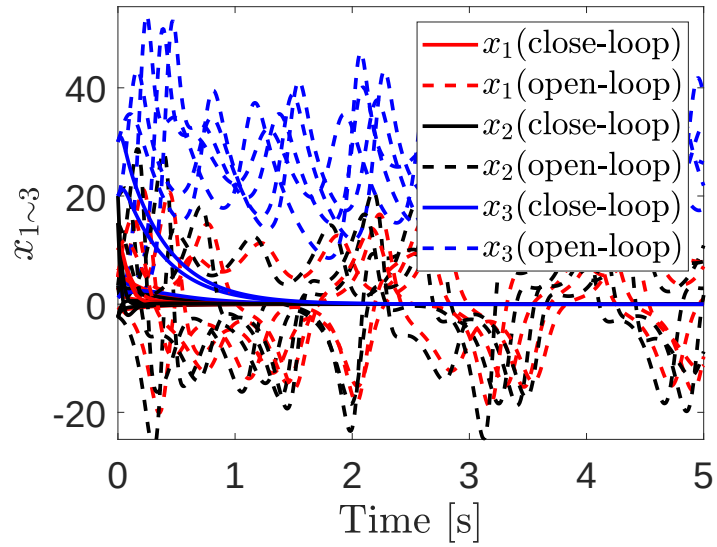

Figure 6.6 $x_{1\sim3}$ vs t

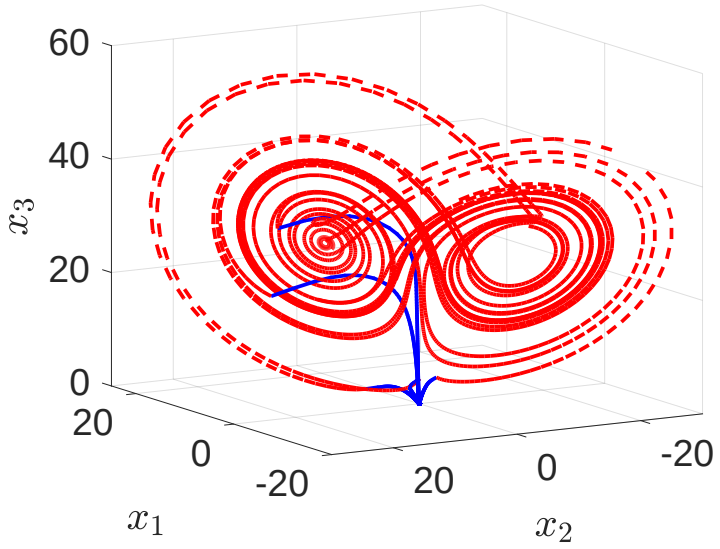

Figure 6.7 Trajectories in 3-D space

Figure 6.8: Lorenz system open-loop and closed-loop trajectories

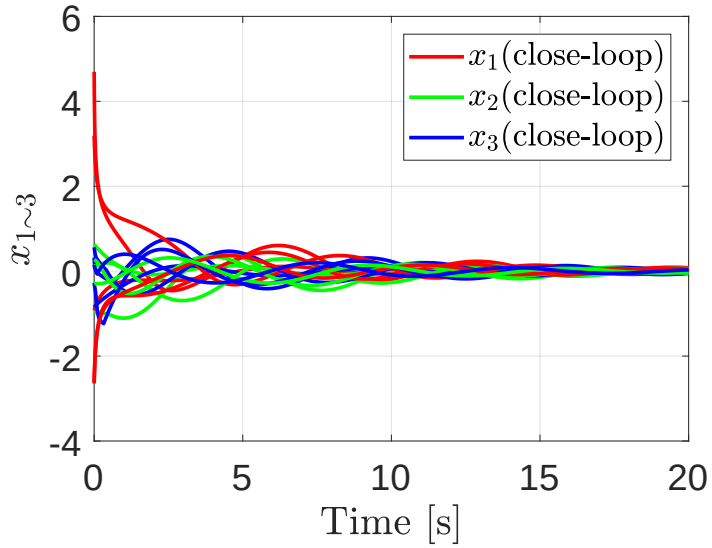

Figure 6.10 $x_{1\sim3}$ vs t

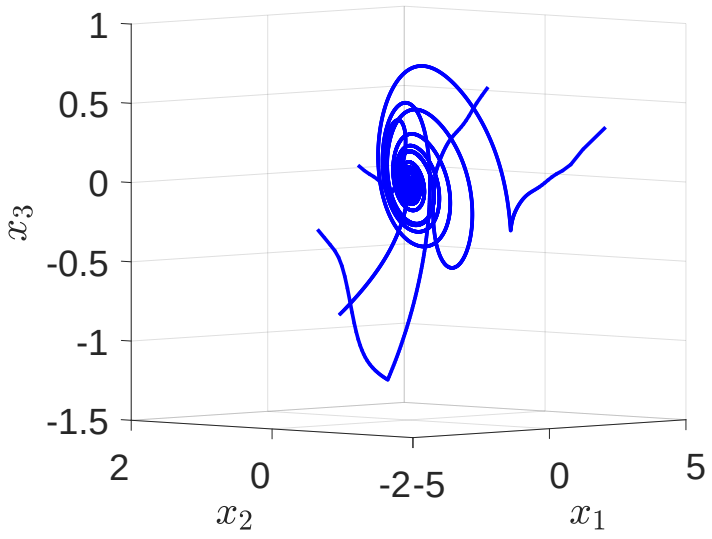

Figure 6.11 Trajectories in 3-D space

Figure 6.12: 3-D integrator system closed-loop trajectories

6.6.4 *3D system with nonlinear g(x)*

The other 3-D example we pick hereKhalil (1996) is with nonlinear control matrix $\mathbf{g}(\mathbf{x})$. The control 3-D system can be written as follows

$$\dot{x}_1 = -x_1 + \left(\frac{2+x_3^2}{1+x_3^2}\right) u, \;\; \dot{x}_2 = x_3, \;\; \dot{x}_3 = x_1 x_3 + u. \tag{6.46}$$

where $\mathbf{x} \in \mathbb{R}^3$ and $u \in \mathbb{R}$ is the single input, and $\mathbf{g}(\mathbf{x}) = [\frac{2+x_3^2}{1+x_3^2}, \; 0, \; 1]^\top$ is nonlinear control matrix for u. In the 3-D nonlinear control example, we generated the time-series data from 50000 random chosen initial conditions from $[-5, 5] \times [-5, 5] \times [-5, 5]$ and propagate each of them for 1 time step with sampling time $\Delta t = 0.01s$.

The objective of this example is stabilization. We are using 800 Gaussian radial basis functions as the basis functions $\mathbf{\Psi}(\mathbf{x})$, with $\sigma = 0.5$, and the centers of basis functions are distributed uniformly within the range of $[-5, \; 5] \times [-5, \; 5] \times [-5, 5]$. In this example, we will apply the stabilization controller design, i.e., solving the convex optimization problem as a feasibility problem. For the validation of the closed-loop stabilization control designed using the Algorithm 3, we perform the closed-loop simulation with five randomly chosen initial conditions in the domain $[-5, \; 5] \times [-5, \; 5] \times [-2.5, 2.5]$. In Fig. 6.14 and Fig. 6.15, we show both the open-loop and the closed-loop trajectories starting from five different initial conditions and all the controlled trajectories are converging to the origin while the uncontrolled trajectories go to infinity. The time trajectories in Fig. 6.14 shows that all the initial conditions can be stabilized to the origin within 10s successfully.

6.7 Conclusion

In this paper, we have provided a convex optimization-based formulation for the optimal control problem in the dual density space. We provided a data-driven approach based on the approximation of the P-F and Koopman operator for the finite-dimensional approximation of the convex optimization problem for optimal control design. Future research efforts will focus on the development of a computationally efficient numerical scheme and the choice of appropriate basis function for the implementation of the developed algorithm to a large dimensional system.

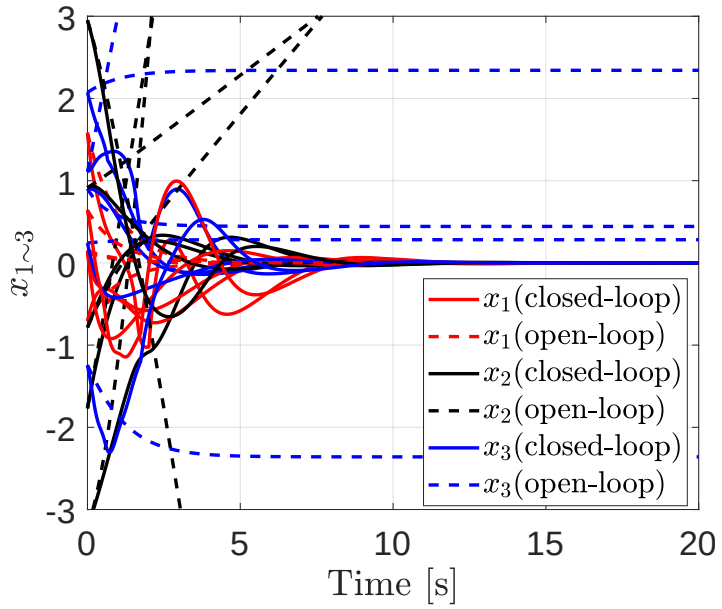

Figure 6.14 $x_{1\sim3}$ vs t

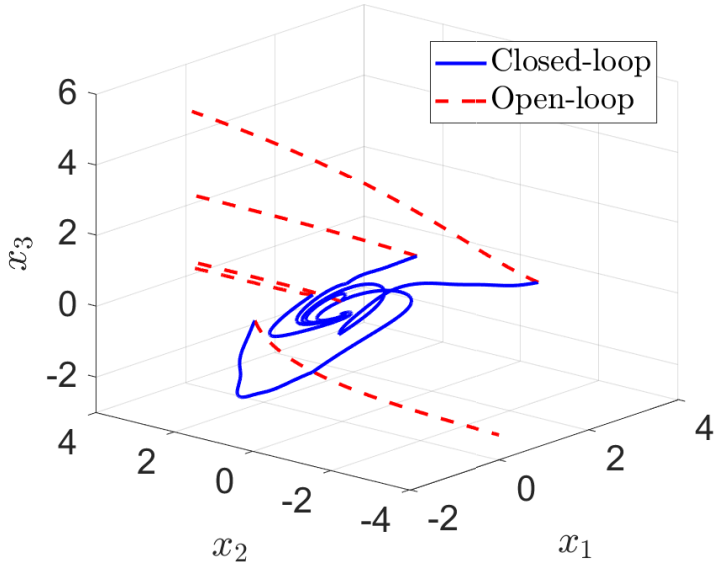

Figure 6.15 Trajectories in 3-D space

Figure 6.16: 3-D nonlinear control system closed-loop trajectories

Algorithm 3: Data-Driven Optimal Control

Data: Generate open-loop time-series data $\{\mathbf{x}_k^0\}_{k=0}^M$, and $\{\mathbf{x}_k^j\}_{k=0}^M$ with unit step for input $\mathbf{u} = \mathbf{e}_j, j = 1, \ldots, p$ in (6.17)

, **Cost**: State cost:$q(\mathbf{x})$, Control Cost: $\mathbf{R}$. **Result:** $\mathbf{u} = \mathbf{k}(\mathbf{x})$

Phase I: PF Approximation

  Choose N Gaussian Radial basis functions with centers uniformly distributed in the domain and σ chosen to satisfy $d \leq 3\sigma \leq 1.5d$

  Let $\mathbf{x}_i^0$ be the data with zero input and $\mathbf{x}_i^j$ is data with step input $\mathbf{u} = \mathbf{e}_j$, $i = 1 \ldots M, j = 1 \ldots p$.

  Obtain $\boldsymbol{G}^j$ and $\boldsymbol{A}^j$ matrices with equation (6.13).

  Solving the NSDMD optimization in (6.15) for the P-F approximation $\mathbf{P}_0 = \Lambda \mathbf{K}_0 \Lambda^{-1}$ and $\mathbf{M}_0$.

  Repeat line 4 to 6 with $j = 1, 2, \ldots, p$ to get $\mathbf{P}_j$ and $\mathbf{M}_j$

end

Phase II: Convex Optimization

  Pick $\ell = \text{argmin}_{i=1,\ldots,N} \|c_i - \mathbf{x}_d\|$, where $\mathbf{x}_d$ is the desired equilibrium point.

  Compute $\mathbf{d} = \int_{\mathbf{X}} q(\mathbf{x}) \boldsymbol{\Psi}^\top d\mathbf{x}$ and $c = (\pi\sigma^2)^{(n/2)}$.

  Remove the ℓth row and ℓth column from $\mathbf{P}_j, \mathbf{M}_j$ and Λ to obtain $\bar{\mathbf{P}}_j, \bar{\mathbf{M}}_j$ $\bar{\Lambda}$ for $j = 1, \ldots, p$. Remove ℓ^{th} element from $\mathbf{d}$.

  Solve the convex problem (6.40) or (6.41) for data-driven approximation of ρ, $\bar{\boldsymbol{\rho}}$, $\mathbf{v}, \mathbf{w}$.

  Insert 0 as ℓth element such that $\mathbf{v}, \mathbf{w} \in \mathbb{R}^N$.

  For the i^{th} basis function, find the optimal feedback weight $k_i^j = \frac{w_i}{v_i}$, $i \neq \ell$, and $k_\ell^j = 0$, $j = 1, \ldots, p$.

end

Phase III: Local Stabilization Control

  Use time series data from zero input $\{x_k^0\}_{k=0}^M$ and unit step input $\{x_k^j\}_{k=0}^M$ for the identification of local linear system dynamics.

  Compute the local linear approximation ($\mathbf{A}$,$\mathbf{B}$) by applying EDMD with $\boldsymbol{\Psi}(\mathbf{x}) = \mathbf{x}$ as basis function using formula (6.42).

  Obtain the LQR controller K_{lqr}, using MATLAB command $\text{lqrd}(\mathbf{A}, \mathbf{B}, \mathbf{Q}, \mathbf{R})$, where $\mathbf{Q} = \frac{\partial^2 q(0)}{\partial \mathbf{x}^2}$.

end

Feedback control $\mathbf{u} = \mathbf{k}(\mathbf{x}) = [k_1(\mathbf{x}), \ldots, k_p(\mathbf{x})]^\top$, where

$$k_j(\mathbf{x}) = \begin{cases} \sum_{i=1}^N k_i^j \psi_i(\mathbf{x}), & \|\mathbf{x} - c_\ell\| > 3\sigma \\ -K_{lqr}\mathbf{x} & \|\mathbf{x} - c_\ell\| \leq 3\sigma \end{cases}, j = 1, \ldots, p.$$

CHAPTER 7. CONCLUSION

In this dissertation, we successfully applied the linear operator theory to identify and design stabilizing and optimal feedback controllers for a nonlinear control system. The proposed framework is data-driven and relies on the use of time-series data generated from the control dynamical system for identification and control design. We employ two dual Koopman and Perron-Frobenius (P-F) operators in our proposed data-driven modeling and control framework.

The modeling and control framework involving the Koopman operator relies on the bilinear lifting of control dynamical system for identification and control of the nonlinear system. In particular, the finite-dimensional bilinear representation in the lifted function space is used to design stabilizing feedback control and optimal control. The stabilizing control relies on the concept of control Lyapunov function for control design. Simultaneously, the optimal control problem using bilinear representation is formulated as a nonconvex optimization problem.

In our second framework involving the P-F operator, we provide a convex formulation to the stabilizing control and optimal control design. The convex formulation was made possible by formulating the control design problem in the dual space of densities. In particular, the duality results in the stability theory of the dynamical system involving the Lyapunov function, and Lyapunov measures or density are exploited for this purpose. The P-F operator is involved in lifting the stability condition and optimal control problem to the dual space of density. This linear lifting using the P-F operator is in contrast to the Koopman-based lifting of control dynamical system leading to the bilinear representation of the control system. Time-series data generated by the control dynamical system is used in the finite-dimensional approximation of P-F operator and associated convex formulation of the stabilization and optimal control problem. This approximation of the P-F operator leads to finite-dimensional convex optimization formulation to approximate optimal control for a nonlinear system.

BIBLIOGRAPHY

Arbabi, H. (2017). *Koopman spectral analysis and study of mixing in incompressible flows*. PhD thesis, UC Santa Barbara.

Arbabi, H., Korda, M., and Mezić, I. (2018). A data-driven koopman model predictive control framework for nonlinear partial differential equations. In *2018 IEEE Conference on Decision and Control (CDC)*, pages 6409–6414. IEEE.

Arbabi, H. and Mezic, I. (2017). Ergodic theory, dynamic mode decomposition, and computation of spectral properties of the koopman operator. *SIAM Journal on Applied Dynamical Systems*, 16(4):2096–2126.

Arimoto, S., Kawamura, S., and Miyazaki, F. (1984). Bettering operation of robots by learning. *Journal of Robotic systems*, 1(2):123–140.

Ariyur, K. B. and Krstić, M. (2003). *Real time optimization by extremum seeking control*. Wiley Online Library.

Artstein, Z. (1983). Stabilization with relaxed controls. *Nonlinear Analysis: Theory, Methods & Applications*, 7(11):1163–1173.

Astolfi, A. (2015). Feedback stabilization of nonlinear systems. *Encyclopedia of Systems and Control*, pages 437–447.

Bagheri, S. (2013). Koopman-mode decomposition of the cylinder wake. *Journal of Fluid Mechanics*, 726:596–623.

Boyd, S., Ghaoui, L. E., Feron, E., and Balakrishnan, V. (1994). *Linear Matrix Inequalities in System and Control Theory*. SIAM.

Brockett, R. W. (1976). Volterra series and geometric control theory. *Automatica*, 12(2):167–176.

Bruder, D., Remy, C. D., and Vasudevan, R. (2019). Nonlinear system identification of soft robot dynamics using koopman operator theory. In *2019 International Conference on Robotics and Automation (ICRA)*, pages 6244–6250. IEEE.

Brunton, B. W., Johnson, L. A., Ojemann, J. G., and Kutz, J. N. (2016a). Extracting spatial–temporal coherent patterns in large-scale neural recordings using dynamic mode decomposition. *Journal of neuroscience methods*, 258:1–15.

Brunton, S. L., Brunton, B. W., Proctor, J. L., and Kutz, J. N. (2016b). Koopman invariant subspaces and finite linear representations of nonlinear dynamical systems for control. *PloS one*, 11(2):e0150171.

Brunton, S. L. and Noack, B. R. (2015). Closed-loop turbulence control: progress and challenges. *Applied Mechanics Reviews*, 67(5):050801.

Brunton, S. L., Proctor, J. L., and Kutz, J. N. (2013). Compressive sampling and dynamic mode decomposition. *arXiv preprint arXiv:1312.5186*.

Budisic, M., Mohr, R., and Mezic, I. (2012). Applied koopmanism. *Chaos*, 22:047510–32.

Camacho, E. F., Bordons, C., and Normey-Rico, J. E. (2003). Model predictive control springer, berlin, 1999, isbn 3540762418, 280 pages. *International Journal of Robust and Nonlinear Control: IFAC-Affiliated Journal*, 13(11):1091–1093.

Charlet, B., Lévine, J., and Marino, R. (1989). On dynamic feedback linearization. *Systems & Control Letters*, 13(2):143–151.

Chen, K. K., Tu, J. H., and Rowley, C. W. (2012). Variants of dynamic mode decomposition: boundary condition, koopman, and fourier analyses. *Journal of nonlinear science*, 22(6):887–915.

Chen, Y. and Vaidya, U. (2019). Sample complexity of nonlinear stochastic dynamics. *American Control Conference*.

Chen, Y. and Wen, C. (1999). *Iterative learning control: convergence, robustness and applications*. Springer.

Choi, H., Vaidya, U., and Chen, Y. (2020). A convex data-driven approach for nonlinear control synthesis.

Chow, J. H. and Cheung, K. W. (1992). A toolbox for power system dynamics and control engineering education and research. *IEEE Transactions on Power Systems*, 7(4):1559–1564.

Das, A. K., Huang, B., and Vaidya, U. (2018). Data-driven optimal control using transfer operators. In *2018 IEEE Conference on Decision and Control (CDC)*, pages 3223–3228. IEEE.

Das, A. K., Raghunathan, A. U., and Vaidya, U. (2017). Transfer operator-based approach for optimal stabilization of stochastic systems. In *2017 American Control Conference (ACC)*, pages 1759–1764. IEEE.

Dawson, S. T., Hemati, M. S., Williams, M. O., and Rowley, C. W. (2016). Characterizing and correcting for the effect of sensor noise in the dynamic mode decomposition. *Experiments in Fluids*, 57(3):42.

Dellnitz, M., Froyland, G., and Junge, O. (2001). The algorithms behind GAIO – set oriented numerical methods for dynamical systems. In Fiedler, B., editor, *Ergodic Theory, Analysis, and Efficient Simulation of Dynamical Systems*, pages 145–174. Springer.

Dellnitz, M. and Junge, O. (2002). Set oriented numerical methods for dynamical systems. *Handbook of dynamical systems*, 2:221–264.

Dellnitz, M. and Junge, O. (2006). Set oriented numerical methods in space mission design. *Modern Astrodynamics*, 1:127–153.

Edwards, C. and Spurgeon, S. (1998). *Sliding mode control: theory and applications*. Crc Press.

Erichson, N. B., Brunton, S. L., and Kutz, J. N. (2016). Compressed dynamic mode decomposition for background modeling. *Journal of Real-Time Image Processing*, pages 1–14.

Formentin, S., Piga, D., Tóth, R., and Savaresi, S. M. (2013). Direct data-driven control of linear parameter-varying systems. In *52nd IEEE Conference on Decision and Control*, pages 4110–4115. IEEE.

Freeman, R. A. and Primbs, J. A. (1996). Control Lyapunov functions: New ideas from an old source. In *Decision and Control, 1996., Proceedings of the 35th IEEE Conference on*, volume 4, pages 3926–3931. IEEE.

Froyland, G. and Dellnitz, M. (2003). Detecting and locating near-optimal almost-invariant sets and cycles. *SIAM Journal on Scientific Computing*, 24(6):1839–1863.

Froyland, G. and Padberg, K. (2009). Almost-invariant sets and invariant manifolds—connecting probabilistic and geometric descriptions of coherent structures in flows. *Physica D: Nonlinear Phenomena*, 238(16):1507–1523.

Fujisaki, Y., Duan, Y., and Ikeda, M. (2004). System representation and optimal control in input-output data space. *IFAC Proceedings Volumes*, 37(11):185–190.

Georgescu, M., Loire, S., Kasper, D., and Mezic, I. (2017). Whole-building fault detection: A scalable approach using spectral methods. *arXiv preprint arXiv:1703.07048*.

Georgescu, M. and Mezić, I. (2015). Building energy modeling: A systematic approach to zoning and model reduction using koopman mode analysis. *Energy and buildings*, 86:794–802.

Guéniat, F., Mathelin, L., and Pastur, L. R. (2015). A dynamic mode decomposition approach for large and arbitrarily sampled systems. *Physics of Fluids*, 27(2):025113.

Halmos, P. R. (1973). The legend of john von neumann. *The American Mathematical Monthly*, 80(4):382–394.

Hansen, N., Niederberger, A. S., Guzzella, L., and Koumoutsakos, P. (2008). A method for handling uncertainty in evolutionary optimization with an application to feedback control of combustion. *IEEE Transactions on Evolutionary Computation*, 13(1):180–197.

Hemati, M. S., Rowley, C. W., Deem, E. A., and Cattafesta, L. N. (2017). De-biasing the dynamic mode decomposition for applied koopman spectral analysis of noisy datasets. *Theoretical and Computational Fluid Dynamics*, 31(4):349–368.

Hemati, M. S., Williams, M. O., and Rowley, C. W. (2014). Dynamic mode decomposition for large and streaming datasets. *Physics of Fluids*, 26(11):111701.

Henrion, D. and Korda, M. (2013). Convex computation of the region of attraction of polynomial control systems. *IEEE Transactions on Automatic Control*, 59(2):297–312.

Heusden, K. v. (2010). Non-iterative data-driven model reference control. Technical report, EPFL.

Hjalmarsson, H., Gunnarsson, S., and Gevers, M. (1994). A convergent iterative restricted complexity control design scheme. In *Proceedings of 1994 33rd IEEE Conference on Decision and Control*, volume 2, pages 1735–1740. IEEE.

Hou, Z.-S. and Wang, Z. (2013). From model-based control to data-driven control: Survey, classification and perspective. *Information Sciences*, 235:3–35.

Hua, J.-C., Gunaratne, G. H., Talley, D. G., Gord, J. R., and Roy, S. (2016). Dynamic-mode decomposition based analysis of shear coaxial jets with and without transverse acoustic driving. *Journal of Fluid Mechanics*, 790:5–32.

Huang, B. and Kadali, R. (2008). *Dynamic modeling, predictive control and performance monitoring: a data-driven subspace approach*. Springer.

Huang, B., Ma, X., and Vaidya, U. (2018). Feedback stabilization using koopman operator. In *2018 IEEE Conference on Decision and Control*, pages 6434–6439. IEEE.

Huang, B., Ma, X., and Vaidya, U. (2019). Data-driven nonlinear stabilization using koopman operator. *arXiv preprint arXiv:1901.07678*.

Huang, B., Ma, X., and Vaidya, U. (2020). Data-driven nonlinear stabilization using koopman operator. In *The Koopman Operator in Systems and Control*, pages 313–334. Springer.

Huang, B. and Vaidya, U. (2018). Data-driven approximation of transfer operators: Naturally structured dynamic mode decomposition. In *2018 Annual American Control Conference (ACC)*, pages 5659–5664. IEEE.

Ikeda, M., Fujisaki, Y., and Hayashi, N. (2001). A model-less algorithm for tracking control based on input-output data. *Nonlinear Analysis: Theory, Methods & Applications*, 47(3):1953–1960.

Kaiser, E., Kutz, J. N., and Brunton, S. L. (2017). Data-driven discovery of koopman eigenfunctions for control. *arXiv preprint arXiv:1707.01146*.

Kappen, H. J. (2007). An introduction to stochastic control theory, path integrals and reinforcement learning. *AIPC*, 887:149–181.

Katayama, T. (2006). *Subspace methods for system identification*. Springer Science & Business Media.

Khalil, H. K. (1996). *Nonlinear Systems*. Prentice Hall, New Jersey.

Kokotovic, P. V. (1992). The joy of feedback: nonlinear and adaptive. *IEEE Control Systems Magazine*, 12(3):7–17.

Kokotovic, P. V., O'Malley Jr, R. E., and Sannuti, P. (1976). Singular perturbations and order reduction in control theory—an overview. *Automatica*, 12(2):123–132.

Koopman, B. and Neumann, J. v. (1932). Dynamical systems of continuous spectra. *Proceedings of the National Academy of Sciences of the United States of America*, 18(3):255.

Koopman, B. O. (1931). Hamiltonian systems and transformation in hilbert space. *Proceedings of the National Academy of Sciences of the United States of America*, 17(5):315.

Korda, M. (2016). Moment-sum-of-squares hierarchies for set approximation and optimal control. Technical report, IGM, Lausanne.

Korda, M., Henrion, D., and Jones, C. N. (2017). Convergence rates of moment-sum-of-squares hierarchies for optimal control problems. *Systems & Control Letters*, 100:1–5.

Korda, M. and Mezić, I. (2018a). Linear predictors for nonlinear dynamical systems: Koopman operator meets model predictive control. *Automatica*, 93:149–160.

Korda, M. and Mezić, I. (2018b). On convergence of extended dynamic mode decomposition to the koopman operator. *Journal of Nonlinear Science*, 28(2):687–710.

Korda, M. and Mezic, I. (2020). Optimal construction of koopman eigenfunctions for prediction and control. *IEEE Transactions on Automatic Control*.

Krstic, M., Kanellakopoulos, I., Kokotovic, P. V., et al. (1995). *Nonlinear and adaptive control design*, volume 222. Wiley New York.

Kutz, J. N., Fu, X., Brunton, S. L., and Erichson, N. B. (2015). Multi-resolution dynamic mode decomposition for foreground/background separation and object tracking. In *2015 IEEE International Conference on Computer Vision Workshop (ICCVW)*, pages 921–929. IEEE.

Lasota, A. and Mackey, M. C. (2013). *Chaos, fractals, and noise: stochastic aspects of dynamics*, volume 97. Springer Science & Business Media.

Ma, X., Huang, B., and Vaidya, U. (2019). Optimal quadratic regulation of nonlinear system using koopman operator. In *2019 American Control Conference*, pages 4911–4916. IEEE.

Mane, R. and Levy, S. (1987). *Ergodic Theory and Differentiable Dynamics*. Ergebnisse der Mathematik und ihrer Grenzgebiete. 3. Folge / A Series of Modern Surveys in Mathematics. Springer Berlin Heidelberg.

Mann, J. and Kutz, J. N. (2016). Dynamic mode decomposition for financial trading strategies. *Quantitative Finance*, 16(11):1643–1655.

Markovsky, I. and Rapisarda, P. (2008). Data-driven simulation and control. *International Journal of Control*, 81(12):1946–1959.

Markovsky, I., Willems, J. C., Rapisarda, P., and De Moor, B. L. (2005). Data driven simulation with applications to system identification. *IFAC Proceedings Volumes*, 38(1):970–975.

Markovsky, I., Willems, J. C., Van Huffel, S., and De Moor, B. (2006). *Exact and approximate modeling of linear systems: A behavioral approach*. SIAM.

Mauroy, A. and Mezic, I. (2013). A spectral operator-theoretic framework for global stability. In *Proc. of IEEE Conference of Decision and Control*, Florence, Italy.

Mauroy, A. and Mezić, I. (2016). Global stability analysis using the eigenfunctions of the Koopman operator. *IEEE Transactions on Automatic Control*, 61(11):3356–3369.

Mayne, D. Q., Rawlings, J. B., Rao, C. V., and Scokaert, P. O. (2000). Constrained model predictive control: Stability and optimality. *Automatica*, 36(6):789–814.

Mehta, P. G. and Vaidya, U. (2005). On stochastic analysis approaches for comparing complex systems. In *Proceedings of the 44th IEEE Conference on Decision and Control*, pages 8082–8087. IEEE.

Mezić, I. (2005). Spectral properties of dynamical systems, model reduction and decompositions. *Nonlinear Dynamics*, 41(1-3):309–325.

Mezić, I. (2013). Analysis of fluid flows via spectral properties of the koopman operator. *Annual Review of Fluid Mechanics*, 45:357–378.

Mezic, I. and Arbabi, H. (2017). On the computation of isostables, isochrons and other spectral objects of the koopman operator using the dynamic mode decomposition. In *2017 International Symposium on Nonlinear Theory and Its Applications(NOLTA)*.

Mezić, I. and Banaszuk, A. (2004). Comparison of systems with complex behavior. *Physica D: Nonlinear Phenomena*, 197(1-2):101–133.

Mohr, R. and Mezić, I. (2014). Construction of eigenfunctions for scalar-type operators via laplace averages with connections to the koopman operator. *arXiv preprint arXiv:1403.6559*.

Mohr, R. M. (2014). *Spectral Properties of the Koopman Operator in the Analysis of Nonstationary Dynamical Systems*. University of California, Santa Barbara.

Moore, K. L. (2012). *Iterative learning control for deterministic systems*. Springer Science & Business Media.

Muld, T. W., Efraimsson, G., and Henningson, D. S. (2012). Flow structures around a high-speed train extracted using proper orthogonal decomposition and dynamic mode decomposition. *Computers & Fluids*, 57:87–97.

Pan, C., Yu, D., and Wang, J. (2011). Dynamical mode decomposition of gurney flap wake flow. *Theoretical and Applied Mechanics Letters*, 1(1):012002.

Park, U. S. and Ikeda, M. (2009). Stability analysis and control design of lti discrete-time systems by the direct use of time series data. *Automatica*, 45(5):1265–1271.

Peitz, S. (2018). Controlling nonlinear pdes using low-dimensional bilinear approximations obtained from data. *arXiv preprint arXiv:1801.06419*.

Peitz, S. and Klus, S. (2019). Koopman operator-based model reduction for switched-system control of pdes. *Automatica*, 106:184–191.

Petersen, K. E. (1989). *Ergodic theory*, volume 2. Cambridge University Press.

Prajna, S., Parrilo, P. A., and Rantzer, A. (2004). Nonlinear control synthesis by convex optimization. *IEEE Transactions on Automatic Control*, 49(2):1–5.

Primbs, J. A., Nevistić, V., and Doyle, J. C. (1999). Nonlinear optimal control: A control Lyapunov function and receding horizon perspective. *Asian Journal of Control*, 1(1):14–24.

Proctor, J. L., Brunton, S. L., and Kutz, J. N. (2016). Dynamic mode decomposition with control. *SIAM Journal on Applied Dynamical Systems*, 15(1):142–161.

Raghunathan, A. and Vaidya, U. (2013). Optimal stabilization using lyapunov measures. *IEEE Transactions on Automatic Control*, 59(5):1316–1321.

Rajaram, R., Vaidya, U., Fardad, M., and Ganapathysubramanian, B. (2010a). Stability in the almost everywhere sense: A linear transfer operator approach. *Journal of Mathematical Analysis and Applications*, 368(1):144 – 156.

Rajaram, R., Vaidya, U., Fardad, M., and Ganapathysubramanian, G. (2010b). Stability in the almost everywhere sense: a linear transfer operator approach. *Journal of Mathematical Analysis and Applications*, 368:144–156.

Rantzer, A. (2001). A dual to Lyapunov's stability theorem. *Systems & Control Letters*, 42:161–168.

Rowley, C. W., Mezić, I., Bagheri, S., Schlatter, P., and Henningson, D. S. (2009). Spectral analysis of nonlinear flows. *Journal of fluid mechanics*, 641:115–127.

Rugh, W. J. and Shamma, J. S. (2000). Research on gain scheduling. *Automatica*, 36(10):1401–1425.

Sauer, P. W. and Pai, M. (1997). Power system dynamics and stability. *Urbana*, 51:61801.

Sayadi, T., Schmid, P. J., Nichols, J. W., and Moin, P. (2014). Reduced-order representation of near-wall structures in the late transitional boundary layer. *Journal of Fluid Mechanics*, 748:278–301.

Schmid, P. J. (2010). Dynamic mode decomposition of numerical and experimental data. *Journal of fluid mechanics*, 656:5–28.

Schmid, P. J., Li, L., Juniper, M., and Pust, O. (2011). Applications of the dynamic mode decomposition. *Theoretical and Computational Fluid Dynamics*, 25(1-4):249–259.

Seena, A. and Sung, H. J. (2011). Dynamic mode decomposition of turbulent cavity flows for self-sustained oscillations. *International Journal of Heat and Fluid Flow*, 32(6):1098–1110.

Sharma, H., Vaidya, U., and Ganapathysubramanian, B. (2019a). A transfer operator methodology for optimal sensor placement accounting for uncertainty. *Building and environment*, 155:334–349.

Sharma, P., Huang, B., Ajjarapu, V., and Vaidya, U. (2019b). Data-driven identification and prediction of power system dynamics using linear operators. In *2019 IEEE Power & Energy Society General Meeting (PESGM)*, pages 1–5. IEEE.

Sinha, S., Vaidya, U., and Rajaram, R. (2016). Operator theoretic framework for optimal placement of sensors and actuators for control of nonequilibrium dynamics. *Journal of Mathematical Analysis and Applications*, 440(2):750–772.

Sontag, E. D. (1989). A 'universal' construction of Artstein's theorem on nonlinear stabilization. *Systems & control letters*, 13(2):117–123.

Sootla, A., Mauroy, A., and Ernst, D. (2018). Optimal control formulation of pulse-based control using Koopman operator. *Automatica*, 91:217–224.

Spall, J. C. (2009). Feedback and weighting mechanisms for improving jacobian estimates in the adaptive simultaneous perturbation algorithm. *IEEE Transactions on Automatic Control*, 54(6):1216–1229.

Spall, J. C. and Chin, D. C. (1997). Traffic-responsive signal timing for system-wide traffic control. *Transportation Research Part C: Emerging Technologies*, 5(3-4):153–163.

Spall, J. C. and Cristion, J. A. (1993). Model-free control of general discrete-time systems. In *Proceedings of 32nd IEEE Conference on Decision and Control*, pages 2792–2797. IEEE.

Spall, J. C. and Cristion, J. A. (1998). Model-free control of nonlinear stochastic systems with discrete-time measurements. *IEEE transactions on automatic control*, 43(9):1198–1210.

Spall, J. C. et al. (1992). Multivariate stochastic approximation using a simultaneous perturbation gradient approximation. *IEEE transactions on automatic control*, 37(3):332–341.

Surana, A. (2016). Koopman operator based observer synthesis for control-affine nonlinear systems. In *2016 IEEE 55th Conference on Decision and Control (CDC)*, pages 6492–6499. IEEE.

Surana, A. and Banaszuk, A. (2016). Linear observer synthesis for nonlinear systems using koopman operator framework. *IFAC-PapersOnLine*, 49(18):716–723.

Susuki, Y. and Mezic, I. (2011). Nonlinear koopman modes and coherency identification of coupled swing dynamics. *IEEE Transactions on Power Systems*, 26(4):1894–1904.

Susuki, Y. and Mezić, I. (2013). Nonlinear koopman modes and power system stability assessment without models. *IEEE Transactions on Power Systems*, 29(2):899–907.

Susuki, Y., Mezic, I., Raak, F., and Hikihara, T. (2016). Applied koopman operator theory for power systems technology. *Nonlinear Theory and Its Applications, IEICE*, 7(4):430–459.

Sutton, R. S. and Barto, A. G. (2018). *Reinforcement learning: An introduction*. MIT press.

Theodorou, E., Buchli, J., and Schaal, S. (2010). A generalized path integral control approach to reinforcement learning. *The Journal of Machine Learning Research*, 11:3137–3181.

Todorov, E. (2009). Efficient computation of optimal actions. *Proceedings of the national academy of sciences*, 106:11478–11483.

Tu, J. H., Rowley, C. W., Luchtenburg, D. M., Brunton, S. L., and Kutz, J. N. (2013). On dynamic mode decomposition: theory and applications. *arXiv preprint arXiv:1312.0041*.

Uchiyama, M. (1978). Formation of high-speed motion pattern of a mechanical arm by trial. *Transactions of the Society of Instrument and Control Engineers*, 14(6):706–712.

Vaidya, U. (2007). Observability gramian for nonlinear systems. In *2007 46th IEEE Conference on Decision and Control*, pages 3357–3362. IEEE.

Vaidya, U., Mehta, P., and Shanbhag, U. (2010a). Nonlinear stabilization via control lyapunov meausre. *IEEE Transactions on Automatic Control*, 55(6):1314–1328.

Vaidya, U. and Mehta, P. G. (2008a). Lyapunov measure for almost everywhere stability. *IEEE Transactions on Automatic Control*, 53(1):307–323.

Vaidya, U. and Mehta, P. G. (2008b). Lyapunov measure for almost everywhere stability. *IEEE Transactions on Automatic Control*, 53(1):307–323.

Vaidya, U., Mehta, P. G., and Shanbhag, U. V. (2010b). Nonlinear stabilization via control lyapunov measure. *IEEE Transactions on Automatic Control*, 55(6):1314–1328.

Van Helvoort, J. J. M. (2007). Unfalsified control: data-driven control design for performance improvement. *Technische Universiteit Eindhoven, Eindhoven, Netherlands*.

Van Overschee, P. and De Moor, B. (2012). *Subspace identification for linear systems: Theory Implementation Applications*. Springer Science & Business Media.

Vander Velde, W. E. (1968). *Multiple-input describing functions and nonlinear system design*. McGraw-Hill, New York.

WATKINS, C. (1989). Learning from delayed rewards. *PhD thesis, Cambridge University*.

Watkins, C. J. and Dayan, P. (1992). Q-learning. *Machine learning*, 8(3-4):279–292.

Weissensteiner, A. (2009). A q-learning approach to derive optimal consumption and investment strategies. *IEEE transactions on neural networks*, 20(8):1234–1243.

Werbos, P. (1992). Approximate dynamic programming for realtime control and neural modelling. *Handbook of intelligent control: neural, fuzzy and adaptive approaches*, pages 493–525.

Werbos, P. J., Miller, W., and Sutton, R. (1990). A menu of designs for reinforcement learning over time. *Neural networks for control*, pages 67–95.

Williams, G., Aldrich, A., and Theodorou, E. A. (2017). Model predictive path integral control: From theory to parallel computation. *Journal of Guidance, Control, and Dynamics*, 40(2):344–357.

Williams, M. O., Kevrekidis, I. G., and Rowley, C. W. (2015). A data–driven approximation of the koopman operator: Extending dynamic mode decomposition. *Journal of Nonlinear Science*, 25(6):1307–1346.

Yin, S. and Kaynak, O. (2015). Big data for modern industry: challenges and trends [point of view]. *Proceedings of the IEEE*, 103(2):143–146.